

24/3140

MONASH UNIVERSITY
THESIS ACCEPTED IN SATISFACTION OF THE
REQUIREMENTS FOR THE DEGREE OF
DOCTOR OF PHILOSOPHY

ON..... 1 March 2002

.....
for Sec. Research Graduate School Committee

Under the copyright Act 1968, this thesis must be used only under the normal conditions of scholarly fair dealing for the purposes of research, criticism or review. In particular no results or conclusions should be extracted from it, nor should it be copied or closely paraphrased in whole or in part without the written consent of the author. Proper written acknowledgement should be made for any assistance obtained from this thesis.

ERRATA

- p.3 paragraph 1, first sentence: "the" for "he"
- p.28 paragraph 3, last sentence: "not" for "most"
- p.40 last paragraph, first sentence: "assumes" for "assume"
- p.65 paragraph 3, 4th line: "Figure 8.2" for "Figure 8.1"
- p.68 5th line: "Figure 8.2" for "Figure 8.1"
- p.136 paragraph 1, 1st line: "CB625" for "CB25"

ADDENDUM

- p.28 paragraph 5, 3rd line: add "are" and read "... and are by no means comprehensive."
- p.49 last paragraph, 1st line: delete "specimen", add "tension" and read "... middle hole tension (MHT)"
- p.102 paragraph 5, last sentence: add missing bracket to end of the sentence and read "... (Figures 6.27 and 6.28 respectively)."

Fracture of Ductile Polymers

*A dissertation submitted for the degree of Doctor of
Philosophy*

by

Henry Beh
B.E. (Hons)

School of Physics and Materials Engineering

Monash University

Clayton, Victoria, 3800

Australia

Submitted March 2000

Revised August 2001

Table of Contents

Contents	i
Abstract	iv
Declaration of Originality	vi
Acknowledgements	vii
List of Publications and Presentations	viii
Nomenclature	x
List of Abbreviations	xii
Chapter 1 Introductory Remarks	1
1.1 Introduction to the Investigation	1
1.2 Layout of the Dissertation	3
Chapter 2 Literature Review	5
2.1 Polymer Blends	5
2.2 Fracture of Ductile Polymers	7
2.2.1 Linear Elastic Fracture Mechanics	8
2.2.2 Elastic/Plastic Fracture Mechanics (J-Integral)	20
2.2.3 Essential Work of Fracture	26
2.2.4 Observations of Deformation in Ductile Polymers	30
2.3 Summary	39
Chapter 3 Methodologies in Predicting Failure	41
3.1 Elastic Analysis of Polymer Articles with Cracks	41
3.1.1 Yielding Methodology	43
3.1.2 LEFM Methodology	43
3.1.3 Effective Crack Tip Blunting Methodology	45

3.2 Application of Elastic Analysis to Complex Geometries.....	47
3.2.1 FEA and Yielding Methodology	48
3.2.2 FEA and LEFM Methodology.....	60
3.2.3 FEA and Effective Crack Tip Blunting Methodology.....	63
3.3 Application of Elastic/Plastic Analysis to Complex Geometries	64
3.3.1 J-Integral Methodology	64
3.4 Designing Polymer Articles.....	65
3.5 Summary.....	67
Chapter 4 Materials and Experimental Methods.....	69
4.1 Materials and Sample Preparation.....	69
4.1.1 Raw Materials.....	69
4.1.2 Processing.....	70
4.2 Experimental Techniques	72
4.2.1 Differential Scanning Calorimetry	72
4.2.2 Impact Tests	72
4.2.3 Izod Impact Tests	72
4.2.4 Finite Element Modelling.....	72
4.2.5 Notching of Polymers.....	73
4.2.6 Tensometer Testing	74
4.2.7 Microscopy.....	74
Chapter 5 Characterisation of Materials	76
5.1 Glass Transition Temperature Measurements	76
5.2 Mechanical Properties	78
5.2.1 Tensile	78
5.2.2 Impact and Izod	82
Chapter 6 Comparison of Experimental and Predicted Failure Loads for Ductile Polymers	84
6.1 Fracture Toughness Measurement - SENT Specimens	84
6.2 Failure Analysis for MHT Specimens.....	91
6.3 Failure Analysis for THT Specimens	96
6.4 Failure Analysis for CT Specimens.....	102
6.5 Failure Analysis for Ribbed Specimens	107
6.6 Summary.....	113

Chapter 7 Microscopy of Crack Tips	115
7.1 Single Phase Polymers	115
7.1.1 PC	115
7.1.2 PET	120
7.1.3 PS	124
7.2 Toughened Polymers - ABS	127
7.2.1 Astalac DMT	128
7.2.2 Astalac MI20	132
7.2.3 CB625	134
7.3 Polymer Blends	137
7.3.1 ABS/PET	137
7.3.2 ABS/PC	142
7.4 Summary	147
Chapter 8 Discussion and Conclusion	149
8.1 Discussion and Concluding Remarks	149
8.2 Recommendations for Future Work	153
References	156

Abstract

Better understating of predicting failure in tough ductile polymers is desirable because of their increasing use in load bearing applications. In this treatise, the use of several methodologies, all of which assume the material to behave elastically, were used to predict failure loads for various injection moulded articles that contained cracks. The motivation for this is to produce a simple means of predicting failure in normally thin walled injection moulded articles.

It was found that a new simple model could predict safe failure loads for thin walled polymer articles with short crack lengths. The model could be applied to articles which are also complex in geometry. This model supposes that sharp flaws in thin walled injection moulded articles blunt themselves to a radius of curvature ρ and this parameter ρ is a characteristic of each material. Brittle polymeric materials such as polystyrene were found to have low values of ρ , whilst tough polymers such as poly-vinyl chloride had high ρ values (up to fifty times the value of polystyrene). Once the parameter ρ is found from simple fracture tests, it is able to be used in predicting failure loads for cracked articles (as in this thesis) or it may also be utilised as a design tool. In design, the simple failure model informs the engineer of the size of the flaw which a component is able to withstand (under service loads) before failing. This allows for better control over the amount of material used and correct allocation of material to regions of probable failure in the manufacture of load bearing components.

Nine types of polymers were studied and four loading situations were investigated. Even under severe loading conditions, such as a crack running along the base of the rib in a ribbed specimen, where a plane strain situation exists, the simple model reliably predicted safe working loads. The cracks are in the order of 15% or less of the article's width. The work covered in this thesis is therefore concerned primarily with cases where the crack is small in comparison to the size of the object. The author feels that consumers will tend to discard components which have large cracks in them thereby making analysis for those cases inconsequential.


It may be worthwhile to state categorically at this point that the parameter ρ is not equal to Irwin's plastic zone size. It is simply a fitting parameter to model the failure behaviour of ductile polymers. As well as this, the simple model proposed is intended for use in

conjunction with linear elastic mechanics and net section yielding. Together, the three procedures predict safe working loads for the crack lengths studied in this thesis. In comparison, the work has shown that if only linear elastic fracture mechanics and net section yielding were relied upon to provide predictions, then premature failure can occur for some materials at crack lengths less than 5% of the specimen's width.

A novel technique of impregnating the crack tip with a thermoset proved effective in providing micrographs having good contrast and detail of the deformation mechanisms involved in failure of thin walled injection moulded articles. The impregnation was performed with the crack under load therefore capturing the event of failure a short time before it happens. Microscopy of the crack tips of eight of the polymers considered, at ninety percent of their failure loads, showed large scale yielding, crazing, microcracking, voiding and stress whitening at the crack tip. This implies that the work done at the end of the flaw allows the polymer to behave as if the crack has blunted itself to a radius of curvature ρ .

Declaration

This thesis contains no material which has been previously accepted for the award of any other degree or diploma in any university or institution. To my knowledge it contains no material previously published or written by any other person, except where due reference is made in the text.



Henry Beh

August 2001

Acknowledgements

I, Henry Beh, would like to thank all those people and organisations who contributed to the work presented in this dissertation.

To my supervisor and friend, Dr. Graham Harold Edward and his family (Carmel, Felicity and Priya), I would like to express my eternal gratitude. He has persevered with me and remained patient despite my sometimes lack of diligence in my work. He has helped to motivate and focus me on the task at hand when I have drifted into areas not associated with my research.

The help given by the staff (academic, secretarial and technical) at the Department of Materials Engineering is appreciated. The skills and quality of work provided by Messrs. Jim Mitchell, Irek Kozicki, Geoff Mead, Silvio Mattievich, Kees De Bruin, Ron Smith (now retired) and Bernard Pownall has been of the highest quality. Special thanks go to Ms. Julie Fraser for her work on the photographs presented in this thesis and materials for my presentations during my candidature.

Thanks to the CRC for Polymers for providing funding for three and a half years. The excellent help of Dr. Ferenc Cser in my microscopy work and Mr. Paul Chaperon in my finite element work is appreciated.

To my fellow colleagues, Dr. Marcus Zipper, Dr. Mark Hodge, Dr. James Mardel, Dr. Jonathan Campbell, Dr. Jim Gonis, Dr. John Forsythe, Messrs. Christopher Wise, Timothy Scott, Anthony Mayr, Aaron Seeber, Mark Forrest, Ms. Katherine Dean and all other post-graduates; your humour and enjoyable conversations have made my stay a happy one. Also, my thanks to Dr. Aubrey Seknow and his family for all their kindness over the years and to all my friends outside Monash University for their support.

Last but most importantly, I would like to dedicate this thesis to my immediate family - grandmother, father and mother for their love and encouragement. I will always be grateful.

List of Publications and Presentations

The following publications have arisen from the work performed during my candidature and other related work. It should be noted that not all publications listed include work presented for examination in this dissertation.

Journal Articles

H. Beh and G.H. Edward, "Failure Prediction of Ductile Polymers", currently being written for *Engineering Fracture Mechanics*.

Conference Publications

H. Beh and G.H. Edward, "Fracture of Tough Ductile Polymers". Faculty of Engineering Graduate Research Scholarship Evening. Melbourne, Australia, 25 September 1996.

H. Beh and G.H. Edward, "Fracture of Toughened Ductile Polymer Blends". 1995 International Chemical Congress of Pacific Basin Societies (Honolulu, Hawaii, USA, 17th-22nd Dec. 1995)

H. Beh and G.H. Edward, "Crack Tip Propagation in Tough Polymer Blends", Fourth Pacific Polymer Conference (Koloa, Kauai, Hawaii, USA, 12th-16th Dec. 1995), 517

H. Beh and G.H. Edward, "Failure Prediction of Ductile Polymers under Complex Stress States". 20th Australian Polymer Symposium (Adelaide, Australia, 5th-9th Feb. 1995), 4-5

H. Beh and G.H. Edward, "Fracture Prediction in Ductile Polymers". Third Pacific Polymer Conference (Gold Coast, Australia, 13th-17th Dec. 1993), 305-306

Invited Lectures

"Fracture of Ductile Polymers", Manufacturing CRCs Postgraduate Student Competition, CSIRO Division of Manufacturing Science and Technology, Preston, Victoria, 2001.

"Prediction of Failure in Ductile Polymers", School of Physics and Materials Engineering student seminars, Monash University, Clayton, Victoria, 1996.

"Toughening Mechanisms of ABS/PET blends", CRC for Polymers student talks, CSIRO Division of Molecular Science, Clayton, Victoria, 1995.

Nomenclature

<u>Symbol</u>	<u>Description</u>
a	Half crack length
b	Semi - minor axis of an ellipse
B	Thickness
c	Semi - major axis of an ellipse
E	Elastic tensile modulus
G	Elastic energy release rate
G_I	Elastic mode I energy release rate
G_{Ic}	Elastic mode I critical energy release rate
J	J-Integral energy release rate
J_I	J-Integral mode I energy release rate
J_{Ic}	J-Integral mode I critical energy release rate
K	Elastic stress intensity factor
K_I	Elastic mode I stress intensity factor
K_{Ic}	Elastic mode I critical stress intensity factor
L	Ligament length
T	Temperature
T_g	Glass Transition Temperature
W	Width

w_e	Specific essential work of fracture
W_e	Essential work of fracture
w_p	Specific non-essential work of fracture
W_p	Non-essential work of fracture
w_f	Specific energy to fracture
W_f	Energy to fracture
Y	Geometric constant
ϵ	Strain
ρ	Radius of curvature at the end of an ellipse or blunting effect parameter
$\bar{\sigma}$	Average stress
σ_a	Applied stress
σ_{vm}	Von-Mises stress
σ_y	Yield stress as measured by a uniaxial tensile test

List of Abbreviations

ABS	Acrylonitrile Butadiene Styrene
CT	Compact Tension
CTOD	Crack Tip Opening Displacement
EWf	Essential Work of Fracture
FEA	Finite Element Analysis
MEK	Methyl - Ethyl Ketone
MHT	Middle Hole Tension
PC	Polycarbonate
PET	Poly(ethylene terephthalate)
PS	Polystyrene
PVC	Polyvinyl chloride
SEM	Scanning Electron Microscopy
SENT	Single Edge Notched Tension
TEM	Transmission Electron Microscopy
THt	Three Hole Tension

Chapter 1

Introductory Remarks

1.1 Introduction to the Investigation

This work was carried out as a continuation to the round robin symposium held by Newman and Loss (1985). The symposium compared numerous fracture mechanics methodologies in predicting failure loads for sheets with various crack lengths made from different metal alloys. Some of the specimens were also complex in stress state. The geometries studied are shown by Figure 1.1.

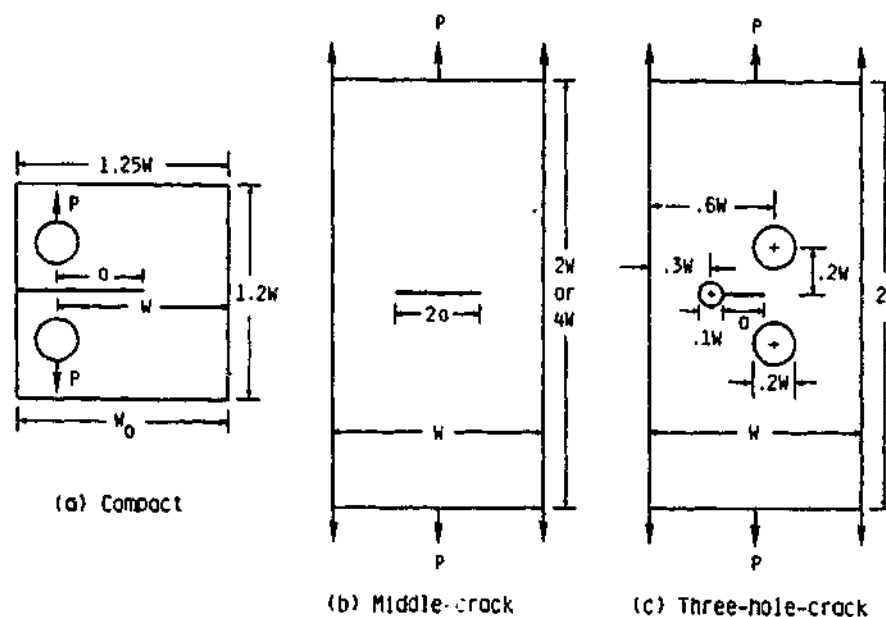


Figure 1.1: Dimensions of specimens as used by Newman and Loss.

In this particular investigation, injection moulded polymer articles of the same geometries as Newman and Loss were used. Injection moulded articles were chosen because they are predominantly thin walled and can be complex in geometry. Apart from specimens shown by Figure 1.1, ribbed specimens were also fractured using pin loading. Under uniform loading, sheets with a centrally drilled hole and cracks emanating from it were also tested as well as sheets with a notch made into the long side of the specimen.

Ribbing in polymeric articles is common because they help to stiffen members, therefore overcoming the problem of low modulus of most polymers. At the junction of the rib and the

flange, a case of plane strain can also exist, in contrast to the plane stress conditions of the other configurations. In fact, because of the constraint on the crack tip, it may cause brittle fracture. That is the primary reason for its inclusion in the experiments.

Nine different types of polymers were used in this study ranging from brittle polystyrene to a tough ABS/PET blend. The wide variety of polymers used, as well as the varied types of loading situations, was intended to validate the simple predictive blunting model described in this thesis.

Simple fracture methodologies such as net section yielding and linear elastic fracture mechanics (LEFM) were used to predict failure for the various articles. The other constraint was that the crack lengths involved were less than fifteen percent of the specimen's width. This thesis is concerned mainly with articles containing short crack lengths because consumers will tend to discard polymer articles with large crack lengths even though they may still be structurally stable for the purpose.

In literature, simple theories for predicting fracture are directed, in the majority, towards metals. The premise is that metals fail before their theoretical strength because they contain sharp imperfections or flaws. Applying this assumption in the analysis of polymeric articles, LEFM and net section yielding predictions were higher than experimental data in some cases, and in practice would be deemed unsafe.

A new simple model was proposed to overcome the inability of LEFM and net section yielding to predict failure. This new model was directed specifically towards tough ductile polymers. The proposal is that sharp imperfections or flaws in polymers blunt themselves to a radius of curvature ρ . This idea has been previously touched upon by Dubey (1998) and Parton (1992). Each material will have a distinctive value of ρ and cracks will behave as if the end has blunted to this effective curvature, but it is not equivalent to the plastic zone described by Irwin. Once the material has been characterised for the parameter ρ and the stress state within the object is well defined, failure loads can be predicted for the article containing the crack. Failure is assumed to occur when the remote applied loads cause the magnified stress at the blunted flaw to reach the yield stress of the material. From observations, the ductile polymeric specimens, when loaded under a constant velocity, go through a maximum load (defined as the point of failure) and continue to neck at lower loads for fairly large extensions (Refer to curve C in Figure 8.2).

Defining the stresses within a component may be done analytically or with the aid of finite element analysis. In this thesis, two specimens with complex geometries required the use of FEA to determine the magnitude of stresses in the regions of interest.

In addition to modelling the failure of ductile polymers with complex stress states, this investigation contains microscopy work on the crack tips of deforming polymer articles. The micrographs were intended to highlight the deformation mechanisms at the crack tips. Previously Bhowmick and De (1991) used fractography, utilising both optical and scanning electron microscopy, on failed rubber components. In 1994, Majumdar et al. (1994) used a double-notch four-point bend specimen in order to capture the moment when the crack was about to propagate under load. In this thesis, the two previous ideas were combined and applied to eight of the materials studied.

The technique can be summarised as follows. Instead of using double-notch four-point bend specimens, cracked polymeric tensile specimens were loaded and their cracks were kept open with the use of wedges. Low viscosity epoxy was poured into the crack mouth and forced into the crack tip using high pressures until the epoxy cured. Optical and scanning microscopy work was then carried out on the crack tip. For metals, the procedure is to use molten rubber instead of epoxy.

Other authors have looked at crack tips [Wu and Mai 1993; Beahan et al. 1975] and fracture surfaces [Horiuchi et al. 1994; Dijkstra and Gaymans 1994] but the idea of forcing epoxy into the crack tip is relatively novel. The other advantage of polymers over metals, especially for polymer blends, is the contrast between phases in the micrographs once an etchant is employed. In Chapter 7, both optical and scanning electron micrographs show large amounts of deformation at the front of the crack tip when it is loaded to ninety percent of its failure load. These images give further evidence to the simple model that to accommodate sharp cracks, ductile polymers effectively blunt the tip to a certain radius of curvature, which is material dependent.

1.2 Layout of the Dissertation

The dissertation is broken up into eight chapters. Before Chapter 1, pages i to xi, could be described as preface. It includes the Table of Contents to List of Abbreviations.

Chapter 1 gives a general overview of the project and some historical reasoning which lead to the current topic of this thesis. It also provides a layout of the dissertation describing the logical structure of the work.

Chapter 2 is a literature survey of previous work done on the subject matter covered by this thesis. The material described in Chapter 2 should be current up to the time of submission and highlights the need for a simple and novel way of predicting fracture in tough ductile polymer articles.

Chapter 3 compares the traditional methodologies used to predict failure in cracked structures with that of the proposed blunting model. The chapter provides a simple example of a crack emanating from a hole in a plate that is loaded uniformly. It then proceeds to apply the theories from that simple case to complex and more engineering relevant structures. It also contains finite element analysis of the stress state within these complex structures.

Chapter 4 gives a description of apparatus and procedures used in attaining the experimental results. It is written in an instructional manner for others who may wish to repeat the experiments.

Simple characterisation tests were performed on the materials used in this thesis. The tests involved observing the change in yield stress or maximum load and elastic modulus as a function of test speed. Impact energy to break and notched Izod energy to break were also noted. The data are reported in Chapter 5.

Results of experimental failure loads of the various specimens used were plotted against the predictive equations (defined in Chapter 3) and are shown in Chapter 6. Micrographs of the crack tips of the deformed articles are printed in Chapter 7. Discussion and analysis of the results are also included within the two chapters.

A summary of the salient findings is given in Chapter 8 as well as ideas for future work. It highlights the incompleteness of this area and the need to explore other aspects of this topic. References are given after Chapter 8.

Chapter 2

Literature Review

2.1 Polymer Blends

Polymer blends are produced by the mixing of two or more polymers together to give an alloy with a specific portfolio of physical properties. This is achieved without having a need to synthesise specialised polymer systems. Polymer blends have the advantage of

1. Higher or equal performance at an equal or lower price compared to current material.
2. Quick modification of performance,
3. Extending the performance of expensive resins.
4. Reuse of plastic scrap; and
5. Formation of unique materials.

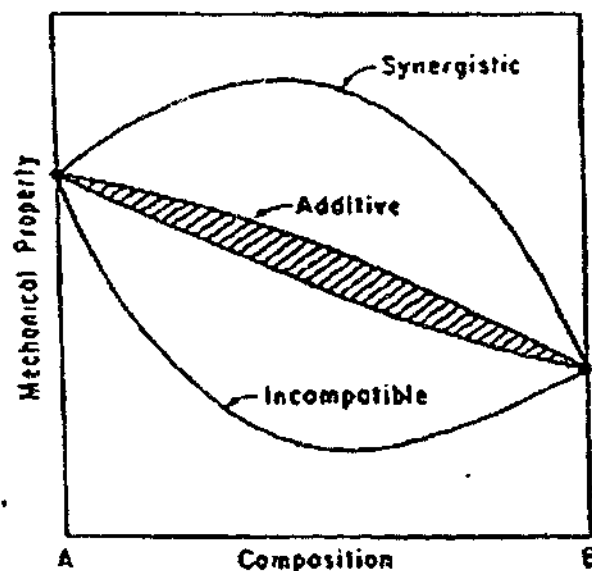


Figure 2.1: Possible variations in mechanical properties for a polymer blend [Paul and Barlow 1980].

The manner in which polymer blends ("blends") are compounded together is of vital importance in controlling the mechanical properties of blends. The mechanical properties of blends are not an average mean of the two or more components, rather they may pass through a minimum somewhere in the composition range. Less likely, synergism may occur whereby the two components produce a blend with enhanced properties relative to each individual component (refer to Figure 2.1).

The textbooks by Utracki (1990) and Paul and Newman (1978) provide an excellent general overview on the topic of polymer blends. These texts give a list of common commercial blends and their uses. More current reviews can be found by reading Lipatov (1992) and Kulshrestha (1993).

A blend is usually toughened by having a brittle matrix with dispersed rubbery inclusions. Another morphology which can produce high toughness materials is the interpenetrating network type of structure (refer to Figure 2.2). Both phases are co-continuous and commingled, thereby physically locking together.

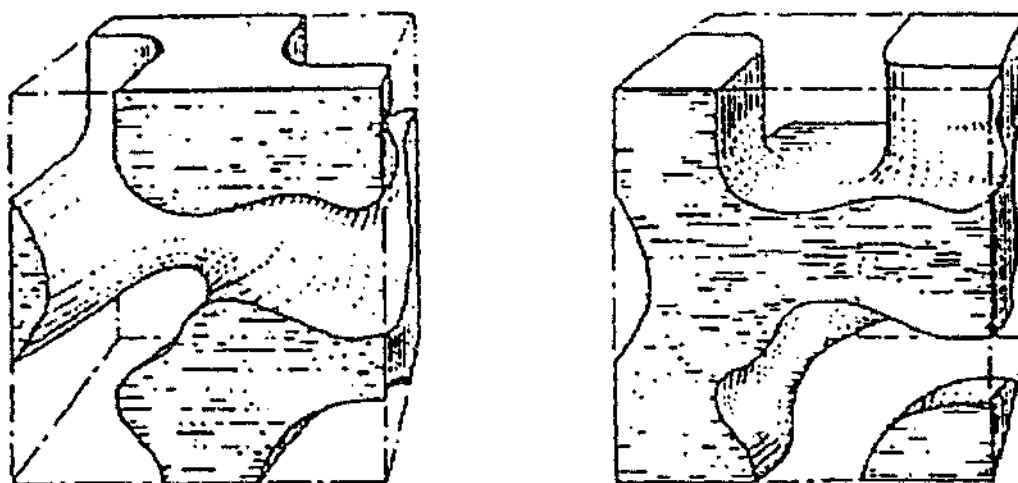


Figure 2.2: Interpenetrating morphology [Edward 1990; Utracki 1990].

In this study, a number of polymers have been experimented upon. They were a range of materials giving a variety of toughness values. Three homo polymers were experimented upon. They were poly(ethylene terephthalate) (PET), polycarbonate (PC) and polystyrene (PS). Information on their chemical structure, general mechanical behaviour and applications can be found in Cook and Guise (1989), Billmeyer Jr. (1984) and MacDonald (1993).

Five polymer blends were considered. There were three grades of acrylonitrile butadiene styrene (ABS) - named Astalac DMT, Astalac M120 and CB625, an ABS/PC blend and an ABS/PET blend. ABS is a blend of three monomeric units. It is a styrene/acrylonitrile copolymer (SAN) matrix containing discrete butadiene based elastomeric particles for toughening. General information on ABS can be found by reading Savenije and Op Zoom (1993) and Chen et al. (1990). Information regarding the exact engineering use of

the ABS/PC blend. Astalac M120 and Astalac DMT can be found in Plast. News Inter. (1997).

The ABS/PET system is a novel material made from the combination of CB625 and PET. It was designed to be a substitute for the ABS/PC blend. The PET phase was chosen because it was cheaper, was a recycled material and performed the same function as the PC. Cook et al. (1996a, 1996b) have characterised this polymer and studied its two phase morphology.

Another variable which can profoundly affect the toughness of the blends is the adhesion between phases. The phases can also be joined at their interfaces using a compatibiliser to produce a tough material. A compatibiliser is often a graft co-polymer of the form A-B. They are designed so that the "A" portion of the graft co-polymer has a physical affinity for one component in the blend and the "B" portion has an affinity for the other to provide a cohesive interface between the two. The compatibiliser itself can be structured in a conventional or tapered manner to connect the two homo polymers (refer to Figure 2.3). Compatibilisers can be used on the dispersed phase structure or the interpenetrating structure. Current research on polystyrene - polyolefin blends [Moad et al. 1994] show the tapered compatibiliser to increase the impact strength of these blends relative to the conventional compatibilisers.

conventional	AAAAAAAAAAAAAAAAABBBBBBBBBBBBBBBBBBBB
tapered	AAAAAAAAABABABABABABBBBAAAAAAAA

Figure 2.3: Conventional and tapered compatibilisers [Moad et al. 1994]

2.2 Fracture of Ductile Polymers

A survey of the literature on fracture of ductile polymers has yielded a large number of articles which examine the fracture toughness of particular polymer systems, and relating this material property to their microstructures.

Before proceeding further, it may be worthwhile to investigate in greater detail the various parameters used to characterise toughness, with an emphasis on polymers. Knott (1973),

Broek (1986), Hearn (1995) and Anderson (1995) provide background reading to fracture mechanics. Bucknall (1977) and Williams (1984) apply the theories to toughened polymers.

2.1.1 Linear Elastic Fracture Mechanics (LEFM)

Materials possess low fracture strengths compared to their theoretical capacity because most materials deform plastically at much lower stress levels and fail by the accumulation of this irreversible damage. In addition components and structures are not perfect. They contain a myriad of material flaws and design flaws.

By analysing a plate (i.e. plane stress conditions) containing an elliptical hole, Inglis (1913) was able to show that the applied stress σ_a was magnified at the ends of the major axis of the ellipse (refer to Figure 2.4) so that

$$\frac{\sigma_{\max}}{\sigma_a} = 1 + \frac{2c}{b}, \quad (2.1)$$

where σ_{\max} is the maximum tensile stress, σ_a is the applied stress normal to the major axis, c is the semi major axis, and b is the semi minor axis.

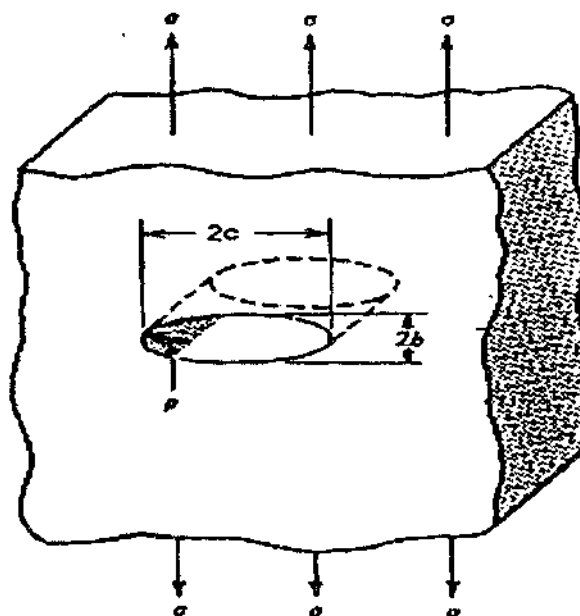


Figure 2.4: Elliptical hole in a large panel
[Hertzberg 1983]

Since the radius of curvature ρ at the end of the semi major axis of the ellipse is given by

$$\rho = \frac{b^2}{c}. \quad (2.2)$$

Eqs. 2.1 and 2.2 may be combined so that

$$\sigma_{\max} = \sigma_a \left[1 + 2\sqrt{\frac{c}{\rho}} \right]. \quad (2.3)$$

In most cases $c \gg \rho$, therefore

$$\sigma_{\max} \approx \left(2\sqrt{\frac{c}{\rho}} \right) \sigma_a. \quad (2.4)$$

The term $2\sqrt{c/\rho}$ is defined as the stress concentration factor k_t and describes the effect of crack geometry on the local crack tip stress level. Many textbooks and standard handbooks describe stress concentration in components with a wide range of crack configurations [Peterson 1953, 1974; Rooke and Cartwright 1976]. Although the exact formulations vary from one case to another, they all reflect the fact that k_t increases with increasing crack length and decreasing crack tip radius. Therefore, to ensure a low σ_{\max} , the crack length must be small or radius of curvature large. That is the reasoning behind drilling holes at the tip of a natural occurring crack, thereby changing the radius of curvature of the sharp crack tip to the radius of the hole. Tough polymers exhibit this property by deformation around a sharp crack, effectively blunting the crack and enlarging its radius of curvature. Results in Chapter 6 tend to support this idea.

After the early development based on stress analysis, Griffith (1920) provided an energy criterion for failure. Griffith noted that a balance must be struck between the decrease in potential energy (related to the release of stored elastic energy and work done by movement of the external loads) and the increase in surface energy resulting from the presence of the crack introduced to a stressed plate of elastic material. Referring to Figure 2.5, Griffith estimated the surface energy term to be the product of the total crack surface area, $2at$ and the specific surface energy, γ_s .

Using the stress analysis of Inglis for an infinitely large plate containing an elliptical crack, he proposed the decrease in potential energy of the cracked plate to be $\pi\sigma_a^2 a^2 t / E$. Therefore the change in the potential energy of the system (i.e. the infinitely large plate) with the introduction of the crack may be expressed by

$$U - U_o = -\left(\frac{\pi\sigma_a^2 a^2 t}{E}\right) + 4at\gamma_s, \quad (2.5)$$

where

U = potential energy of body with crack.

U_o = potential of the body without crack.

σ_a = applied stress.

E = modulus of elasticity.

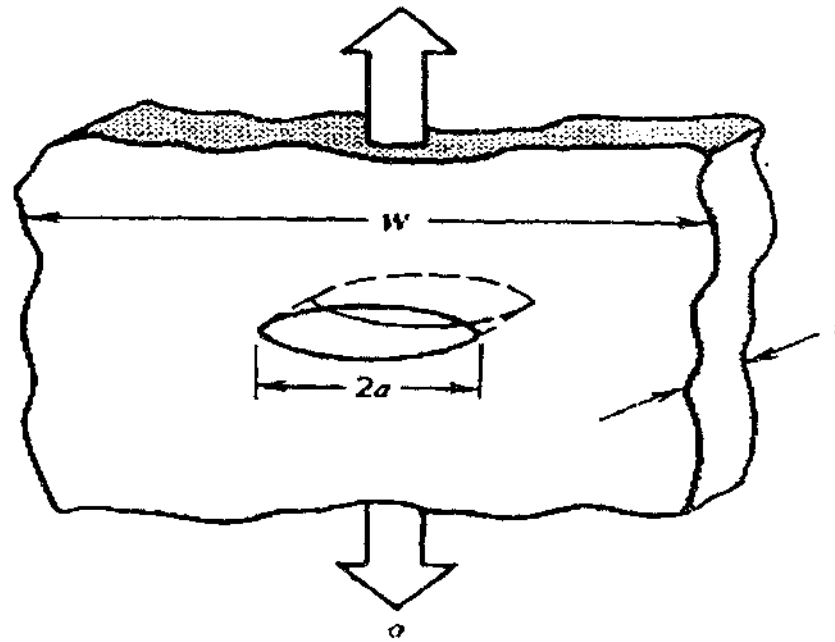


Figure 2.5: Crack in a large panel [Inglis 1913]

Eq. 2.5 can be rewritten in the form

$$U = 4at\gamma_s - \frac{\pi\sigma_a^2 a^2 t}{E} + U_o. \quad (2.6)$$

Differentiating the potential energy with respect to crack length and setting $\partial U / \partial a$ to zero (note: $\partial U_o / \partial a = 0$ because U_o accounts for the potential energy of the body without a crack and hence does not vary with crack length) gives the condition of instability:

$$\frac{\partial U}{\partial a} = 4t\gamma_s - \left(\frac{2\pi\sigma_a^2 a t}{E} \right) = 0, \quad (2.7)$$

which reduces to:

$$2\gamma_s = \frac{\pi\sigma_a^2 a}{E}. \quad (2.8)$$

The nature of the instability condition of Eq. 2.8 can be found by differentiating equation 2.7 again. Since

$$\frac{\partial^2 U}{\partial a^2} = -\frac{2\pi\sigma_a^2 t}{E}, \quad (2.9)$$

is negative, the crack is unstable and will always grow.

Griffith rewrote Eq. 2.8 to state that fracture will occur when

$$\sigma_a = \sqrt{\frac{2E\gamma_s}{\pi a}}, \quad (2.10)$$

for the case of plane stress, and

$$\sigma_a = \sqrt{\frac{2E\gamma_s}{\pi a(1-\nu^2)}}, \quad (2.11)$$

for the case of plane strain where ν is Poisson's ratio.

It is important to recognise that the Griffith relationship was derived for an elastic material containing a very sharp crack. Although Eqs. 2.10 and 2.11 do not explicitly involve the crack tip radius ρ , as was the case for the stress concentration in Eq. 2.4, the radius of the crack tip is assumed to be very sharp. As such, the Griffith relationship as written should be considered as a necessary but not sufficient condition for failure. The crack tip radius also would have to be atomically sharp to raise the local stress above the cohesive strength of the material.

To verify his equations for fracture, Griffith performed several experiments. Thin round tubes and spherical bulbs of soda-lime glass were cracked to various crack lengths with a sharp instrument, then annealed to eliminate any residual stresses associated with the cracking process and fractured by internal pressure. Griffith then computed values of $\sigma\sqrt{a}$ and compared them to $\sqrt{2E\gamma_s/\pi}$ (refer to Eq. 2.10). γ_s was determined from experimental surface tension values of glass fibres. No significant difference was found between computed and experimental values. Plastic deformation processes in amorphous glasses are very limited and the difference in surface energy and fracture energy values do not differ greatly. This is not true for metals and polymers. Orowan (1950) recognised this fact and suggested that Eq. 2.10 be modified to include the energy of plastic deformation in the fracture process so that

$$\sigma_a = \sqrt{\frac{2E(\gamma_s + \gamma_p)}{\pi a}} = \sqrt{\frac{2E\gamma_s}{\pi a} \left(1 + \frac{\gamma_p}{\gamma_s}\right)}. \quad (2.12)$$

where γ_p is the energy consumed in the region surrounding the crack.

If γ_p is much greater than γ_s ,

$$\sigma_a \approx \sqrt{\frac{2E\gamma_s}{\pi a} \left(\frac{\gamma_p}{\gamma_s}\right)}. \quad (2.13)$$

The applicability of Eqs. 2.10 or 2.12 or 2.13 in describing the fracture of real materials will depend on the sharpness of the crack and the relative amount of plastic deformation. The theoretical amount of energy to form two new fracture surfaces $2\gamma_s$ in a solid is

$$\sigma_c = \sqrt{\frac{E\gamma_s}{a_0}}, \quad (2.14)$$

where σ_c is the critical fracture stress.

Combining Eq. 2.4 and Eq. 2.14, and letting σ_{\max} equal σ_c , the applied stress for fracture will be

$$\sigma_a = \frac{1}{2} \sqrt{\frac{E\gamma_s}{a_0} \left(\frac{\rho}{a} \right)} = \sqrt{\frac{2E\gamma_s}{\pi a} \left(\frac{\pi\rho}{8a_0} \right)}. \quad (2.15)$$

The similarity between Eqs. 2.13 and 2.15 suggests a correlation between γ_p/γ_s and $\pi\rho/8a_0$. Plastic deformation can be related to a blunting process at the crack tip, with ρ increasing with γ_p . Comparing Eqs. 2.10 and 2.15 indicates that the Griffith relation is valid for cracks with a radius of curvature at the tip which is in the vicinity of $8a_0/\pi$. Eq. 2.10 is also believed to be applicable also where $\rho < (8a_0/\pi)$, since it would be unreasonable to assume that fracture will occur at zero stress as the crack root radius became infinitely small. When $\rho > (8a_0/\pi)$, Eqs. 2.14 and 2.15 would control the failure condition.

For the case of materials capable of plastic deformation, Irwin (1948) chose to use the energy source term $\delta U/\delta a$ (i.e. the elastic energy per unit crack length increment), rather than develop an explicit relationship in terms of the energy sink terms, γ_s or $\gamma_s + \gamma_p$. Denoting $\delta U/\delta a$ as G , Irwin showed that

$$\sigma_a = \sqrt{\frac{EG}{\pi a}}, \quad (2.16)$$

which is one of the most important relationships in the literature of fracture mechanics. By comparison of Eqs. 2.12 and 2.16, it is seen that

$$G = 2(\gamma_s + \gamma_p). \quad (2.17)$$

At the point of instability, the elastic energy release rate G (also referred to as the crack driving force) reaches a critical value G_c whereupon fracture occurs. This critical elastic energy rate may be interpreted as a material parameter and can be measured in the laboratory with sharply notched test specimens.

Measurement of G_c requires further development of a number of equations. Theory suggests that if the crack extends by an amount da , the necessary additional surface energy is obtained from the work done by the external load. For a plate of unit thickness the condition for crack growth becomes

$$\frac{d}{da}(U - F + W) = 0 \text{ or } \frac{d}{da}(F - U) = \frac{dW}{da}, \quad (2.18)$$

where U is the elastic energy contained in the plate, F is the work performed by the external force and W is the energy for crack formation.

For an elastically loaded body containing a crack of length a (refer to Figure 2.6a), the amount of stored elastic strain energy is given by

$$U = \frac{1}{2} Pu = \frac{1}{2} \frac{P^2}{k}, \quad (2.19)$$

where U is the stored strain energy of the body, P is the applied load, u is the load displacement, and $k = P/u$ is the body stiffness for crack length a .

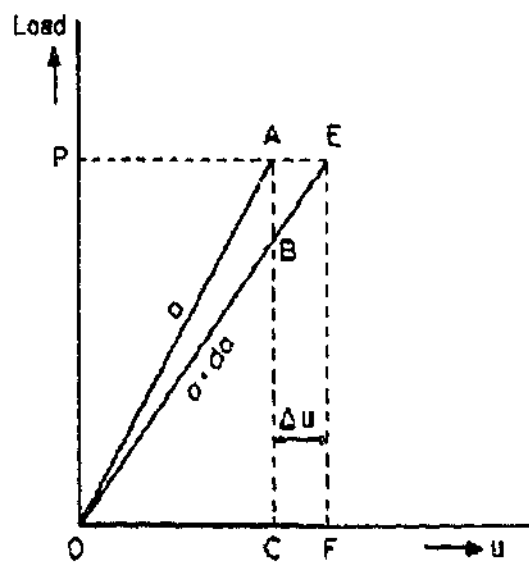


Figure 2.6a: Stored elastic strain energy [Broek 1986]

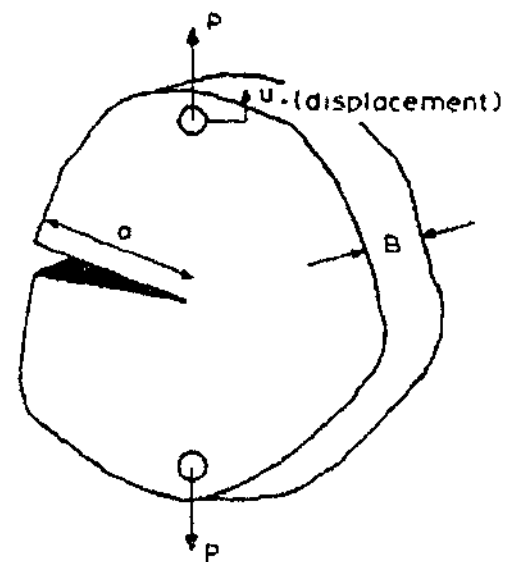


Figure 2.6b: Load and displacement for a cracked plate [Broek 1986]

Alternatively, consider a cracked plate of thickness B under a load P , as shown by Figure 2.6b. Under the action of the load, the load-application points undergo a relative displacement u . When the crack increases in size by an amount da the displacement will increase by an amount du . Hence, the work done by the external force is Pdu . As a result, it follows that:

$$G = \frac{dW}{da} = \frac{d}{da}(F - U) = \frac{1}{B} \left(P \frac{du}{da} - \frac{dU}{da} \right), \quad (2.20a)$$

where B is the thickness of the plate.

Assuming all the deformations are elastic and there is no crack growth, the displacement u is proportional to load. Therefore $u = CP$ where C is the compliance of the plate. For an uncracked plate of length L , width W and thickness B , the compliance is given by

$$C = L/(WBE), \quad (2.20b)$$

where E is the Young's modulus of the plate material.

By using Eq. 2.20b an evaluation can be made of Eq. 2.20a which yields

$$G = \frac{1}{B} \left(P^2 \frac{\partial C}{\partial a} + CP \frac{dP}{da} - \frac{1}{2} P^2 \frac{\partial C}{\partial a} - CP \frac{dP}{da} \right) = \frac{P^2}{2B} \frac{\partial C}{\partial a}, \quad (2.21)$$

The terms with dP/da cancel which means that G is independent of whether the load is constant or not. Therefore

$$G = \frac{P^2}{2B} \frac{\partial C}{\partial a} = \frac{1}{B} \left(\frac{dU}{da} \right)_P = - \frac{1}{B} \left(\frac{dU}{da} \right)_u, \quad (2.22)$$

G is always proportional to the derivative of the elastic energy (apart from the difference in sign: at constant load U increases or at fixed displacement U decreases).

The fracture of flawed components may also be analysed by a stress analysis based on concepts of elastic theory. Irwin (1957, 1958), modifying the results by Westergaard (1939), published solutions for crack tip stress distributions associated with three major modes of loading (refer to Figure 2.7). Mode I loading is encountered in the overwhelming majority of actual engineering situations involving the fracture process.

Consider a plane stressed solid (refer to Figure 2.8) with the co-ordinate system X and Y . The equilibrium conditions are

$$\begin{aligned}\frac{\partial \sigma_x}{\partial x} + \frac{\partial \tau_{xy}}{\partial y} &= 0 \\ \frac{\partial \sigma_y}{\partial y} + \frac{\partial \tau_{xy}}{\partial x} &= 0 \\ \left(\frac{\partial^2}{\partial x^2} + \frac{\partial^2}{\partial y^2} \right) (\sigma_x + \sigma_y) &= 0\end{aligned}\quad (2.23)$$

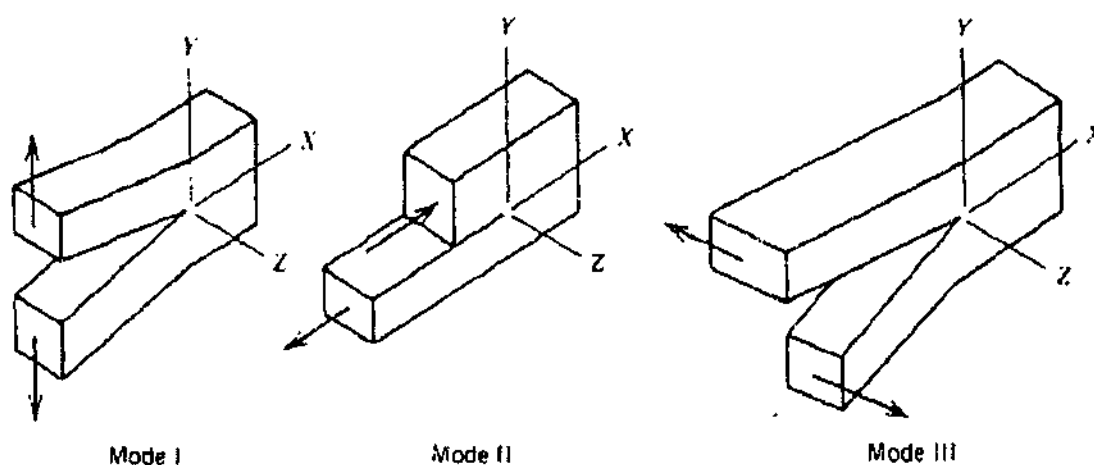


Figure 2.7: Three major modes of loading [Hertzberg 1983].

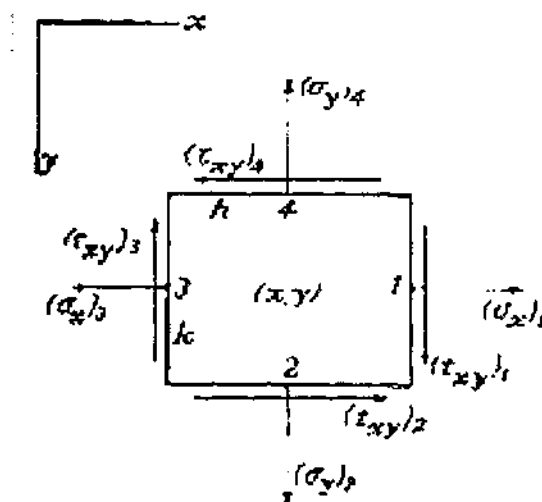


Figure 2.8: Plane stress element [Timoshenko and Goodier 1970].

If the displacements in x and y direction are u and v respectively, the expressions for the strains are

$$\begin{aligned}\varepsilon_x &= \frac{\partial u}{\partial x}, \\ \varepsilon_y &= \frac{\partial v}{\partial y}, \\ \gamma_{xy} &= \frac{\partial u}{\partial y} + \frac{\partial v}{\partial x}.\end{aligned}\tag{2.24}$$

The equilibrium equations [Timoshenko and Goodier 1970] are automatically satisfied if

$$\begin{aligned}\sigma_x &= \frac{\partial^2 \psi}{\partial y^2}, \\ \sigma_y &= \frac{\partial^2 \psi}{\partial x^2}, \\ \tau_{xy} &= -\frac{\partial^2 \psi}{\partial x \partial y}, \\ \frac{\partial^4 \psi}{\partial x^4} + 2 \frac{\partial^4 \psi}{\partial x^2 \partial y^2} + \frac{\partial^4 \psi}{\partial y^4} &= 0 \text{ or } \nabla^2(\nabla^2 \psi) = 0,\end{aligned}\tag{2.25}$$

where ψ is Airy's stress function.

Westergaard proposed stress functions for the crack tip in mode I cracking

$$\psi = \operatorname{Re} \overline{f(z)} + y \operatorname{Im} \overline{f(z)}\tag{2.26}$$

where

$$\begin{aligned}\frac{d \overline{f(z)}}{dz} &= \overline{f'(z)}, \\ \frac{d \overline{f(z)}}{dz} &= f(z), \\ \frac{df(z)}{dz} &= f'(z).\end{aligned}$$

The complex function $f(z)$, to be analytical, must satisfy the Cauchy-Riemann [Kreyszig 1988] conditions of

$$\begin{aligned}\frac{\partial \operatorname{Re} f(z)}{\partial \bar{z}} &= \frac{\partial \operatorname{Im} f(z)}{\partial z} = \operatorname{Re} \frac{\partial f(z)}{\partial z}, \\ \frac{\partial \operatorname{Im} f(z)}{\partial \bar{z}} &= -\frac{\partial \operatorname{Re} f(z)}{\partial z} = \operatorname{Im} \frac{\partial f(z)}{\partial z}.\end{aligned}\quad (2.27)$$

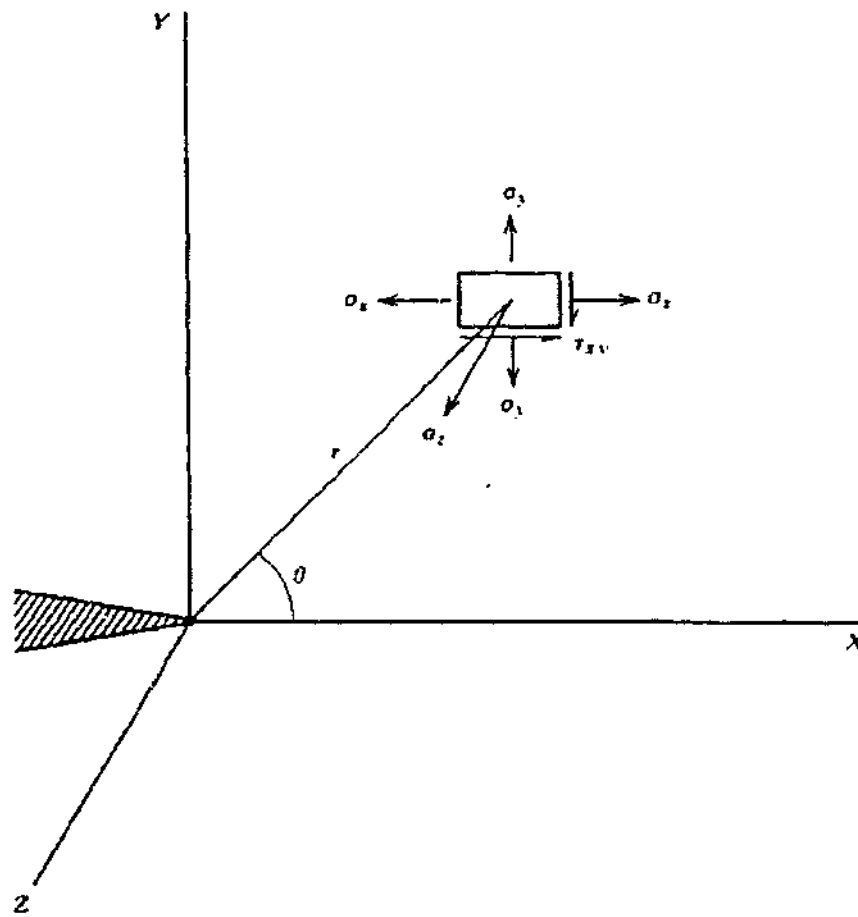


Figure 2.9: Stresses near the crack tip [Broek 1986].

It follows that by applying the Cauchy-Riemann equations to the Westergaard function, the following is obtained

$$\nabla^2 \operatorname{Re} f(z) = \nabla^2 \operatorname{Im} f(z) = 0. \quad (2.28)$$

which satisfies the Airy's stress equilibrium condition. Therefore, using Eq. 2.26, the stresses will be

$$\begin{aligned} \sigma_x &= \operatorname{Re} f(z) - y \operatorname{Im} f(z)' \\ \sigma_y &= \operatorname{Re} f(z) + y \operatorname{Im} f(z)' \\ \tau_{xy} &= -y \operatorname{Re} f(z)' \end{aligned} \quad (2.29)$$

A function $f(z)$ which satisfies the boundary conditions under consideration will hence give a complete description of the stresses in that solid. For a general crack tip (refer to Figure 2.9), the function $f(z)$ is assumed to be

$$f(z) = \frac{A}{\sqrt{z}} \quad (2.30)$$

where A is real constant.

Taking the limiting case

$$f(z)_{z \rightarrow 0} = \frac{K_I}{\sqrt{2\pi z}}, \quad (2.31)$$

and substituting $z = re^{i\theta}$, the stresses around the crack tip are:

$$\begin{aligned} \sigma_x &= \frac{K_I}{\sqrt{2\pi r}} \cos \frac{\theta}{2} \left(1 - \sin \frac{\theta}{3} \sin \frac{\theta}{3} \right) - \sigma, \\ \sigma_y &= \frac{K_I}{\sqrt{2\pi r}} \cos \frac{\theta}{2} \left(1 + \sin \frac{\theta}{3} \sin \frac{3\theta}{2} \right), \\ \tau_{xy} &= \frac{K_I}{\sqrt{2\pi r}} \sin \frac{\theta}{2} \cos \frac{\theta}{3} \cos \frac{3\theta}{2}. \end{aligned} \quad (2.32)$$

The parameter K_I in the equations is known as the stress intensity factor for mode I cracking and is a measure of the stress singularity at the crack tip. In order to give proper dimension to the stresses, K_I must have dimensions of σ by the square root of length. For the case of the

crack loaded in uniaxial tension and elastic, σ must be the remote applied stress σ_a , and the characteristic length is the crack length a . Hence K_I must take the form of:

$$K_I = Y\sigma\sqrt{a\pi} \quad (2.33)$$

where Y is a geometric constant. Eq. 2.33 can thus be related back to Eq. 2.16.

2.2.2 Elastic/Plastic Fracture Mechanics (J-Integral)

When materials fail at stresses appreciably lower than their yield stress under plane strain conditions and the plastic size ahead of the crack tip is small compared to the crack size, LEFM can be applied. Either K_{Ic} or G_{Ic} are therefore capable of characterising the fracture process.

For situations where the structure is thin-walled such as those commonly found in injection moulded articles, the plastic zone will be larger than those of plane strain situations. However if fracture takes place at loads lower than the yield stress, LEFM still applies. Once the plastic zone is large compared to the remaining uncracked area, LEFM no longer applies.

A polymer blend may exhibit high toughness and low yield strength making characterisation

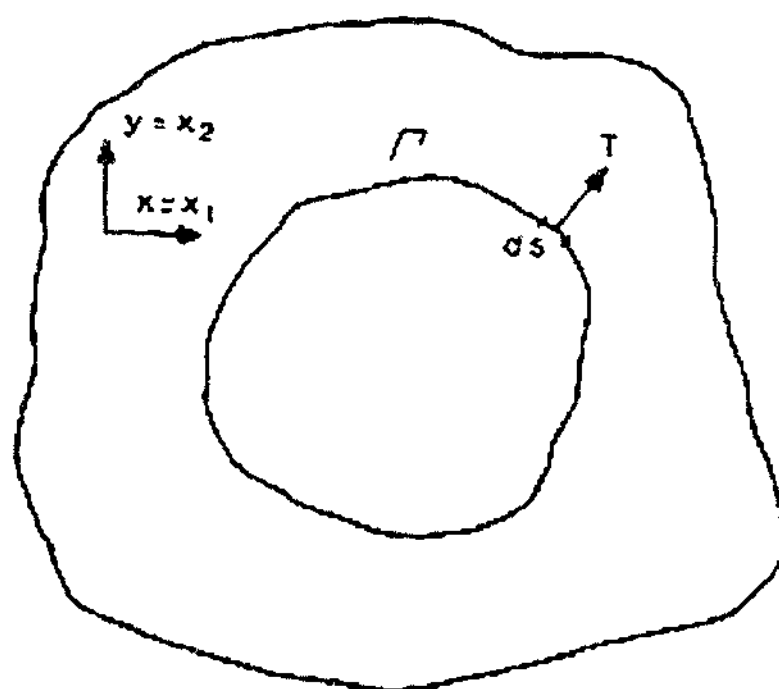


Figure 2.10: Definition of the J integral.

of its fracture parameters is difficult. The J-integral seems capable of characterising such materials, in light of its recent successes at being applied to metals [ASTM E813-89 1990; Ansafari and Andrews 1993] and polymers [Crist et al. 1991; Kim et al. 1990a; Frontini et al. 1992] and some polymer blends [Herpels and Mascia 1990; Huang 1991].

Advancement of fracture mechanics to cater for materials which are tough occurred in the 1960's. The J-integral provided a means of determining an energy release rate for cases where plasticity effects were not negligible. Eshelby (1974) had defined a number of contour integrals which were path independent by virtue of the theorem of energy conservation [Knowles and Sternberg 1972]. The two-dimensional form of these integrals can be written as

$$J = \int \left(W dy - T \frac{\partial u}{\partial x} ds \right), \quad (2.34)$$

$$\text{where } W = W(x, y) = W(\varepsilon) = \int_0^\varepsilon \sigma_y d\varepsilon_y. \quad (2.35)$$

Consider a situation where Γ is a closed contour followed counter clockwise, as shown by Figure 2.10, in a stressed solid. T is the tension vector (traction) perpendicular to Γ in the outside direction, where $T_i = \sigma_{ij} n_j$, n_j is the unit vector perpendicular to σ_j , u is the displacement in the x-direction and ds is an element of Γ . It can be shown that $J = 0$ along any closed contour.

Rice (1968) applied this integral to crack problems. Consider the closed contour ABCDEF around the crack tip in Figure 2.11a. The integral is zero around this contour. Since $T = 0$ and $dy = 0$ along the parts CD and AF, the contribution of these parts to the integral is zero. Therefore the contribution of ABC must be equal, but opposite in sign, to the contribution of DEF. This means that the integral, if taken only along Γ_1 or Γ_2 will have the same value, i.e. $J_{\Gamma_1} = J_{\Gamma_2}$ in Figure 2.11b. Hence the integral is path-independent.

The J-integral is an energy related quantity since the two terms in the integrand, namely W and Tdu/dx , both have dimensions of $\sigma\epsilon$, which is strain energy. Previously Rice (1967) and Drucker (1962) showed that the J-integral as defined along the contour around the crack tip in Figure 2.11b is the change in potential energy for a virtual crack extension da :

$$J = -\frac{\partial V}{\partial a}, \quad (2.36)$$

where V is the potential energy.

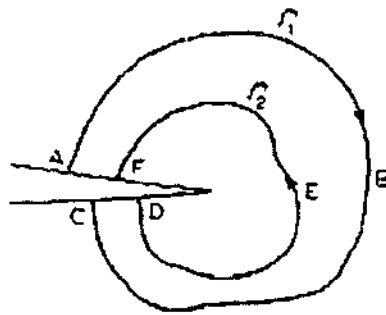


Figure 2.11a: Application of closed contours to crack problems [Broek 1986].

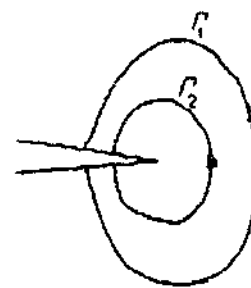


Figure 2.11b: Change in potential energy [Broek 1986].

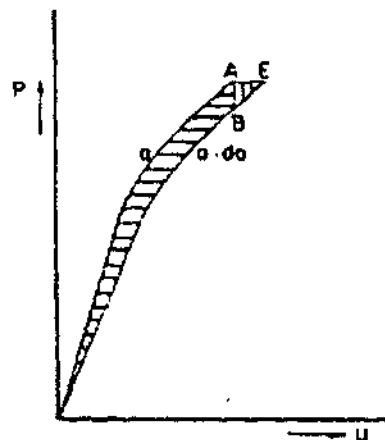


Figure 2.11c: Graphical interpretation of the J-integral [Broek 1986].

For a linear elastic material $-\delta V/\delta a = G$ which means that

$$J = G, \quad (2.37a)$$

for the linear elastic case. By analogy with the elastic case

$$J = \left(\frac{\partial V}{\partial a} \right)_p = - \left(\frac{\partial V}{\partial u} \right)_u, \quad (2.37b)$$

so that, again, the same results are obtained regardless of the end conditions (i.e. fixed displacement, u or constant load, P). However, in the linear elastic case, one can immediately write

$$- \left(\frac{\partial V}{\partial u} \right)_p = \frac{1}{2} P \frac{\partial u}{\partial a} \quad (2.38)$$

and

$$- \left(\frac{\partial V}{\partial a} \right)_u = \frac{1}{2} u \frac{\partial P}{\partial a}, \quad (2.39)$$

whereas in the non-linear elastic case, these equations become:

$$J = \left(\frac{\partial V}{\partial a} \right)_p = \int_0^P \left(\frac{\partial u}{\partial a} \right)_p dP, \quad (2.40)$$

and

$$J = - \left(\frac{\partial V}{\partial u} \right)_u = \int_0^u \left(\frac{\partial P}{\partial a} \right)_u du. \quad (2.41)$$

The graphical interpretation to Eqs. 2.40 and 2.41 is shown by Figure 2.11c. Figure 2.11c shows that the material unloads along the same curve as that along which it was loaded, showing non-linear but elastic stress strain behaviour. It also shows there is negligible difference between the energy release rate for the constant load and constant displacement case. As a result, determination of the crack tip strain energy using the J-integral is valid as long as no unloading occurs because permanent deformation is not accounted for. This implies the J-integral can be used as a fracture criterion for cases where crack tip plasticity is not negligible because many problems in plasticity can be solved by treating the material as

non-linear elastic through the deformation theory of plasticity or by the incremental theory of plasticity.

In the linear elastic case J is equal to G and therefore also J is equal to K^2/E . One can postulate that crack growth or fracture occurs if J exceeds a critical value J_{Ic} , which is analogous to G_{Ic} , and equal to G_{Ic} if the material is essentially linear elastic.

There is obviously a strong analogy between the two parameters G and J . Since G in essence is also a measure for the crack tip stress field through $K^2 = EG$, it must be expected that J is also a stress field parameter. This is clearly the case for a linear elastic material where $J = G$, but it remains true for a non-linear elastic material as well.

Consider a non-linear elastic material for which the stress-strain curve can be represented by the Ramberg-Osgood equation

$$\frac{\varepsilon}{\varepsilon_o} = \frac{\sigma}{\sigma_o} + \alpha \left(\frac{\sigma}{\sigma_o} \right)^n, \quad (2.42)$$

where ε_o is the strain at flow, σ_o is the stress at flow, n is the strain hardening exponent and α is a constant.

For small strains exceeding the elastic limit, the equation above can be rewritten as

$$\frac{\varepsilon}{\varepsilon_o} = \alpha \left(\frac{\sigma}{\sigma_o} \right)^n. \quad (2.43)$$

The J-integral is defined as

$$J = \int \left(W dy - T \frac{\partial t}{\partial x} ds \right),$$

where Γ is an arbitrary contour around the crack tip (beginning and ending at the opposite crack face). Taking a circular contour of radius r from the crack tip, the J-integral will be

$$J = \int_{-\pi}^{\pi} \left(W \cos \theta - T \frac{\partial u}{\partial x} \right) r d\theta, \quad (2.44)$$

where θ is the polar angle, and W , T , and $\partial u / \partial x$ depend upon r and θ .

The expression for W is

$$W = \int_0^{\epsilon} \sigma_{ij} d\epsilon_{ij},$$

so that W has the dimensions of $\sigma_{ij}\epsilon_{ij}$. The traction T has dimensions of stress and du/dx is dimensionless. Therefore T also has dimensions of $\sigma_{ij}\epsilon_{ij}$. The terms in parenthesis from Eq. 2.44 after integration is proportional to $\sigma_{ij}\epsilon_{ij}$:

$$J = f n (\sigma_{ij}\epsilon_{ij}) r. \quad (2.45)$$

Making use of the stress-strain relation of Eq. 2.43, it follows that

$$\epsilon(r) = \frac{C_1}{r^{n/(n+1)}} \text{ and } \sigma(r) = \frac{C_2}{r^{1/(n+1)}}. \quad (2.46)$$

For the case of a linear elastic material (i.e. $n = 1$), the above equations become

$$\epsilon(r) = \frac{C_1}{\sqrt{r}} \text{ and } \sigma(r) = \frac{C_2}{\sqrt{r}}, \quad (2.47)$$

which are in accordance with equations found previously.

The constants C_1 and C_2 can be expanded and Hutchinson (1968) derived the crack tip stress and strain fields to be

$$\begin{aligned} \sigma_{ij} &= \sigma_o \left(\frac{J}{\alpha \sigma_o \epsilon_o I_n r} \right)^{1/(n+1)} f_{ij}(\theta) \\ \epsilon_{ij} &= \alpha \sigma_o \left(\frac{J}{\alpha \sigma_o \epsilon_o I_n r} \right)^{n/(n+1)} g_{ij}(\theta) \end{aligned} \quad (2.48)$$

where I_n is a constant depending on the stress-strain relationship.

These equations highlight that J can be a stress field parameter likened to K even though Eqs. 2.48 are related to the material behaviour more closely by the exponent n in the equations.

2.2.3 Essential Work of Fracture

Broberg (1968, 1975) suggested that the non-elastic region at the crack tip should be divided into two parts. There should be an end region, where the fracture process takes place, and an outer region where screening plastic deformation takes place in order to accommodate the large strains in the end region.

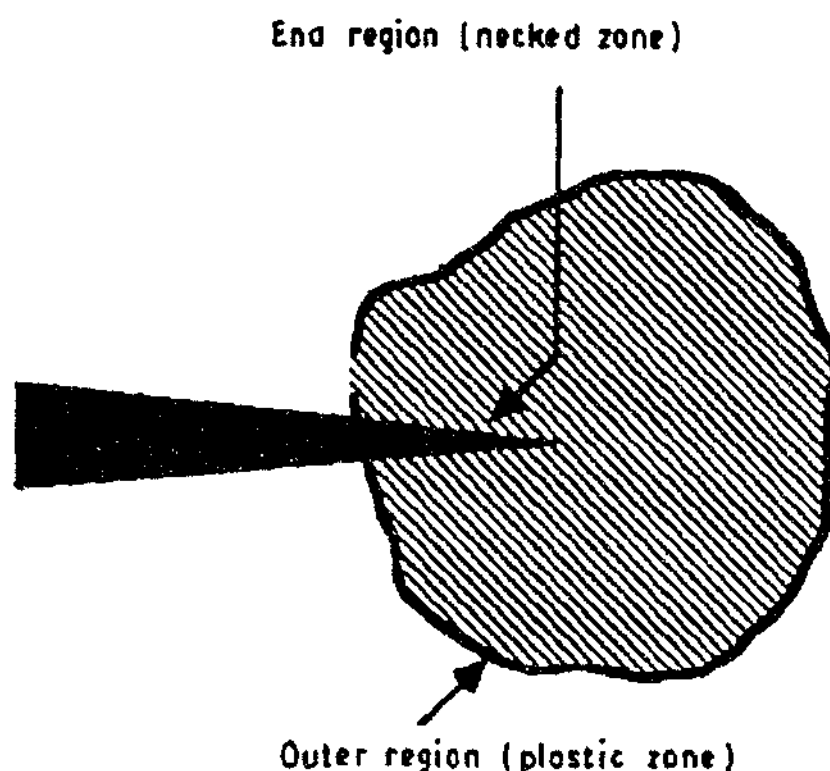


Figure 2.12: Broberg's interpretation of the fracture process in polymers [Hashemi and O'Brien 1993].

The essential work method divides the input energy into two parts, namely the essential work and the non-essential work:

$$W_f = W_e + W_p \quad (2.49)$$

where W_f is the energy to fracture, W_e is the essential work of fracture and W_p is the non-essential work of fracture.

W_e accounts for the necking and fracture of the material in the fracture process zone. W_p accounts for the plastic deformation in the outer plastic zone, which for metals will involve shear and for polymers can involve micro voiding, crazing, cavitation, crack bridging, and shear yielding.

When the plastic zone reaches the edge of the material, it can be assumed the plastic zone area is proportional to the ligament length (width minus crack length) squared (Cotterell and Reddel 1977; Chan and Williams 1994). The essential work of fracture is only proportional to the ligament length. Therefore Eq. 2.49 can be rewritten as.

$$W_f = w_e LB + w_p \beta L^2 B, \quad (2.50)$$

where

B is thickness of the specimen,
 L is the ligament length,
 w_e is the specific essential work of fracture,
 w_p is the specific non-essential work of fracture and
 β is the shape factor.

Eq. 2.50 can be rewritten as

$$w_f = w_e + w_p \beta L, \quad (2.51)$$

where $w_f = W_f/LB$ and is the specific work to fracture.

If a set of specimens with varying ligament lengths is tested and W_f found, then divided by LB and plotted against L , a linear relationship should result. If L is extrapolated back to zero, then w_e can be found which is assumed to be a material constant, as shown by Eq. 2.51.

Two restrictions are applicable to the essential work of fracture. Firstly the maximum ligament length used for extrapolation must be less than one third of the specimen width or the plastic zone size, whichever is the lower:

$$L < \min\left(\frac{W}{3}, 2r_p\right), \quad (2.52)$$

where W is the specimen width and $2r_p$ is the plastic zone size.

This condition ensures complete yielding of the ligament before crack propagation and the plastic deformation is restricted to the ligament area, away from the lateral boundary of the specimen. The second restriction is that the ligament length should be three to five times the specimen thickness, to ensure it is not in the plane stress-plane strain transition region where the theory breaks down.

The disadvantage with the essential work of fracture method to date is its lack of application to predicting failure in engineering structures. It remains at present (to the author's knowledge) a characterisation tool for measuring and comparing the fracture toughness of materials, but is most used to predict failure loads for given geometries or designs.

Although the J-integral and the essential work (w_e) method approach the elastic-plastic fracture problem differently, it has been shown that the two resulting critical fracture parameters are compatible. Since the J-integral is an established method for testing the fracture toughness of ductile materials, the w_e method can also be used to characterise the fracture toughness of ductile materials. The w_e method has been successfully applied to thin sheets of metals [Mai and Cotterell 1985; Knuk and Read 1986] and polymers [Mai and Cotterell 1986; Hashemi 1993; Wu et al. 1993].

It may be worthwhile at this stage to compare some fracture toughness values, previously found by other workers, as measured by LEFM, J-Integral and w_e method (shown in Table 2.1). The values are for materials used in this thesis and by no means comprehensive. They should simply be viewed as being a guide to the toughness of each material.

Ashby and Jones (1986) gave a range of G_{Ic} values between 0.1 and 10 kJ/m² for general engineering polymers. The toughness values found by other workers fall into this expected range except for the ABS/PC blend which did not fall between 0.1 and 10 kJ/m². Materials

will tend to have a spread of toughness values due to the method of testing, geometry of specimens and variations in the same grade of material (due to processing conditions, amount of rubber in the matrix etc.). ABS shows this variability in Table 2.1 and PET and PC show this in fracture experiments in Chapter 6.1.

PS seems to be the most brittle material and ABS/PC the toughest, given the G_{Ic} values in Table 2.1. The essential work of fracture approach gave toughness values which were higher than the range given by Ashby and Jones and in the case of PC, higher than LEFM or the J-Integral methodology.

Table 2.1: Fracture toughness values as measured by different methods.

Material	G_{Ic} (kJ/m ²)	J_{Ic} (kJ/m ²)	w_e (kJ/m ²)
PS	1.2 [#] [Ashby and Jones 1986]	1.4 [Yee 1990]	1.1 [%] [Mai and Cotterell 1986]
PC	2.5 [Kim et al. 1990b]	2.5 [Kim et al. 1990b]	19-28 [Hashemi 1997]
ABS	1.6-4.1* [Paul et al. 1991]	3.6-8.1 [Bernal and Frontini 1992]	12.5-13 [Ching et al. 2000]
PET	5.9 ^{\$}	—	36-68 [Hashemi 1997]
ABS/PET	6.7 ^{\$}	—	—
ABS/PC	18.9 [Herpels and Mascia 1990]	23.2 [Herpels and Mascia 1990]	3.7 [Santana et al. 1997]

* Assuming E is equal 1800 MPa

[#] Assuming E is equal to 3165 MPa

[%] Measured on High Impact Polystyrene

^{\$} As measured in this thesis

2.2.4 Observations of Deformation in Ductile Polymers

Toughness of polymers can also be explained by the energy absorbing mechanisms which impede crack advancement - particle deformation/cavitation, shear yielding and crazing. Figures 2.13 to 2.15 [Kinloch and Young 1983; Argon and Cohen 1994] show these mechanisms schematically. Takemori (1990), and Bucknall (1977) provide overviews on these toughening mechanisms.

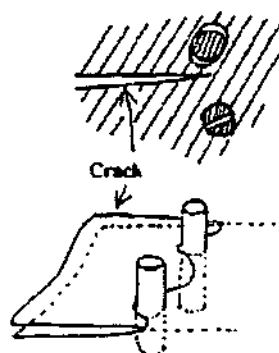


Figure 2.13: Particle cavitation.

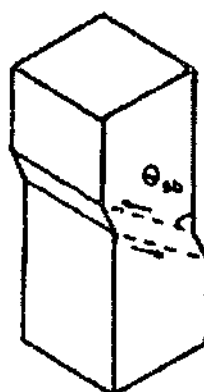


Figure 2.14: Shear yielding.



Figure 2.15: Crazing.

Microscopy of deformed regions in tough polymers provides a qualitative approach to the understanding of fracture in polymers. The enhanced toughness of rubber modified materials such as high impact polystyrene (HIPS) and acrylonitrile butadiene styrene (ABS) is due to their ability to provide a much greater volume of polymer to be involved in the energy absorbing process. Incorporating a second phase of rubbery particles initiates localised energy absorbing mechanisms from many sources rather than a few isolated ones around the crack tip. ABS utilises the three methods of toughening described in Figures 2.13 to 2.15.

The first method is particle deformation/cavitation. Essentially, the rubber particles are considered to bridge the crack as it propagates through the material or cavitate due to the triaxial stresses set up in front of a notch (shown by Figure 2.16). The increase in toughness of the multiphase polymer may be identified with the amount of elastic energy stored in the rubber particles during stretching which is then dissipated irreversibly when the particles rupture. This model was developed by Kunz-Douglass (1980) and Kunz (1981), but the model could not explain the stress whitening observed in most rubber-toughened plastics.

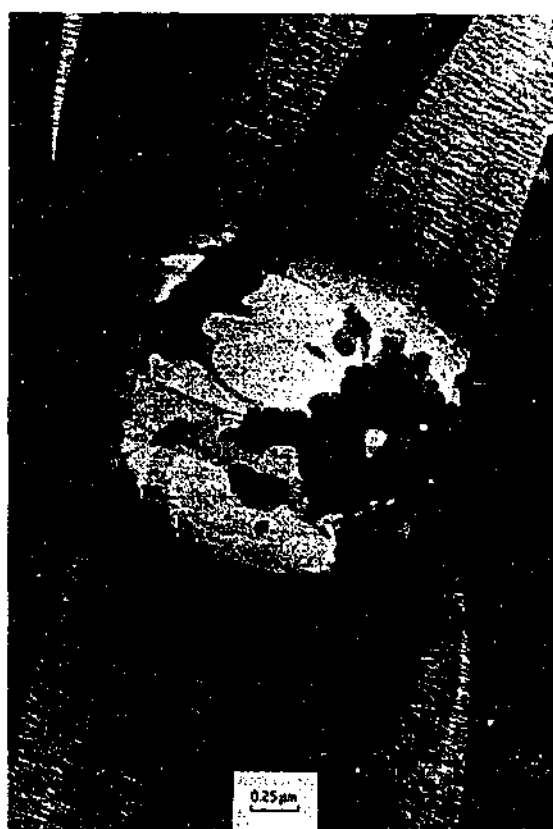


Figure 2.16: Internal voiding of a rubber particle in ABS - stained with OsO_4 [Donald and Kramer 1992].

Thus whilst ligaments of rubber spanning a crack must reduce the stress concentration at the crack tip and their fracture involves only some energy dissipation, it appears that this mechanism is usually only of secondary importance in increasing the toughness of such multiphase polymers. It is principally the deformation of the matrix, enhanced by the presence of the second phase, which improves the toughness.

The second method of toughening is by shear yielding of the matrix. Extensive shear yielding accompanying the fracture process is a major mechanism in many tough single phase polymers and this mechanism may be greatly enhanced in many otherwise brittle polymers by the second rubbery particulate phase. Optical microscopy studies on ABS materials revealed that the material, in a uniaxial tensile test, had undergone localised plastic deformation around virtually every rubber particle (shown by Figure 2.17).

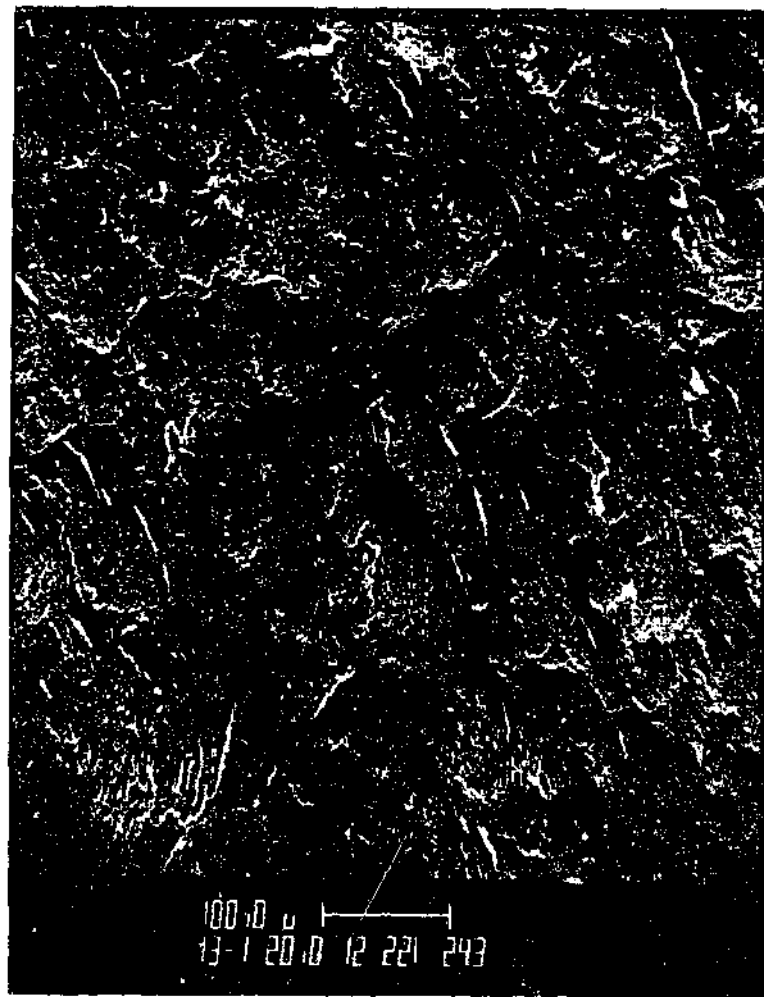


Figure 1.17: SEM scan showing shear bands in the free surface of a drawn ABS sample [Chen and Sauer 1990].

The third method of toughening is by crazing. The function of the rubbery particles is to initiate multiple craze growth in the material matrix. Bucknall and co-workers (1976) suggested that under an applied tensile stress, crazes are initiated at points of maximum triaxial stress concentrations, which are usually near the equators of the rubber particles. The rubber particles are also craze terminators (refer to Figure 2.18), preventing the growth of very large crazes which could act as sites for premature crack initiation and growth. Therefore the rubber particles induce a large number of small crazes to be generated instead of the formation of large crazes in a matrix without the rubber particles.

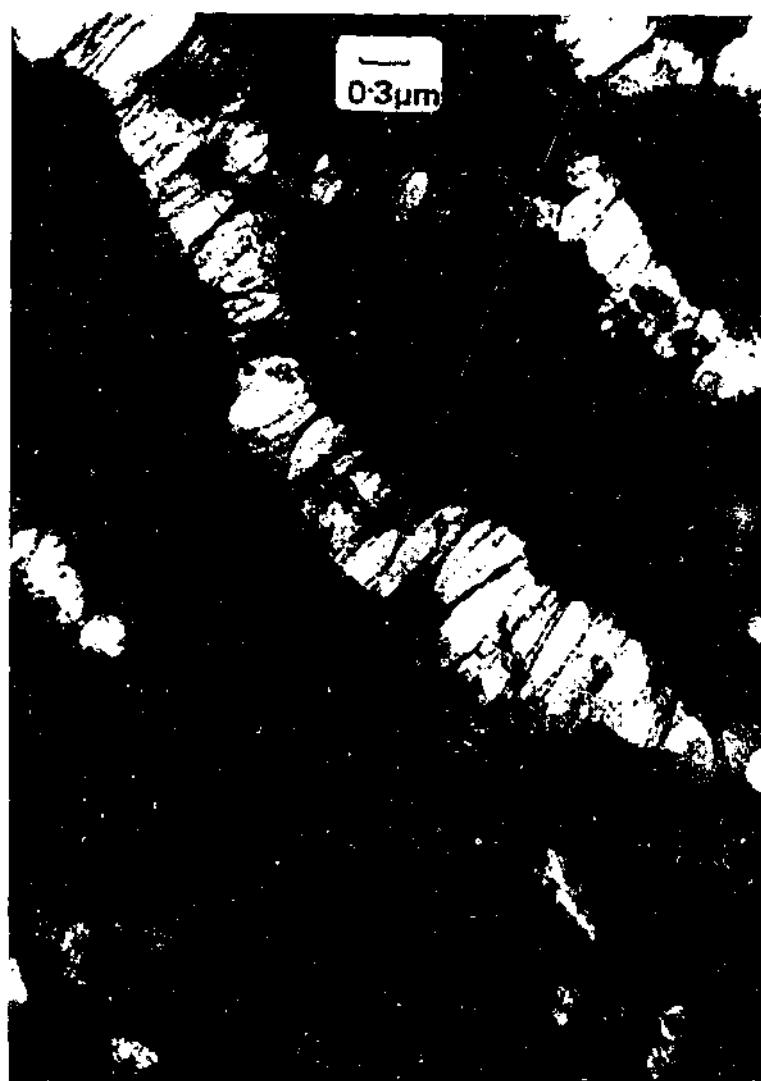


Figure 2.18: Crazing in ABS [Donald and Kramer 1982].

Kinloch and Young have shown (Figure 2.19) that all three modes of toughening can occur during loading. In many toughened polymers such as ABS and rubber-toughened PVC, the mechanisms of cavitation, shear yielding and crazing may be observed. As a general rule the mechanism which is dominant in the toughened polymer will simply reflect the main mechanism which is operative in the matrix when it is modified. Thus, in HIPS, crazing is usually the dominant mechanism whilst shear yielding is generally the major mechanism in rubber-toughened PVC and epoxy resins. However, microstructural features of the toughened polymer, such as particle size, will affect which mechanism will be preferred, as will the strain rate and temperature of the test.



Figure 2.19: TEM of a replica of a 50/50 blend of HIPS and poly(2, 6-di methyl-1, 4-phenylene oxide). Arrow indicates direction of applied stress [Kinloch and Young 1983].

The simultaneous initiation of shear bands and crazes is shown in Figure 2.19. The shear bands are formed approximately along planes of maximum resolved shear stress and therefore intersect crazes at an angle of about 45 degrees. These observations led Bucknall and co-workers (1976) to suggest that in addition to increasing the energy absorption, shear bands act as effective craze terminators for growing crazes. Hence, in those polymers where shear banding occurs in addition to crazing, the necessity for relatively large rubber particles to function as craze terminators is removed.

The nature of crack propagation in other engineering polymers has also been investigated. Beahan et al. (1975) studied the fracture process of an amorphous single phase glassy

polymer - polystyrene. They showed that the material precrazes before the crack advances. The crack path can be broken up into regions (Figure 2.20). In the initiation and intermediate region, fracture progresses through the precrazed matter in one of several ways. Initially, the crack grows by the nucleation and growth of conically shaped voids along the mid-plane of the craze (refer to Figure 2.21). As the crack velocity increases, the crack tends to grow alternately along one craze-matrix boundary interface and then the other. Consequently, the fracture surface contains islands or patches of craze matter attached to one-half of the fracture surface (Figure 2.22 and 2.23) which mate with detachment zones on the mating surface.

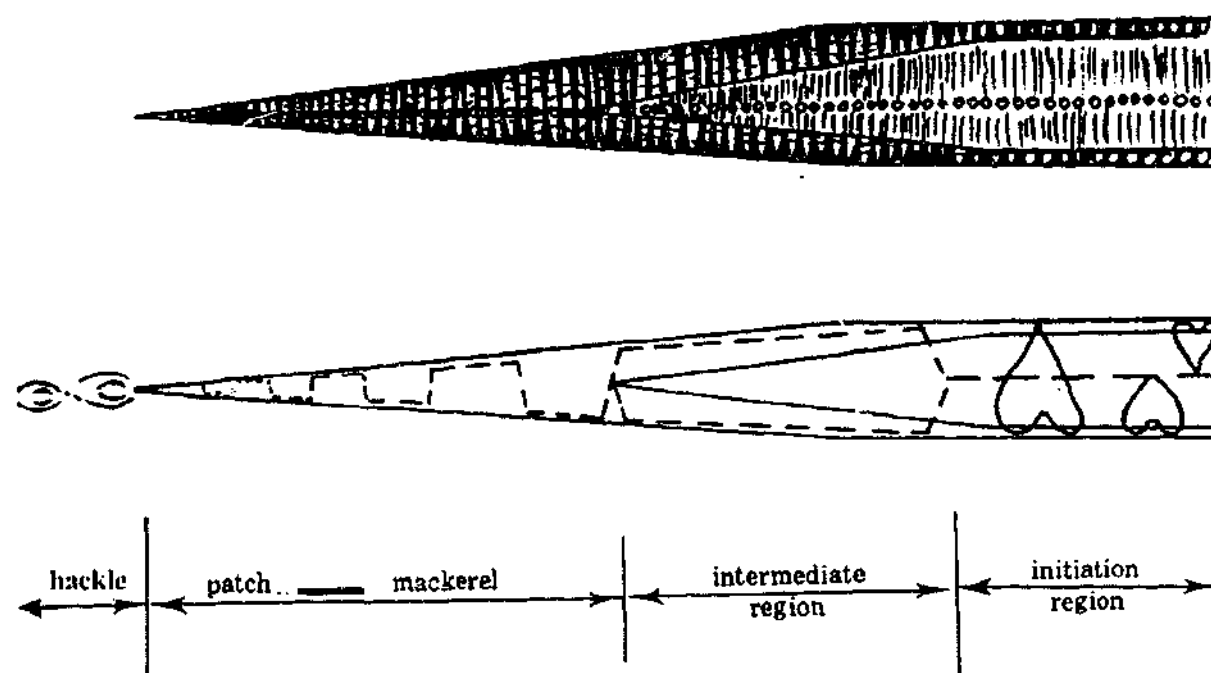


Figure 2.20: Schematic of fast fracture [Beahan et al. 1975].

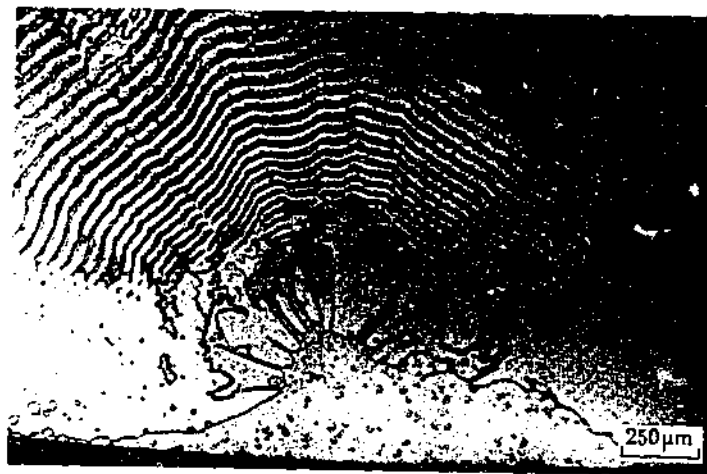


Figure 2.21: Optical micrograph of the nucleation and mackerel regions [Beahan et al. 1975].

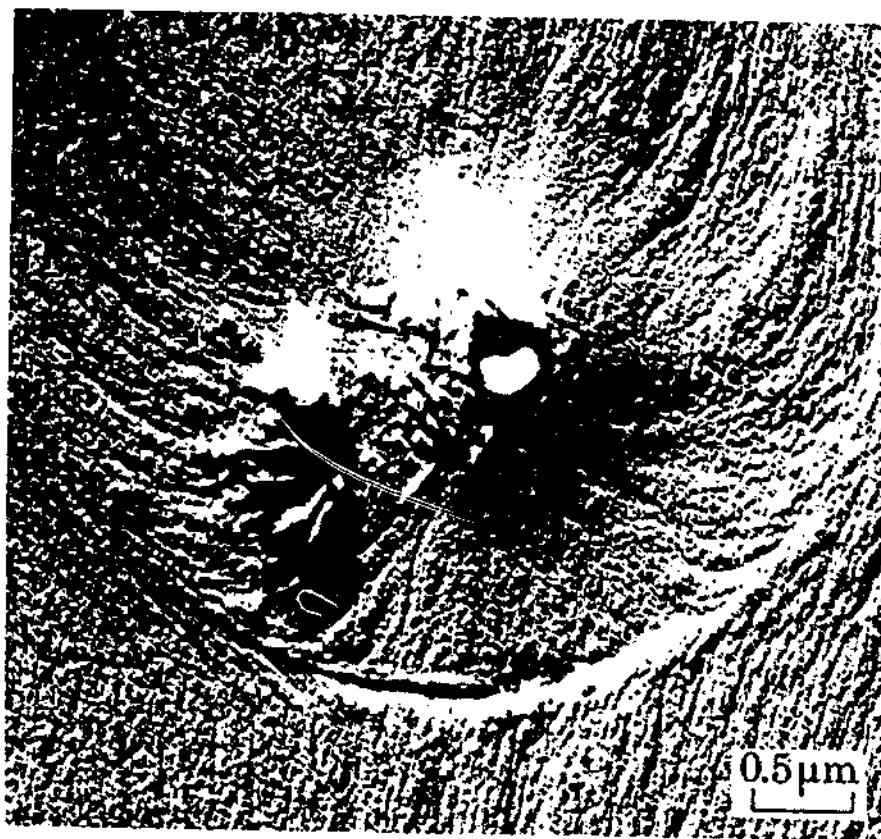


Figure 2.22: SEM image revealing conical voids along mid-plane of the craze [Beahan et al. 1975].

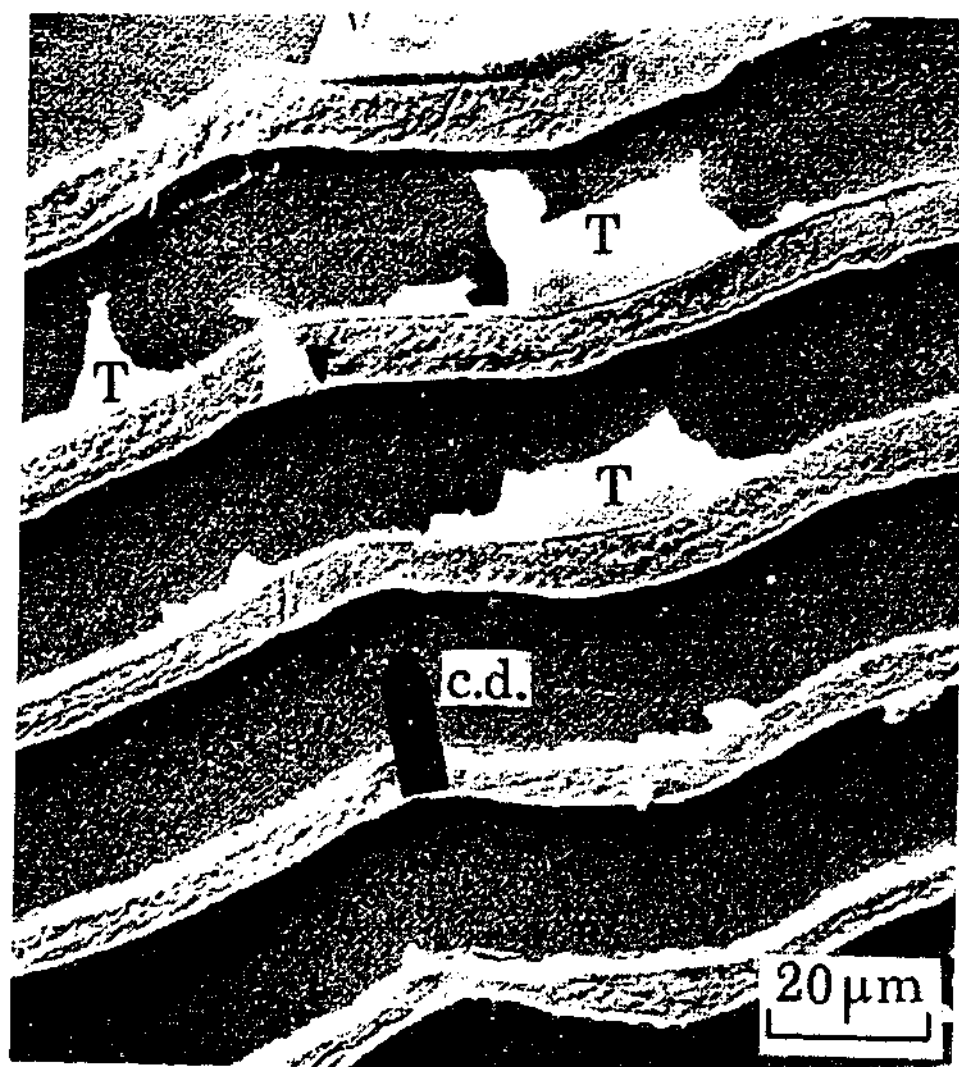


Figure 2.23: Mackerel pattern [Beahan et al. 1975].

During the terminal stage of fast fracture, the crack front outpaces the craze tip, with continued crack extension taking place through bundles of secondary crazes that form at the crack tip. The banded nature of this surface (referred to as "hackle" bands) suggests that the crack propagates through one bundle of crazes, at which point a new craze bundle is formed and the process repeated. A close examination of the hackle zone reveals the patch morphology described above. This part of the fracture surface takes on a "misty" appearance because of the rougher surface and the fact there contains bundles of crazes (refer to Figure 2.24).

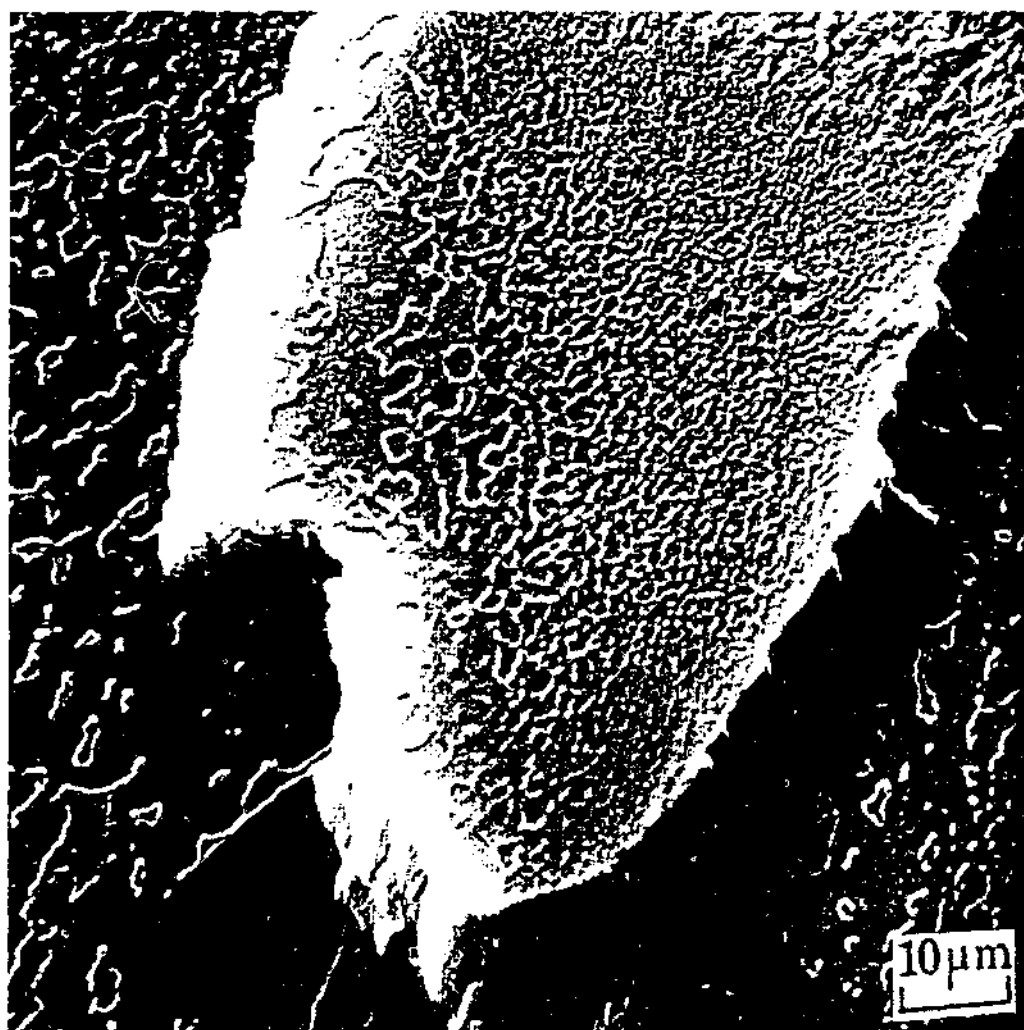


Figure 2.24: Scanning electron micrograph taken from the hackle region showing two craze levels [Beahan et al. 1975].

Curtin and Xiao (1995) have modelled this fracture process. They used a spring network to approximate the fibrils holding the crazed material together. However this model was not tried on more ductile materials.

For the tough single phase polymers used in this study (PC and PET) stress whitening and shear yielding was observed in front of the crack tip at the time of failure. Severe blunting of the crack tip in tough polymer blends has been observed by Wu and Mai (1993) as shown in Figure 2.25.



Figure 2.25: Crack tip blunted by deformation of the surrounding material [Wu and Mai 1993].

2.3 Summary

The fundamentals of fracture mechanics has been described in Chapters 2.2.1 to 2.2.2. It shows why materials fail at lower loads when compared to the bond strength as given by atomic theory. The reason is that materials are imperfect and contains flaws. Flaws in brittle materials are sharp and experiments by Griffith on soda glass has proven this.

However, for metals, these imperfections are not as sharp when compared to glass. In fact, for metallic materials, there is a yielded zone that develops in front of the crack tip. This gave rise to Irwin's idea of a plastic zone size which in turn led to corrections to Griffith's equations. Elastic-plastic fracture mechanics was researched in the 1960's in order to also model the fracture behaviour of metals and tough metal alloys. Some of the fundamental work (such as the J-Integral) has proved effective in explaining the tough nature of metals.

A new class of materials has now emerged which are tough and have low yield stresses when compared to metals. This new class of materials is polymers and polymer blends. In Chapter 2.2.4, workers have studied the behaviour of a flaw in these ductile materials. They noted a large number of toughening mechanisms at work to severely blunt any existing sharp flaw. In

the case of metals, yielding of the crack tip is the primary means of blunting whereas in polymers, cavitation, crack bridging, shear yielding and many other methods are possible.

Workers [Huang 1991; Bucknall et al. 1993; Raab 1993] have proposed models which link the microfeatures observed in crack tip deformation of some polymers to its toughness but only the essential work of fracture (EWF) idea is general enough to take into account all the possible toughening mechanisms. To achieve this, EWF essentially lumps all the mechanisms into a process zone ahead of the crack tip. The exact nature of the theory is described in Chapters 2.2.3 and will not be repeated here. Suffice to say, it has proven to be an important tool for the characterisation of toughness for polymers.

Chapter 2 has described the fundamentals of fracture for brittle to extremely tough materials. Unfortunately, the application of theory to engineering situations has not been discussed. Chapter 3 will seek to correct this and it will also develop a simple model which may be used to predict failure for polymeric materials. The premise of this new model is that polymeric materials blunt sharp imperfections or cracks to a radius of curvature ρ , and each material has its own characteristic value. Brittle materials have low values whilst tough polymers have high values.

This simple model assumes that polymers will use all available means available to it, in order to blunt the sharp flaws which exist within it. The model only describes the behaviour of polymers with cracks and the value of ρ obtained is not equal to the plastic zone size. In this regard, it is dissimilar to Broberg and Mai's EWF idea, and Irwin's plastic zone size idea for metals. Both these theories assume that the process area ahead of the crack encapsulates all the energy absorbing phenomenon to blunt the crack whereas the effective crack tip parameter is only a modelling tool and has no physical interpretation unlike the previous two parameters. As we shall see later though, the new model is an effective means of predicting failure for tough and ductile polymers.

Chapter 3

Methodologies in Predicting Failure

3.1 Elastic Analysis of Polymer Articles with Cracks

Background theory in analysing polymer sheets with cracks has been given in Chapter 2.2. Observations have also been made on the propagation of cracks in sheets of tough engineering polymers. However, the application of theory and observations, to configurations commonly found in engineering practice is most important to a failure analyst or designer.

Deutschman et al. (1975) stated that:

".....it is very necessary to understand that the mathematical model chosen and the subsequent calculations that are made merely approximate reality. One must, therefore, be fully aware of the various assumptions and limitations (for example, of linearity, homogeneity, and so on) that were made in deriving the equations used in the study of the engineering sciences...."

Therefore, it is very important to keep in mind that good design is based upon good theory while emphasising that the numbers that result from applying the theory are merely ball park figures, which give the design engineer a rational basis for substantiating her/his work...."

Therefore from the quotation above, it would be sensible to acknowledge that the methodology offered to an engineer or designer should be simple and one which will provide "ball park" working loads which are safe for all configurations.

Consider a simple engineering configuration, that of a crack emanating from a hole (refer to Figure 3.1) in a uniformly loaded plate and also treat the material to be linear elastic. Therefore what tools are available to predict the remote applied load required to cause failure for such an article made from a tough ductile polymer?

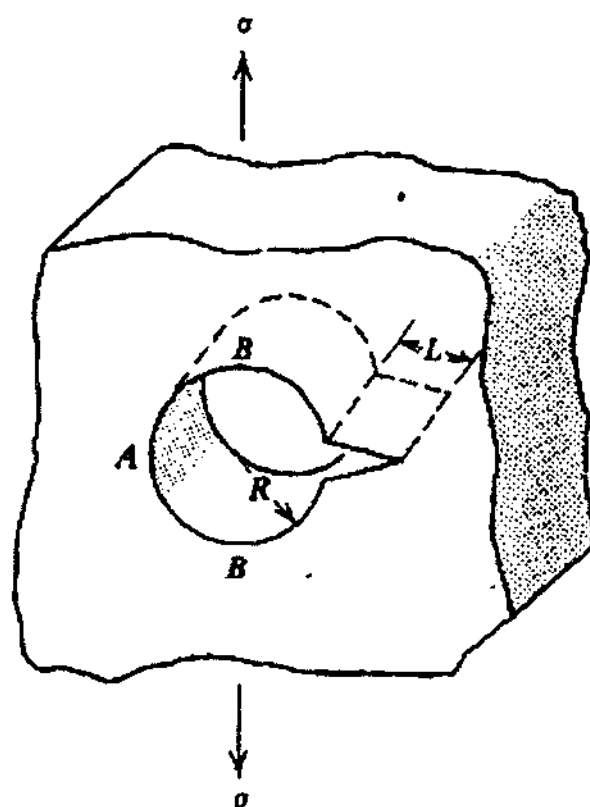


Figure 3.1: Crack emanating from a hole.
[Hertzberg 1983]

3.1.1 Yielding Methodology

The simplest method of prediction is to assume the article fails when the stress across the ligament length (i.e. the width of the specimen minus the diameter of the hole and crack) is equal to the yield stress obtained from a uniaxial tensile test. In this thesis, the term net section yielding is used to describe this mode of failure. The equation for failure would be when

$$\begin{aligned}\frac{P}{B[W - (L + 2R)]} &= \sigma_y, \\ \frac{P}{BW\left(1 - \frac{L + 2R}{W}\right)} &= \sigma_y, \\ \frac{\sigma_a}{\left(1 - \frac{L + 2R}{W}\right)} &= \sigma_y, \\ \sigma_a &= \sigma_y \left(1 - \frac{L + 2R}{W}\right).\end{aligned}\tag{3.1}$$

where σ_a is the remote applied stress, σ_y is the yield stress of the material as obtained from a uniaxial tensile test, B is the thickness and W is the width of the specimen. It is worth noting that for more complex configurations and stress states, the definition of failure by net section yielding is when the average Von-Mises stress across a section of material reaches the yield stress as defined by the Von-Mises criterion. The Von-Mises criterion was chosen over the Tresca criterion because it is a better description of the yielding phenomenon in ductile materials [Bacoffen 1972; Calladine 1969].

3.1.2 LEFM Methodology

A second methodology which one may use to predict failure for an article shown by Figure 3.1 is LEFM. Eq. 2.33 states that failure will occur when

$$K_{Ic} = Y\sigma_a\sqrt{\pi a},$$

where K_{Ic} is the fracture toughness of the material (also equal to \sqrt{EG}), a is the crack length and Y is a geometric factor which describes the stress state of the structure. For the case of a crack emanating from a round hole, the crack length is equal to L and Y is equal to 3 [Howland 1930] multiplied by 1.12 because there exists stress concentration effects from

the hole and edge effects from the finite size of the plate. If the plate was very wide, K_t would be equal to 3 (which is the stress concentration around a hole) as no edge effects would be present.

Therefore substituting the appropriate terms into Eq. 2.33, one obtains

$$K_{Ic} = (1.12)(3)\sigma_a \sqrt{\pi L}.$$

Transposing the equation, the applied stress required for failure is

$$\begin{aligned} \sigma_a &= \frac{K_{Ic}}{(1.12)(3)\sqrt{\pi L}}, \\ \sigma_a &= \frac{K_{Ic}}{(1.12)(3)(\sqrt{W})\sqrt{\pi \frac{L}{W}}}. \end{aligned} \quad (3.2)$$

An alternative approach is to suppose that the hole is part of the crack. This is particularly meaningful if L is much greater than R , when the crack length is assumed to be $\frac{L + 2R}{2}$.

Failure occurs when

$$\begin{aligned} K_{Ic} &= (1.12)\sigma_a(\sqrt{\pi})\sqrt{\frac{L + 2R}{2}}, \\ \sigma_a &= \frac{K_{Ic}}{(1.12)\sqrt{\pi}(\sqrt{W})\sqrt{\frac{L + 2R}{2W}}}. \end{aligned} \quad (3.3)$$

For small cracks, Eq. 3.2 is more appropriate to use, as it assumes the stress concentration has an effect upon the crack. This form of analysis is followed where the crack lengths are short relative to the dimensions of the structure. Short crack length is also the condition that is imposed on fracture specimens used in this thesis.

A plastic correction factor may be made to Eq. 3.2. Irwin proposed that the material in front of the crack tip yields to a circular shape with a radius r_p . Therefore the total crack length is $L+r_p$, and LEFM predicts failure to occur when

$$\sigma_a = \frac{K_{Ic}}{(1.12)(3)(\sqrt{W})\sqrt{\pi \frac{L+r_p}{W}}}, \quad (3.4)$$

$$\text{where } r_p = \frac{(K_{Ic})^2}{2\pi(\sigma_y)^2}. \quad (3.4a)$$

In LEFM, the geometric factor Y is an important term. In the situations considered in this thesis, where the cracks are small, Y can be thought of as a stress concentration factor. It describes the magnified stresses which the crack experiences when it is near a stress concentrator. Y is well defined for simple geometries but for more complex configurations, finite element analysis is employed to find the highly stressed regions in a component.

3.1.3 Effective Crack Tip Blunting Methodology

A third approach to predicting failure in ductile polymers with cracks has been hinted at by Dubey (1998) and Parton (1992) and from observations of crack tip deformation in polymers.

This methodology assumes that the crack effectively blunts itself to an effective radius of curvature ρ (refer to Figure 3.2) which is different for each material. This effective radius of curvature, assumed to be a material constant, is not necessarily related to the plastic zone size, or to the observed shape of the yielded/crazed/cavitated region at the crack tip. It is simply a material parameter that describes its behaviour, and could accommodate combinations of plastic yielding, crazing, cavitation, fibre pullout, crack bridging and other polymeric toughening mechanisms.

Geometrically, an ellipse with semi-minor axis b and semi-major axis c will have a radius of curvature ρ equal to b^2/c [Jennings 1994; Roe 1993]. Any ellipse may be formed to approximate the end of a crack but every material is assumed to have a distinctive ρ . Therefore the tensile stress state at the end of the crack, in the y direction will be

$$\sigma_{\text{tip}} = \left[\sigma_a \left(1 + 2\sqrt{\frac{a}{\rho}} \right) \right] (Y), \quad (3.5)$$

where Y is a geometric constant as defined in Chapter 3.1.2.

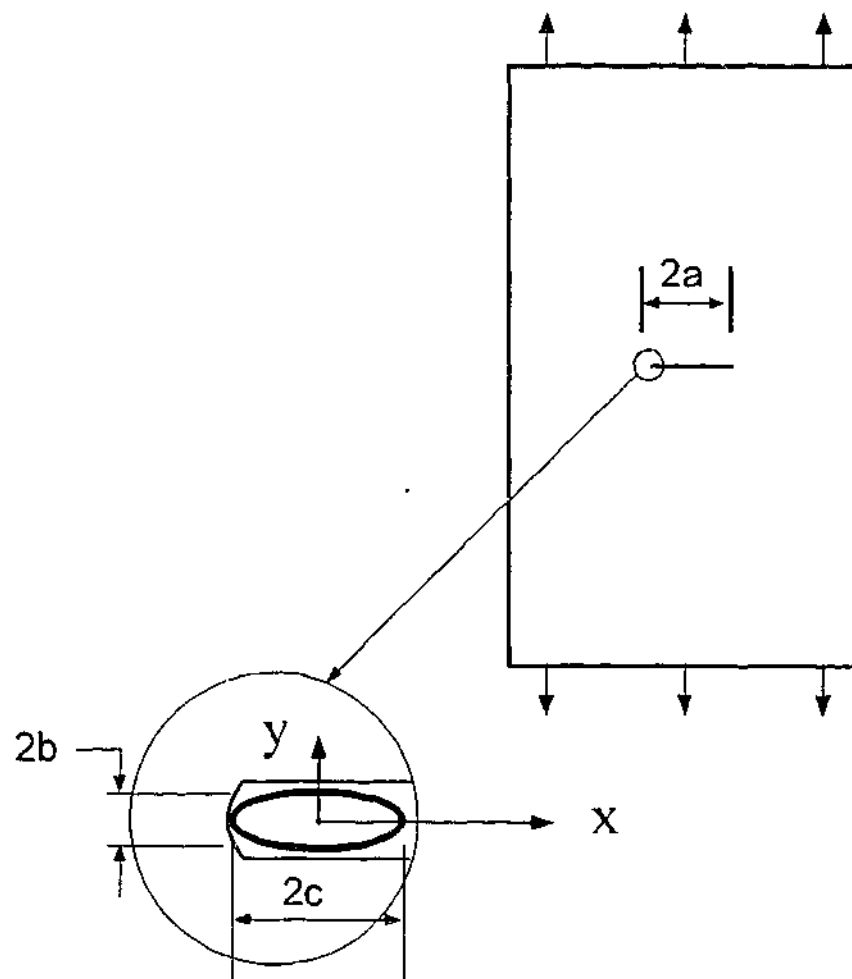


Figure 3.2: Effective crack tip blunting model.

The key supposition is that failure will occur when the stress at the tip causes the material to further yield (i.e. when $\sigma_{tip} = \sigma_y$). For the example of a crack emanating from a hole (shown by Figure 3.1), failure occurs when

$$\sigma_a = \frac{\sigma_y}{\left(1 + 2\sqrt{\frac{L}{\rho}}\right)} \quad (3.12)$$

$$\sigma_a = \frac{\sigma_y}{\left\{1 + 2\left[\left(\sqrt{\frac{W}{\rho}}\right)\left(\sqrt{\frac{L}{W}}\right)\right]\right\}} \quad (3.6)$$

If one includes the plastic zone correction, Eq. 3.6 becomes

$$\sigma_a = \frac{\sigma_y}{\left\{1 + 2\left[\left(\sqrt{\frac{W}{\rho}}\right)\left(\sqrt{\frac{L + r_p}{W}}\right)\right]\right\}} \quad (3.7)$$

3.2 Application of Elastic Analysis to Complex Geometries

The principles of predicting fracture have been looked at in Section 3.1. The example of predicting failure for a simple article such as a crack emanating from a hole showed the logical steps required in three different, simple methodologies. The question which now arises is, how does one apply the principles of the three methodologies to the five configurations tested in this thesis.

3.2.1 FEA and Yielding Methodology

Figure 3.3 shows a single edge notched tensile (SENT) specimen. The component is loaded uniformly and along the mould filling direction with the gate being at the 75mm end. The specimen is also experiencing a plane stress condition as it is a thin sheet with no constraint in the thickness direction.

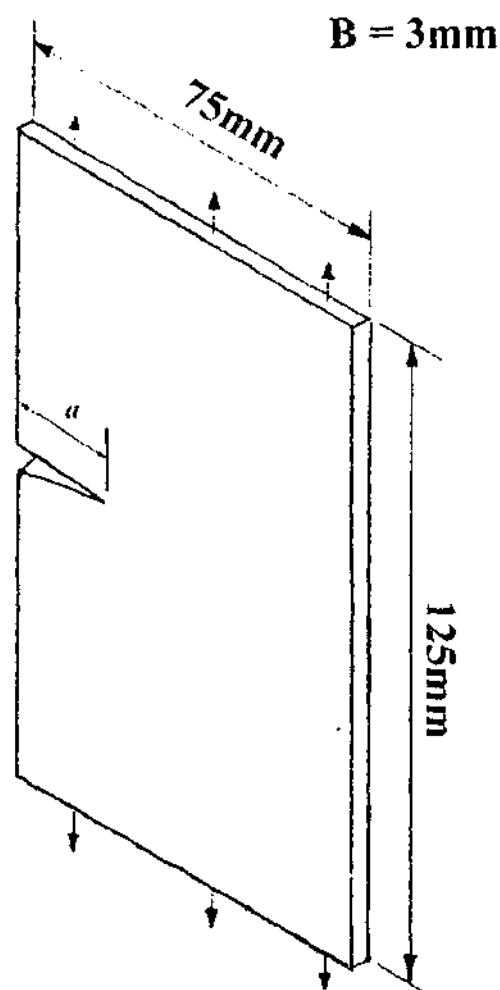


Figure 3.3: Dimensions of SENT specimen.

The first methodology used to predict failure is net section yielding. Yielding would occur across the ligament length when the net section stress equals the yield stress of the material. Therefore failure occurs when

$$\begin{aligned}\frac{P}{B(W-a)} &= \sigma_y, \\ \frac{P}{BW\left(1-\frac{a}{W}\right)} &= \sigma_y, \\ \sigma_a &= \sigma_y\left(1-\frac{a}{W}\right),\end{aligned}\tag{3.8}$$

where a is the crack length. The variables in Eq. 3.8 are all defined, hence failure loads can be found for varying values of crack length.

It is also worth mentioning at this stage that the SENT specimen was used to characterise the parameters K_{Ic} and ρ . However this will be explained in more detail in Chapter 6.

The second specimen to be considered in this thesis is a middle hole specimen (MHT) specimen. The dimensions of the article is shown by Figure 3.4. Compared to a SENT specimen, the MHT article is complicated by the addition of a stress concentrator which is the hole. However the problem is still one of plane stress. Furthermore, stress concentration effects from holes is well analysed and finite element analysis is not required.

To predict failure by yielding, one can follow the same arguments as in Chapter 3.1.1. The remote stress for failure is

$$\begin{aligned} \frac{P}{BW \left(1 - \frac{2a + 2R}{W} \right)} &= \sigma_y, \\ \frac{\sigma_a}{\left(1 - \frac{2a + 2R}{W} \right)} &= \sigma_y, \\ \sigma_a &= \sigma_y \left(1 - \frac{2a + 2R}{W} \right). \end{aligned} \quad (3.8a)$$

where $2R$ is the diameter of the hole.

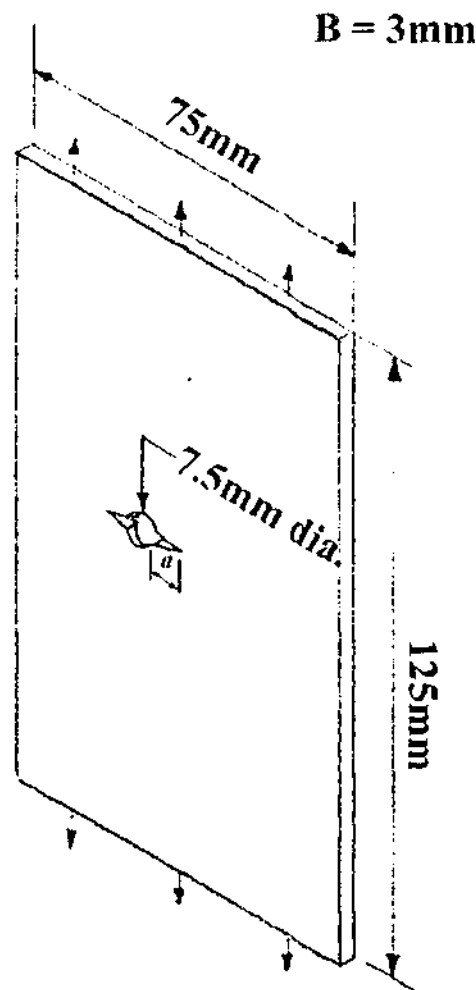


Figure 3.4: Dimensions of MHT specimen.

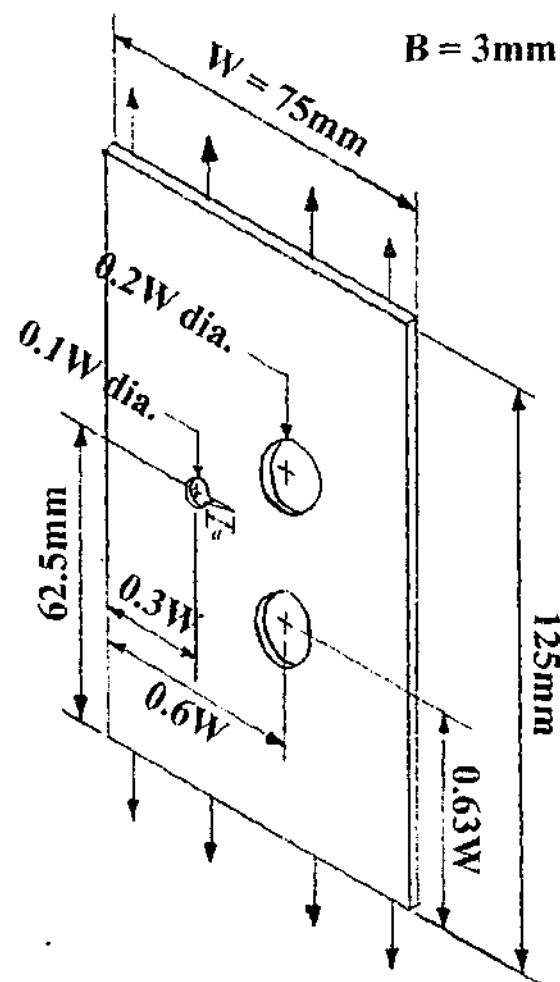


Figure 3.5: Dimensions for THT specimen.

The third specimen was a three-hole tension (THT) specimen shown by Figure 3.5. The dimensions were proportional to those used by Newman et al. (shown in Figure 1.1).

The three-hole tension specimen is an example of a more complex injection moulded article and as a result, finite element analysis (FEA) is required to solve the problem. A simple methodology for analysing the problem is by considering whether the crack emanating from the smaller hole is influenced by the stress concentration of the small hole. If it is not, then the crack and small hole is treated as one unified crack.

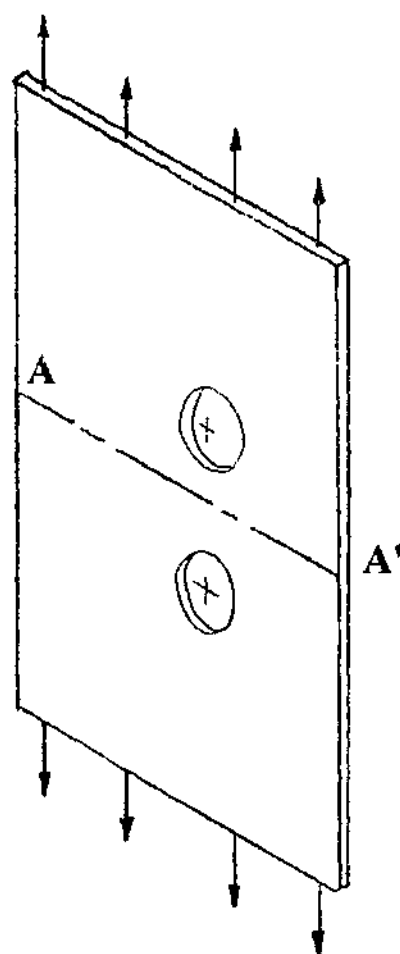


Figure 3.6: FE model for unified hole and crack.

Two finite element analyses were performed. The first considered the small hole and crack to be a single large crack. Therefore a plate with only the two larger holes was modelled (as shown by Figure 3.6). The only region of interest is the midplane, AA'. The stress distribution is plotted on Figure 3.7. The drop in stress concentration between the two large holes shows the shielding effect of the holes against the applied stress.

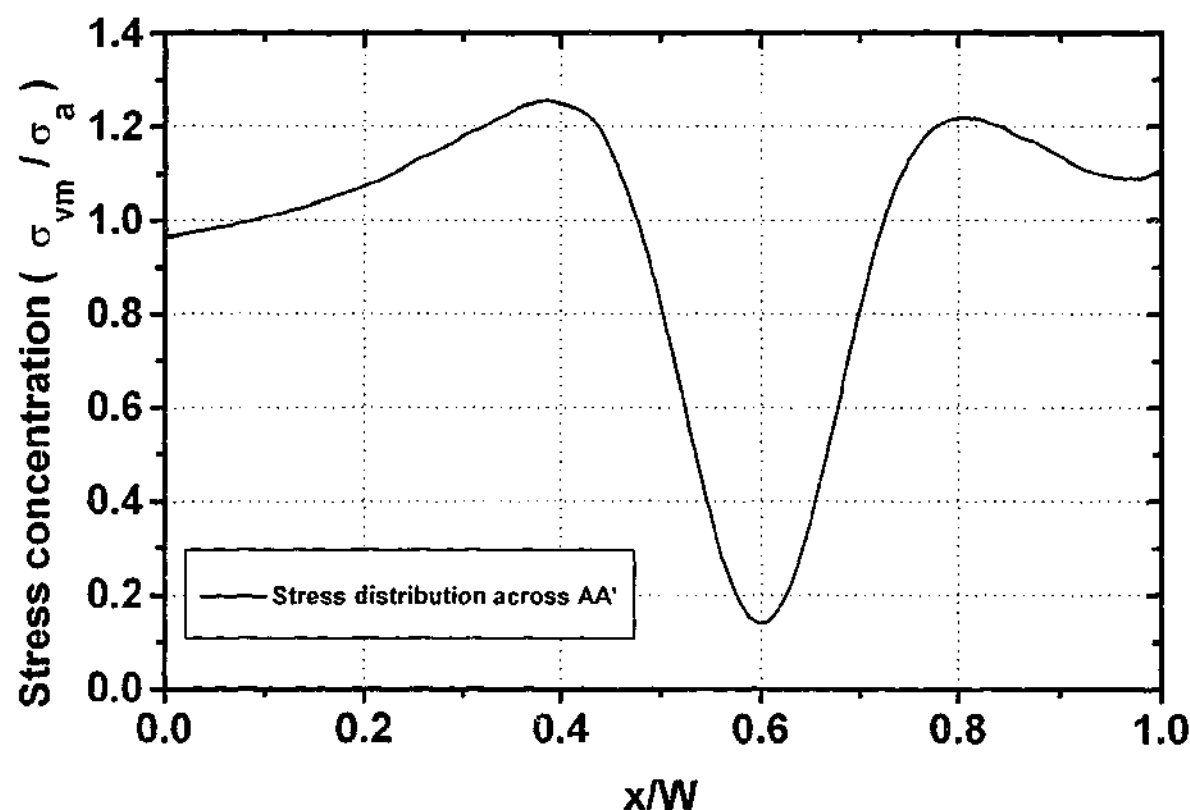


Figure 3.7: Stress distribution across AA' for unified crack in a THT specimen.

In terms of net section yielding, the above result is not as relevant as for the case when the small hole influences the flaw. As discussed in Chapter 1, this thesis deals mainly with small crack sizes which means the hole should have an effect on the crack. The second finite element model considered the crack to be independent of the small hole. Therefore the analysis included the small hole as well as the two large holes (as shown by Figure 3.8). However in this situation, there are several regions where the structure could fail and the stress distribution needs to be well described.

The edge of the specimen to that of the small hole, identified as CC' in Figure 3.8, is an area of possible failure by yielding while the material joining the small hole and larger hole, identified as DD', may also deform plastically.

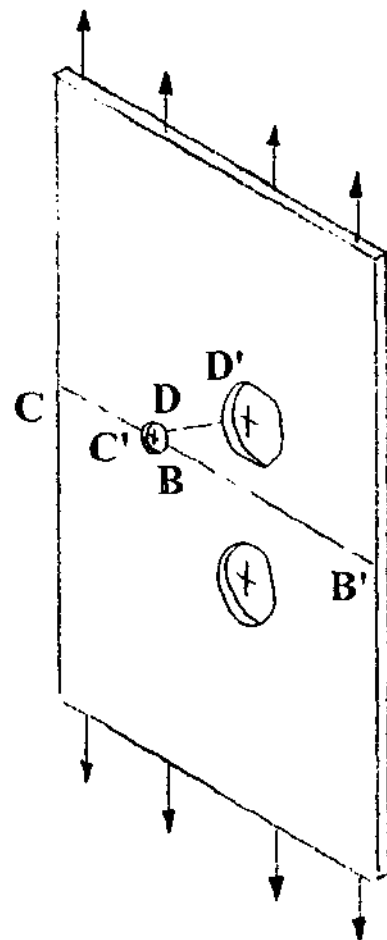


Figure 3.8: THT specimen used in finite element analysis.

The stress distribution for CC' and BB' are plotted on Figure 3.9. The stress distribution across DD' is plotted in Figure 3.10. Figure 3.9 is a plot of σ_{vm} / σ_a versus x/W , where x is position along the midplane. Figure 3.9 shows the highly stressed region in front of the small hole decreasing rapidly once it reaches the shielded area provided by the two larger holes.

The area of interest between the small hole and larger hole is considered to be the plane of material joining the centre of the small hole to the centre of the larger hole. This may not necessarily be where the maximum stresses lie but it contains the least amount of material. Figure 3.10 shows the Von-Mises stress distribution across plane DD' . High stresses exist at the edge of the small hole and drop to unity only at the circumference of the larger hole.

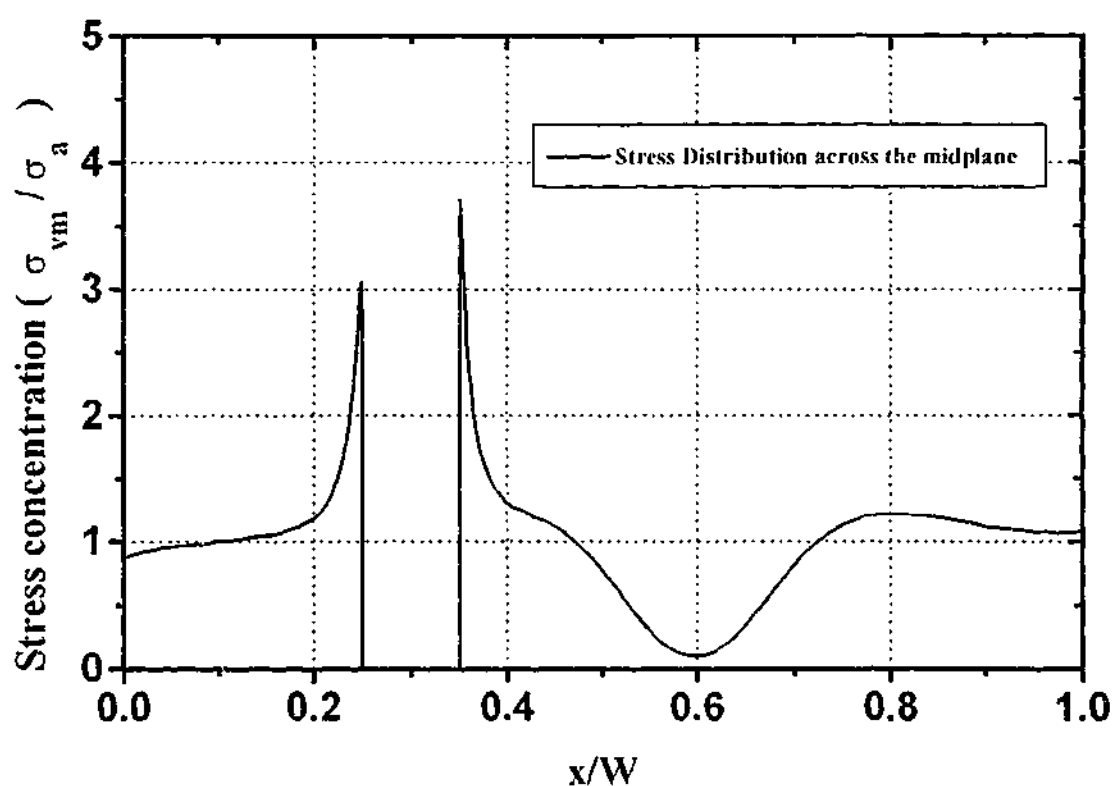


Figure 3.9: Finite element analysis of stress along the midplane of the THT specimen.

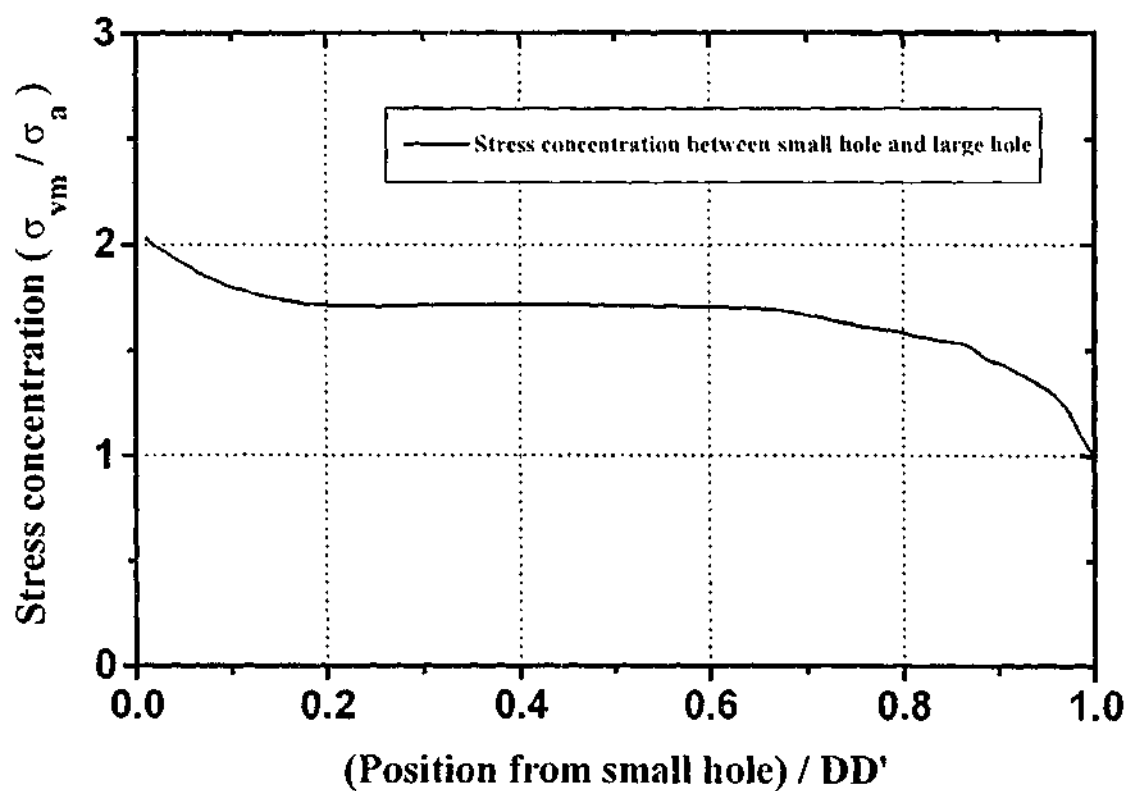


Figure 3.10: Finite element results for the plane DD'.

Failure by net section yielding is predicted to occur if the average stresses across ligament CC' or DD' reaches the yield stress as defined by the Von-Mises yield criterion. Table 3.1 gives the average stress across CC' and DD' - two areas where cross section yielding may be possible.

Table 3.1: Average stresses across regions of possible failure

Region	Average Stress Concentration $(\bar{\sigma}/\sigma_u)$
CC'	1.147
DD'	1.664

The Von-Mises criterion (in terms of principal stresses) can be expressed [Hosford and Caddell 1993] as

(3.9a)

$$(\sigma_1 - \sigma_2)^2 + (\sigma_2 - \sigma_3)^2 + (\sigma_3 - \sigma_1)^2 = q^2,$$

where q is a function of the yield stress as obtained from a uniaxial tensile test. Substituting

$$\sigma_1 = \sigma_y,$$

$$\sigma_2 = 0 \text{ and}$$

$$\sigma_3 = 0,$$

into Eq. 3.9a results in q^2 being equal to $2\sigma_y^2$.

The evaluated yield stress can now be used in place of q in the Von-Mises criterion and dividing both sides by 3, the equation becomes

$$\frac{(\sigma_1 - \sigma_2)^2 + (\sigma_2 - \sigma_3)^2 + (\sigma_3 - \sigma_1)^2}{3} = \frac{2\sigma_y^2}{3}.$$

Taking the square root of both sides, the equation becomes

$$\sqrt{\frac{(\sigma_1 - \sigma_2)^2 + (\sigma_2 - \sigma_3)^2 + (\sigma_3 - \sigma_1)^2}{3}} = \sqrt{\frac{2}{3}}\sigma_y. \quad (3.9b)$$

Failure occurs when the function of the stress state on the left hand side of Eq. 3.9b reaches the Von-Mises defined yield stress on the right hand side. The left hand side of Eq. 3.9b is also the function used to calculate stresses in the finite element analysis.

From the values given by Table 3.1, the ligament DD' experiences the largest average stress. In fact, for every 1 unit of remote applied stress, the average Von-Mises stress is 1.664 times higher. Therefore using Eq 3.9b and Table 3.1, yield failure occurs when

$$\sigma_a = \frac{\sqrt{\frac{2}{3}}\sigma_y}{1.664} \quad (3.10)$$

As the CT specimen is pin loaded (shown in Figure 3.11), the approach needed to predict failure by yielding will vary slightly when compared to the previous three specimens which were uniformly loaded. In this case, the pin loads act as leveraging forces trying to pull apart two beams with the crack separating the beams. The point of failure will therefore be at the end of the crack, which can be regarded as the end of the beam.

An analytical solution exists for describing the stress distribution at the crack tip of a CT specimen. It is given in the book by Atkins and Mai (1985). To predict failure for pin loaded cases, they considered the problem to be a summation of two loading situations - shown by Figure 3.12. One load is tensile whilst the other is considered to be a bending moment. The stresses at the end of the crack can be evaluated by stating that

$$\sigma_r = \frac{P}{B(W-a)} + \frac{My}{I}$$

where

$$M = P(W-a)/2,$$

$$y = (W-a)/2 \text{ and}$$

$$I = B(W-a)^3/12.$$

Substituting and simplifying, the result is

$$\sigma_y = \frac{6P}{BW} \left[\frac{a/W + ((2/3)(1 - a/W))}{(1 - a/W)^2} \right]$$

Failure is assumed to occur when σ_y is equal to the yield stress. The required applied load (normalised by dividing against thickness and width) is given by

$$\frac{P}{BW} = \sigma_a = \frac{\sigma_y}{6} \left[\frac{(1 - a/W)^2}{a/W + ((2/3)(1 - a/W))} \right]$$

Predictions of failure loads caused by yielding can therefore be made for all crack lengths.

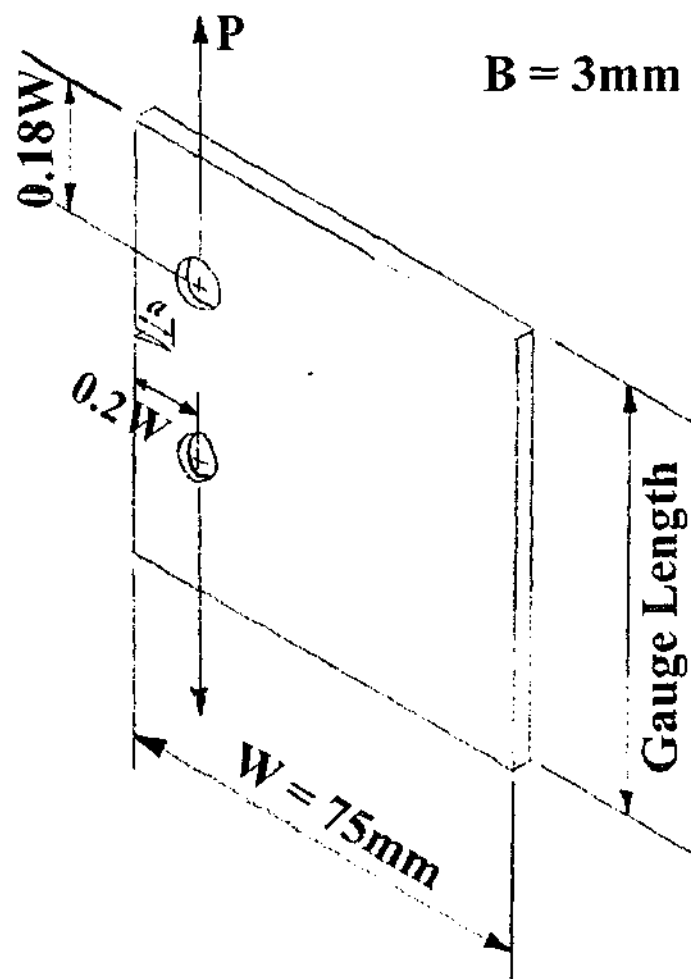


Figure 3.11: Dimensions for CT specimens.

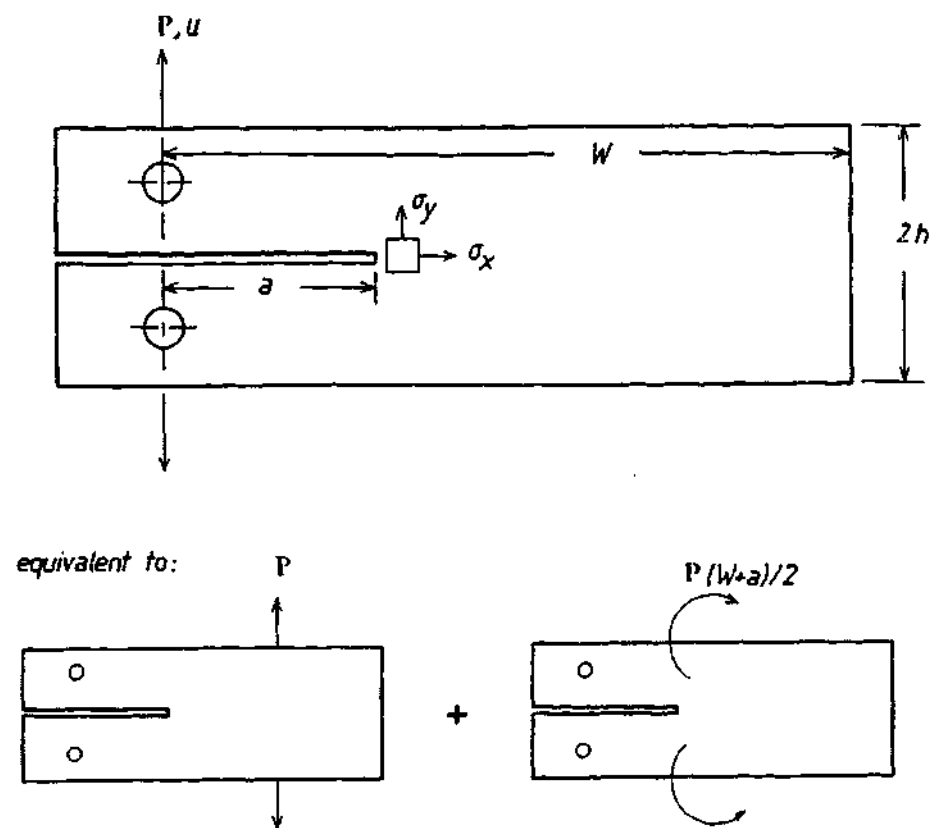


Figure 3.12: Analytical solution to pin loaded cases [Atkins and Mai 1985].

Analysis for net section yielding of the ribbed specimen (shown by Figure 3.13) was the same as for the CT specimen. They were essentially both pin-loaded cases. In this thesis, the plane strain condition which exists when the crack is at the junction of the "T" intersection is not taken into account in the predictions. This was done for the purpose of simplicity.

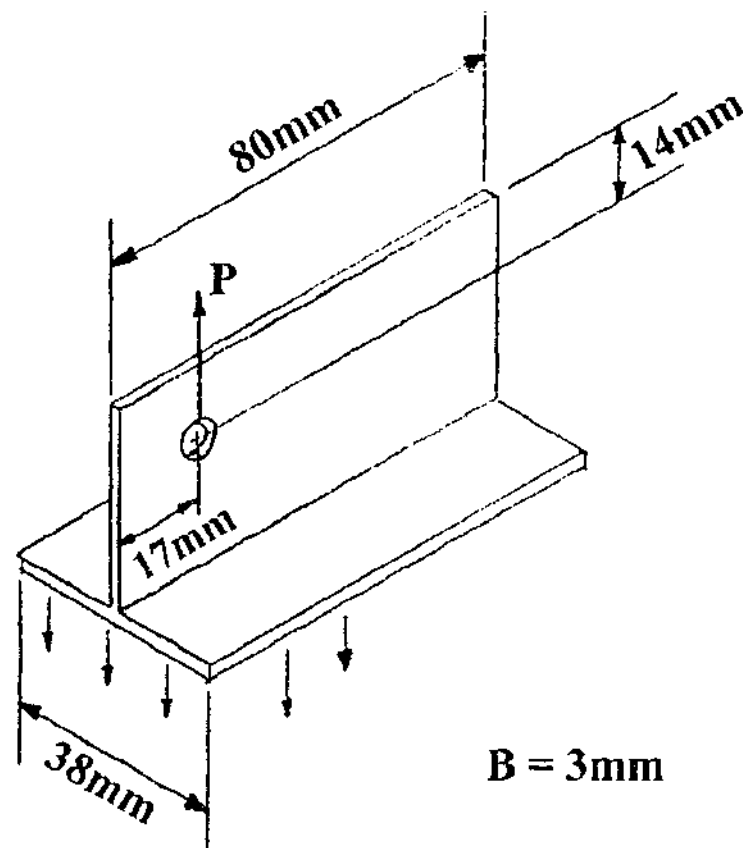


Figure 3.13: Dimensions of ribbed specimens.

3.2.2 FEA and LEFM Methodology

In LEFM, the simplest equation used to forecast the fracture in a cracked specimen is,

$$\sigma_a = \frac{K_{Ic}}{Y\sqrt{W} \sqrt{\pi \frac{a}{W}}} \quad (3.11)$$

Irwin modified this equation to

$$\sigma_a = \frac{K_{Ic}}{Y\sqrt{W} \sqrt{\pi \frac{a + r_p}{W}}} \quad (3.12)$$

with the addition of the plastic zone to the overall crack length. Eq. 3.12 is used to generate curves to predict failure by LEFM because it provides lower loads as well as a better

representation of the ductility present in many materials when compared to Eq. 3.11. In Eq. 3.12, K_{Ic} is a constant (for a particular material) along with r_p . a is the independent variable, leaving Y as the parameter that needs to be defined. Y describes the stress concentration (or stress state) in the region of interest within the structure in question. It is a function of position in that body. In the case of a SENT specimen,

$$Y = 1.12 - 0.23\left(\frac{x}{W}\right) + 10.5\left(\frac{x}{W}\right)^2 - 21.71\left(\frac{x}{W}\right)^3 + 30.38\left(\frac{x}{W}\right)^4, \quad (3.13)$$

where x is the position along the midplane of Figure 3.3.

For any crack length, the stress state is found by substituting the equivalent value for x . It is interesting to note that for small cracks, Y is equal to 1.12. This value, slightly greater than unity, indicates that there are stress concentration effects present in SENT specimens from the edges.

For the MHT specimens,

$$Y = \frac{1}{2} \left[2 + \left(\frac{r}{x+r} \right)^2 + 3 \left(\frac{r}{x+r} \right)^4 \right], \quad (3.14)$$

where x is position as measured from the edge of the hole along the midplane (refer to Figure 3.4) and r is the radius of the hole. Eq. 3.14 describes the stress concentration of the hole in a uniformly loaded plate. When x is equal to 0, Y is equal to 3, which is the expected result. As x increases, the stress concentration drops away rapidly.

The stress state for the uniformly loaded THT specimen has no analytical solution and hence FEA was utilised to gain an answer. Y for the THT article is plotted in Figure 3.9 and the region of interest is BB' as shown by Figure 3.8. The plane BB' has a high stress concentration near the hole, and it is the region where a crack was introduced, but it drops to unity quickly.

No analytical solution was found for an unnotched CT specimen and as a result FEA was used to define the stress state. The specimens were pin loaded and as a result Hertzian stresses were encountered (Timoshenko 1970). For the case of the CT specimens, only one region of stress distribution is important. It is at the midplane of the specimens, shown by EE' in Figure 3.14.

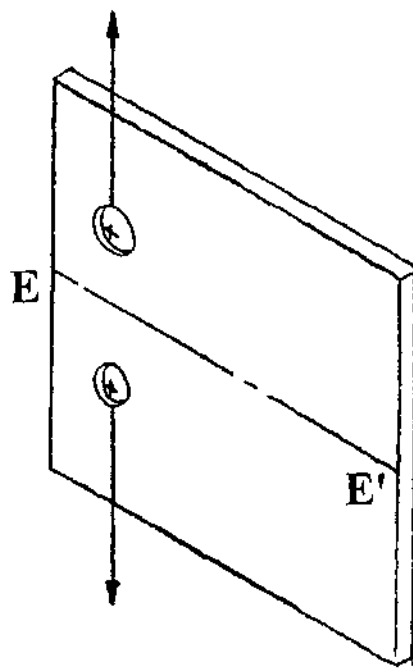


Figure 3.14: CT specimen used in FEA, showing the plane of interest EE'.

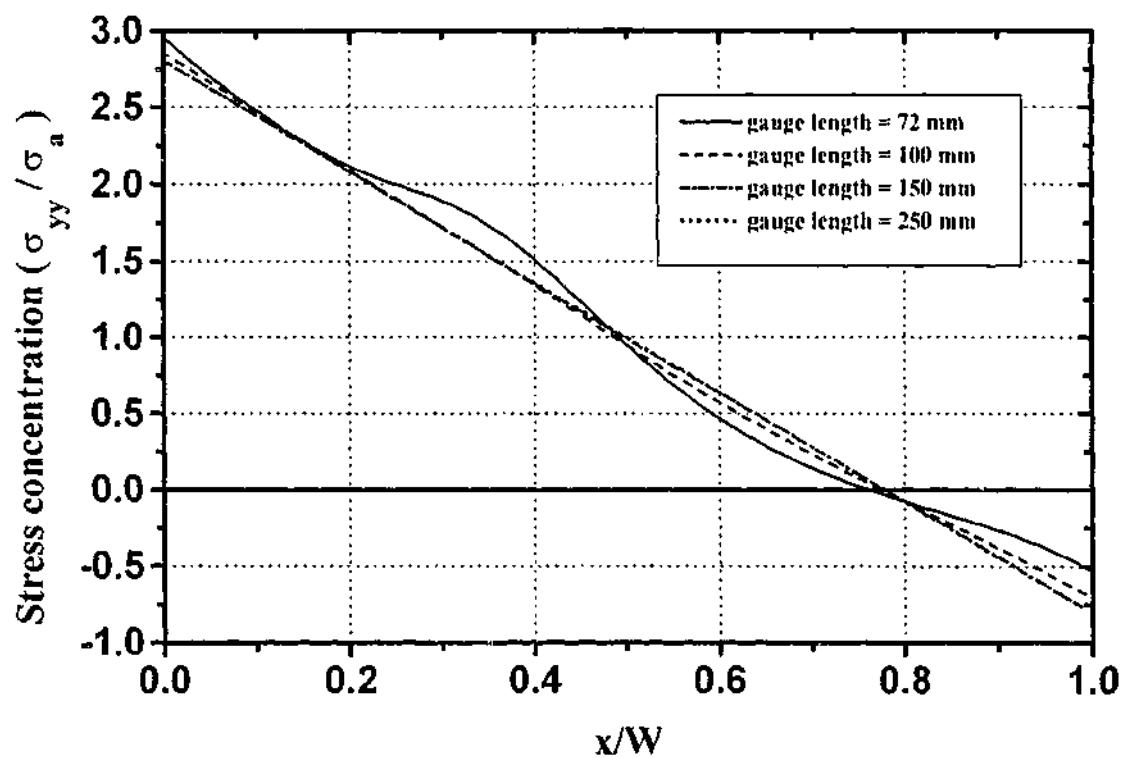


Figure 3.15: FEA calculated stress distribution across EE' for the CT specimen. $W = 75\text{mm}$ for all specimens.

Figure 3.15 shows the stress distribution σ_{yy} / σ_a across EE' for CT specimens with various gauge lengths. The stresses decrease away from the edge and loading points and become compressive for x/W greater than approximately 0.78. This is true for all gauge lengths. Therefore even at reasonably long gauge lengths, the ratio of σ_{yy} to σ_a is not unity, indicating a bending moment effect is present.

For the specimen with a gauge length of 72 mm (which is the gauge length of the experimental specimens), there is a rise in stresses associated with the loading pins, which are located at $x/W = 0.2$. This is due to the close proximity of the two loading points and the effect of having a concentrated pin load directed at a surface of the holes.

As stated in Section 3.2.1, Y for the ribbed specimen did not differ from that of the CT specimen in order to maintain the simplicity of the problem. Therefore the finite element solution (shown by Figure 3.13) was used in the analysis of CT and ribbed specimens.

3.2.3 FEA and Effective Crack Tip Blunting Methodology

Application of the crack tip blunting methodology does not differ greatly from that of LEFM. The general equation for predicting failure by this method is

$$\sigma_a = \frac{\sigma_y}{\left(1 + 2\sqrt{\frac{a}{\rho}}\right)Y}, \quad (3.15)$$

and including the plastic zone size,

$$\sigma_a = \frac{\sigma_y}{\left(1 + 2\sqrt{\frac{a + r_p}{\rho}}\right)Y}. \quad (3.16)$$

As in the previous section, all relevant parameters are known. ρ is a material constant, Y is defined by FEA or analytically and a is the independent variable plotted against. Eq. 3.16 states that for increasing values of ρ (i.e. tough materials), the stress required to cause failure rises. This is in accordance with intuition.

3.3 Application of Elastic/Plastic Analysis to Complex Geometries

3.3.1 J-Integral Methodology

The energy argument for fracture was shown by Eq. 2.16 to be

$$\frac{Y^2 \sigma_a^2 \pi a}{E} = G,$$

where Y is a geometric constant which describes the stress state of the structure before a crack is introduced. The equation is useful because it permits the use of stresses to be used in the solution of the equation.

Fracture occurs when the applied stress increases the left hand term of the equation to the value of G_{Ic} . This equation can also be rewritten in a form which will contain strain. Substituting σ/ϵ for E , the equation becomes

$$Y^2 \sigma_a \epsilon \pi a = G. \quad (3.17)$$

Furthermore, an elastic-plastic material can be modelled using the Ramsberg-Osgood equation, which relates stress and strain by

$$\epsilon = \frac{\sigma_a}{E} + \frac{(\sigma_a)^n}{F} \text{ or } \epsilon = \epsilon_{el} + \epsilon_{pl}. \quad (3.18)$$

Substituting Eq. 3.18 into Eq. 3.17, one gets

$$\frac{Y^2 (\sigma_a)^2 \pi a}{E} + \frac{Y^2 (\sigma_a)^{n+1} \pi a}{F} = J. \quad (3.19)$$

The right hand term of the equation is no longer G but J , to denote an elastic-plastic material.

The first term on the left hand side of the equation,

$$\frac{Y^2(\sigma_a)^2 \pi a}{E},$$

is the elastic component of the energy release rate. The second term

$$\frac{Y^2(\sigma_a)^{n+1} a}{F},$$

signifies the plastic component of the energy release rate.

Equation 3.19 is useful in engineering because the left hand side of the equation is expressed in stresses. The equation states that fracture will occur when the applied stress increases the total on the left hand side of the equation to a value of J_{Ic} , which is the fracture toughness of the material. The solution to Eq. 3.19 requires iteration and performing a tensile test to evaluate E and F . Y is once again found analytically or by using finite element analysis for more complex geometries.

To obtain an iterative solution is not as simple as in the elastic case. Admittedly, the use of computers could aid in the solving of the problem but ductile polymers provide another barrier. The main hurdle is the tensile curve does not match the stress-strain relation given by Eq. 3.18. The curve (shown as curve C in Figure 8.1) rises to a maximum load and then continues to neck at lower loads. For increasing strain, the stress does not continue to increase in an exponential manner as for metals.

3.4 Designing Polymer Articles using Elastic Analysis

Instead of applying the discussed methodologies to articles with cracks already present in them, they may be used upon uncracked objects. The question posed from this alternative viewpoint is - what size flaw can a complex structure withstand before failure? A further question is - which methodology will provide a consistently safe result?

Take the simple example of an everyday injection moulded article that is also complex in geometry such as a telephone casing. If it is subjected to some external loading condition, what size flaw could it tolerate without failing?

The initial step would be to perform an FEA analysis because an analytical solution would probably be either impossible or too time consuming to attain. The FEA analysis would then give a stress distribution of the telephone casing under service loads. There would probably be several regions where high stresses are situated. The designer would then focus her attention onto these important areas and use the FEA data to make appropriate calculations.

In order to check for the occurrence of net section yielding, one would transpose Eq. 3.10 to:

$$\bar{\sigma}_{vm} = \sqrt{\frac{2}{3}} \sigma_y, \quad (3.20)$$

where $\bar{\sigma}_{vm}$ is the average Von-Mises stress over a ligament length.

Eq. 3.20 states that if any of the regions had an average Von-Mises stress over the yield stress (according to the Von-Mises criterion), then the component would fail. A redesign would then be necessary perhaps simply by increasing the wall thickness to decrease the stresses in any critical regions.

Similarly one could alter Eq. 3.12 and Eq. 3.16 to have crack length a as the dependent variable. Eq. 3.12 would become

$$a = \left[\frac{K_{Ic}}{(\sigma_{x,y,z})\pi} \right]^2 - r_p, \quad (3.21)$$

and Eq. 3.16 will be

$$a = \left[\frac{\rho}{4} \left(\frac{\sigma_y}{\sigma_{x,y,z}} - 1 \right)^2 \right] - r_p, \quad (3.22)$$

where $\sigma_{x,y,z}$ is the point of maximum stress and is also equal to σ_a multiplied by Y .

Equations 3.21 and 3.22 both state that for increasing stress, the allowable crack size decreases, since K_{Ic} and ρ are constants. This is in accordance with intuition.

From results in Chapter 6, it can be argued that the crack lengths solved using Eq. 3.21 will be larger than those of Eq. 3.22. However ductile polymers are not able to withstand the large cracks predicted by LEFM.

Following on from this argument, should an engineer choose to base her/his calculation upon LEFM, the amount of material used would be less than necessary (i.e. thin wall thickness increases the maximum stress) in order to accommodate a small flaw. The object may fail prematurely. The other option is to accept calculations based upon the simple crack blunting model. The crack lengths as calculated from Eq. 3.22 would be smaller but is a safe design. Hence wall thickness can be increased to allow for larger cracks, decreased to allow for smaller cracks or remain the same if the predicted tolerable crack size is within specification.

3.5 Summary

In this chapter, three simple methodologies were described that could be used to predict failure in polymeric articles with cracks. It was also shown how these three methodologies could just as easily be used as design tools to ascertain what crack length an article could withstand before failure during service.

The three methodologies used were:

- net section yielding.
- LEFM and
- effective crack tip blunting.

The effective crack tip blunting methodology is the simple idea proposed in this thesis. The supposition is that a crack in a polymer behaves as if it has blunted to an effective radius of curvature ρ . In turn, this curvature ρ will produce a certain stress concentration and failure is assumed to occur when the magnified stresses at the crack tip reaches the yield stress of the material. Each material will have a distinct value of ρ . It should also be noted that ρ is not equal to Irwin's plastic zone size r_p . In fact, to effectively blunt the crack, polymers use a variety of mechanisms – cavitation, crack bridging, shear yielding, microcracking, crazing and various other means, whereas the plastic zone size is only based on the yielding of material in front of the crack.

Chapter 3 formulates the logical sequence of steps necessary to apply the three methodologies to complicated geometries. The five types of geometries tested ranged from plane stress to plane strain conditions. Case studies of fractured components [Herrera et al. 1995a; Herrera et al. 1995b] and use of simple methodologies to predict failure in engineering articles [Shi 1993; Guagliano and Vergani 1994] have been applied to metals but

discussion is lacking when it comes to injection moulded structures made from tough ductile polymers. In this thesis, only simple criteria for failure were utilised. In all three methods, the material was assumed to behave in a linear elastic manner. Elastic-plastic fracture mechanics was avoided because of its complexity. Also the stress-strain equations involved in the analysis assume a work hardening material. As shown by Figure 8.1 (curve C), this is not the case for polymers. Essential work of fracture (EWF) was not used because to the author's knowledge, it has only been applied to polymers as a characterisation tool.

Chapter 4

Materials and Experimental Methods

4.1 Materials and Sample Preparation

4.1.1 Raw Materials

Eight materials were studied. They were PC, PET, PS, three types of ABS and two polymer blend systems - ABS/PC and ABS/PET. All the polymers are commercially available except for the ABS/PET system.

Table 4.1 shows the materials used, their corresponding tradenames and place of purchase. Tradenames will be used to differentiate the three grades of ABS. The three ABS materials were CB625, Astalac DMT and Astalac M120. CB625 is a general purpose grade ABS. Astalac DMT is a high flow, injection moulding grade ABS while Astalac M120 is an extrusion grade with high rubber content [Plast. News Int. 1997].

Table 4.1: Tradenames and manufacturers of materials used.

Material	Tradename	Manufacturer
ABS	Astalac DMT	Marplex Australia Ltd.
ABS	Astalac M120	Marplex Australia Ltd.
ABS	CB625	Monsanto
PC	Lexan 111	GE Plastics
PET	Kodak PET 9921W	Eastman Chemical Company
PS	PS 103	Huntsman Chemical Company
ABS/PET		CRC for Polymers
ABS/PC	Astaloy 800	Marplex Australia Ltd.

The PS and PC were general purpose injection moulding grade materials while the PET was a blow moulding grade. In industry, the blow moulding grade PET is first injection moulded into a preform before being expanded into a bottle. This particular grade of material can

therefore be used for the purpose of injection moulding plaques and tensile specimens for use in this thesis.

Two polymer blend systems were considered in this study - ABS/PC and ABS/PET. The ABS/PC is a commercially available injection moulding grade, specifically catered for the automotive industry. The blend has 50% by weight of each component. The ABS/PET blend was designed by the CRC for Polymers and it also contains 50% by weight of each component. The ABS used in the ABS/PET blend was CB625 and the PET component was Kodak PET 9921W.

The ABS/PET blend was intended to be a cheaper alternative to the ABS/PC system and the combination of CB625 and Kodak PET 9921W showed a synergistic effect at 50/50 blend ratio. It increased the toughness of the material in notched Izod impact tests above that which was expected from a linear interpolation [Cook et al. 1996a].

4.1.2 Processing

Table 4.2: Drying temperatures and time for pellets before injection moulding

Material	Drying temperature and time
PET	177 °C for 4 hours
PC	110 °C for 8 hours
ABS/PET	100 °C for 12 hours
ABS/PC	100 °C for 6 hours
Astalac DMT	80 °C for 12 hours
Astalac M120	80 °C for 12 hours
CB625	80 °C for 12 hours
PS	70 °C for 4 hours

CB625 and Kodak PET 9921W were melt blended in an intermeshing, counter-rotating JSW twin screw extruder at 230°C / 240°C and pelletised [Cook et al. 1996b]. Pellets of each material were pre-dried at the temperatures stated in Table 4.2, under a nitrogen atmosphere. They were then fed into a Cincinnati Milacron Vista Sentry injection moulder hopper (under

nitrogen atmosphere) and processed into end-gated plaques and tensile bars. The processing conditions for the materials are shown by Figure 4.1.

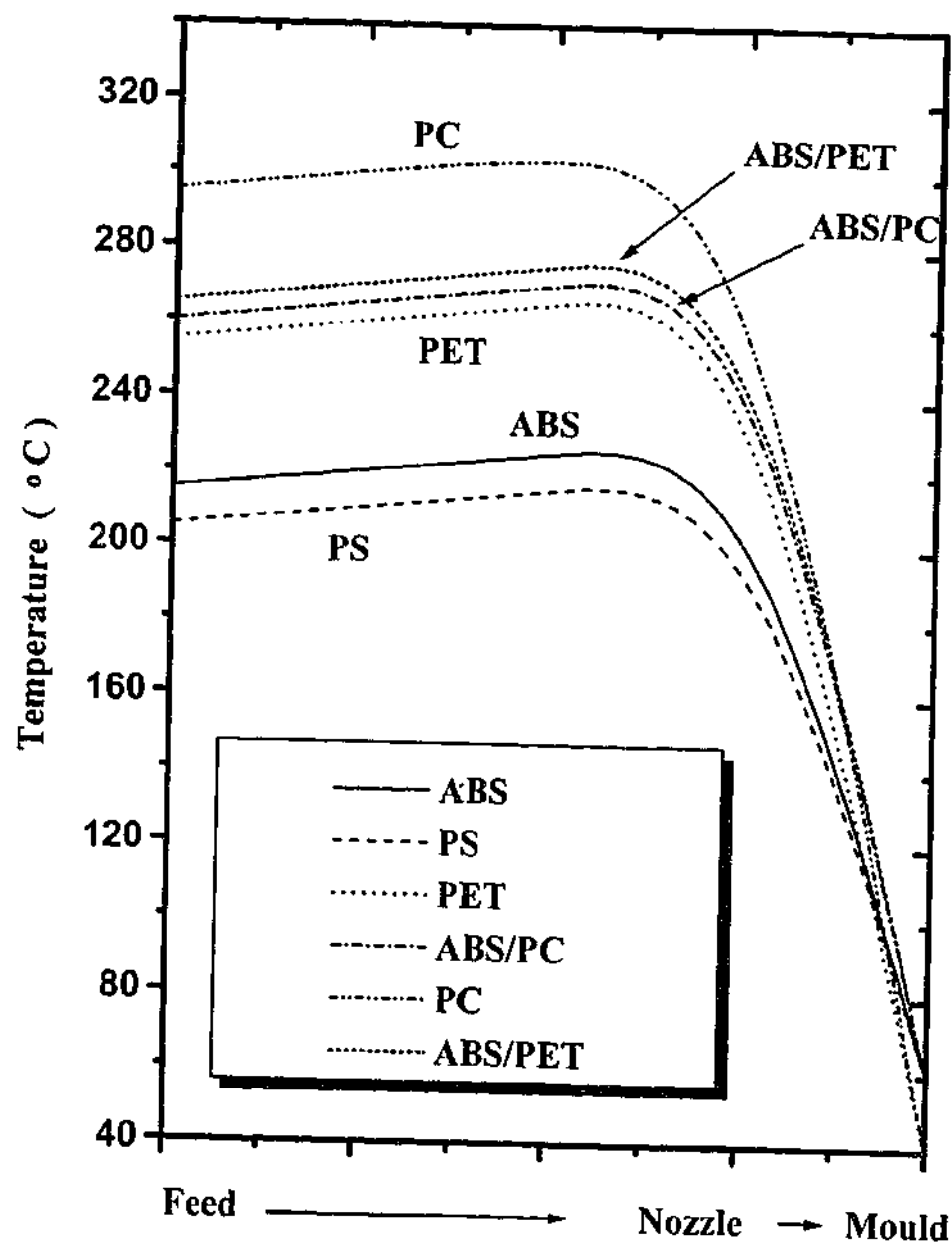


Figure 4.1: Injection moulding conditions for all the materials studied.

4.2 Experimental Techniques

4.2.1 Differential Scanning Calorimetry

Differential scanning calorimetry (DSC) was used to find the glass transition temperatures for the homopolymers and blends. Samples of 10 to 20mg were guillotined from the end-gated injection moulded tensile bars [Zipper 1995].

The samples were tested in aluminium pans on a Perkin Elmer DSC7 at a scan rate of 10°C/min, commencing at 50°C, with a nitrogen gas flow of 20 lbs/in². Indium (transition point of 156.60°C and transitional energy of 28.45J/g) and zinc (transition point of 419.47°C) were used to calibrate the temperature and transitional energy scales. A scan over the temperature range of the experiment using two empty aluminium pans provided a baseline with which the sample trace could be subtracted from. Perkin Elmer PC Series Software (Version 3.1) was used to analyse the data.

4.2.2 Impact Tests

Impact tests were performed at room temperature on end-gated injection moulded plaques of dimensions 125mm by 75mm with a thickness of 3mm. An instrumented ICI impact tester (PCB 223B Model transducer) was used. Three to five specimens of each polymer were tested. The Radmana Instrumented Impact Tester Software Version 4.3 calculated the energy to break for each sample.

4.2.3 Izod Impact Tests

Rectangular strips with dimensions of 80mm by 10mm and 3mm thickness were made by cutting along the long side of the injection moulded plaques. The strips were notched using a broach as specified in ASTM D256-97 (1999) and tested at room temperature on a Zwick Impact Tester. Ten specimens were tested for each material.

4.2.4 Finite Element Modelling

The THT specimen and CT specimen with different gauge lengths were modelled using MechanicaTM Version 16 on a Silicon Graphics R5000.

The size and geometry of the plates were specified and the meshing was automatically generated. For the THT specimen, the uniformly loaded ends were not allowed to contract

laterally, simulating the grips used in experiments. A 1MPa stress was applied to the ends of the THT specimen.

For the CT specimen, four gauge lengths were modelled - 72mm, 100mm, 150mm and 250mm. A compressive traction equal to 1kN was placed on the upper half of the hole, and no constraints were applied to the specimen, simulating a pin loaded case.

For THT and CT specimens, the finite element analysis was solved for the elastic case and under plane stress conditions.

4.2.5 Notching of Polymers

The dimensioning for SENT, MHT, THT, CT and ribbed specimens are described by Figures 3.2, 3.5, 3.11 and 3.15.

SENT and CT specimens were prepared from injection moulded plaques. The gate for the plaques were at the 75mm end. They were notched along the width direction, perpendicular to the mould filling direction using a slitting saw on a milling machine. A 2.5mm thick slit was used for specimens with a/W ratios less than 0.3, and a 5mm slit was used for larger a/W ratios. The notches were milled until it was 1mm from the desired crack length. The crack tip was extended and sharpened with a scalpel blade. Holes were drilled in the CT specimens to locate the pins.

MHT and THT specimens were also made from plaques by drilling the required holes on a bench drill. A fine saw was used to extend the crack from the 7.5mm diameter hole for a/W ratio less than 0.3. Longer cracks were milled using a slotting drill of 3.5mm diameter. A scalpel blade was used to sharpen the starting notch.

Ribbed specimens were prepared from extruded PVC "T" sections bought from a local supplier. The PVC was cut to 80mm lengths and cracks were made using a fine hacksaw and sharpened with a razor blade. A hole was drilled into the upright of the specimen (as shown in Figure 3.13) to cater for the pin.

Tensile bars were used to prepare specimens for microscopy of the crack tip. Notches were made using a 2.8mm thick slitting saw in the middle of the bar. Notches were milled to a depth of 2.5mm and extended to 3mm by a scalpel blade.

To relieve the machining stresses, the samples were placed flat in an oven at a temperature of 5°C higher than their glass transition temperature for 10 minutes.

4.2.6 Tensometer Testing

Tensile tests were performed at room temperature according to ASTM 638.98 (1999). The specimens had widths of 10mm, thickness of 3mm and gauge lengths of 75mm. Yield stresses of each material were found for a variety of nominal strain rates - 1×10^{-6} strain/s to 10 strain/s. For nominal strain rates below 0.15 strain/s, an Instron 4505 screw driven tensometer (5kN load cell) was used. The Instron Series IX software downloaded the raw datafile for analysis. At higher strain rates, a MTS 810 hydraulic tensometer (10kN load cell) was used.

Elastic Modulus was also found for a variety of strain rates (up to 0.15 strain/s) using an 50 mm extensometer. The experiments were only performed on the Instron 4505.

SENT, MHT, THT, CT and ribbed specimens were tested at a displacement rate of 5mm/min on the Instron 4505. For the SENT, MHT and THT specimens, this corresponded to a strain rate of 8.777×10^{-4} strain/s.

4.2.7 Microscopy

Notched tensile specimens were uniformly loaded to 90% of their failure load on the Instron 4505. When required, the crack tip opening was maintained by wedging a piece of polymer into the notch.

An area, 10mm by 10mm, around the crack was removed from the tensile bar. It was placed in a cylindrical mould and a small piece of metal was then laid on top of the specimen to stop it from floating in the mixture. "Struers" resin and hardener (which is a mix designed for polymer microscopy, as it is a low exothermic thermoset) were pre-mixed and poured into the cylindrical mould. In order to force resin into the crack tip, the mould and sample was placed in a plastic bag with the resin and isostatically pressed.

In the case of optical microscopy, the specimens were polished and photographs were taken on an Olympus PMG 3 microscope. For SEM, the specimens were polished until a 1 mm layer of hardened resin was left to protect the surface. The specimen was then reduced to a 5mm by 5mm area around the crack tip. This smaller specimen was then microtomed. The

microtomed face was etched with an appropriate chemical and scanning electron micrographs were taken on a Jeol JSM-840A SEM.

Chapter 5

Characterisation of Materials

5.1 Glass Transition Temperature Measurements

The results from the DSC scans on all the materials considered in this thesis are plotted on Figure 5.1. The midpoint in the change of slope of the trace is considered to be the T_g of the material and is represented with a vertical dash on the curve. Numerical values of the glass transition temperatures are given on Table 5.1.

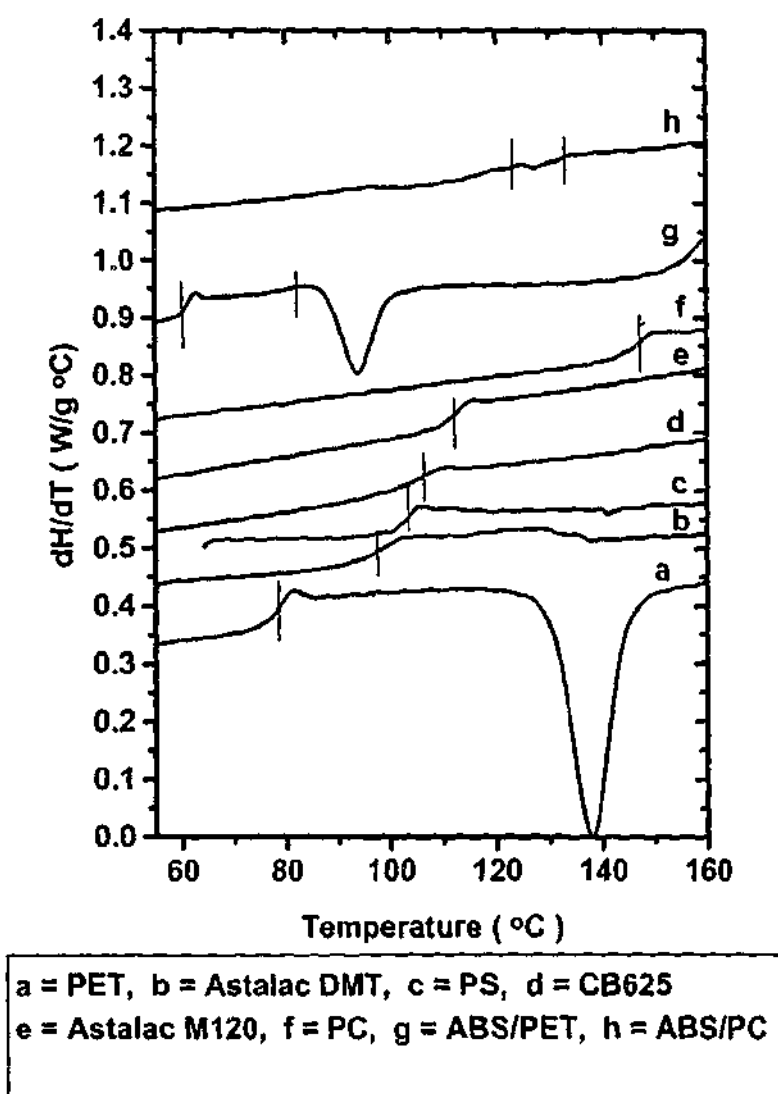


Figure 5.1: DSC curves and glass transition temperatures of all materials studied.

Table 5.1: Glass Transition Temperatures for the materials studied.

Material	Glass Transition Temperature (°C)
PET	77.3
Astalac DMT	98.8
PS	103.0
CB625	103.7
Astalac M120	108.5
PC	145.9
ABS/PET	69.2 / 101.3
ABS/PC	126.6 / 141.9

In Figure 5.1, a single well defined T_g was observed for the homopolymers (curves a to f). PET had the lowest T_g while PC had the highest. PET was also the only semi-crystalline material investigated in this thesis - a fact shown by the downward peak on the DSC trace. The ABS/PC blend showed higher T_g 's than the ABS/PET blend and the T_g 's of all the polymers and blends were above room temperature.

The ABS and PET blend has been well characterised by Cook et al. (1996). With the use of differential scanning calorimetry, they were able to show two distinct T_g 's. This suggests an immiscible blend. For this particular composition, they also noted the T_g of the ABS was masked by the endothermic downward peak of the PET (curve g in Figure 5.1). For the ABS/PC blend, Paul et al. (1994) have reported the dual phase nature of the material. However, with the resolution of the available equipment, there was difficulty in ascertaining the sharp transitions observed by previous workers. It is interesting to note that the ABS/PET blend had T_g 's lower than its original components of CB625 and Kodak PET 9921 W.

5.2 Mechanical Properties

5.2.3 Tensile

Figures 5.2 to 5.9 show the yield stress and elastic modulus behaviour of the polymers under a variety of nominal strain rates. Yield is defined as the maximum load attained during a tensile test. There was an increase in tensile strength and Young's modulus for increasing strain rate. This is in accordance with work done by Ward (1986) and highlights the visco-elastic nature of polymers.

The embrittlement of polymers with increasing strain rate is the result of a lack of time for the polymer chains to relax. However, the changes in the studied systems are occurring over many decades, as shown by the flat trend observed in the plots. Therefore, for engineering components/parts with stress concentrations where the local strain rates are higher than the average strain rate, the material properties will not differ significantly from the surrounding material in most cases.

Scatter in the results at high strain rates was apparent in all the materials tested. A possible reason may have been the lack of resolution of the equipment. At such high speed tests, the amount of data collected may not have been of sufficient accuracy and quantity.

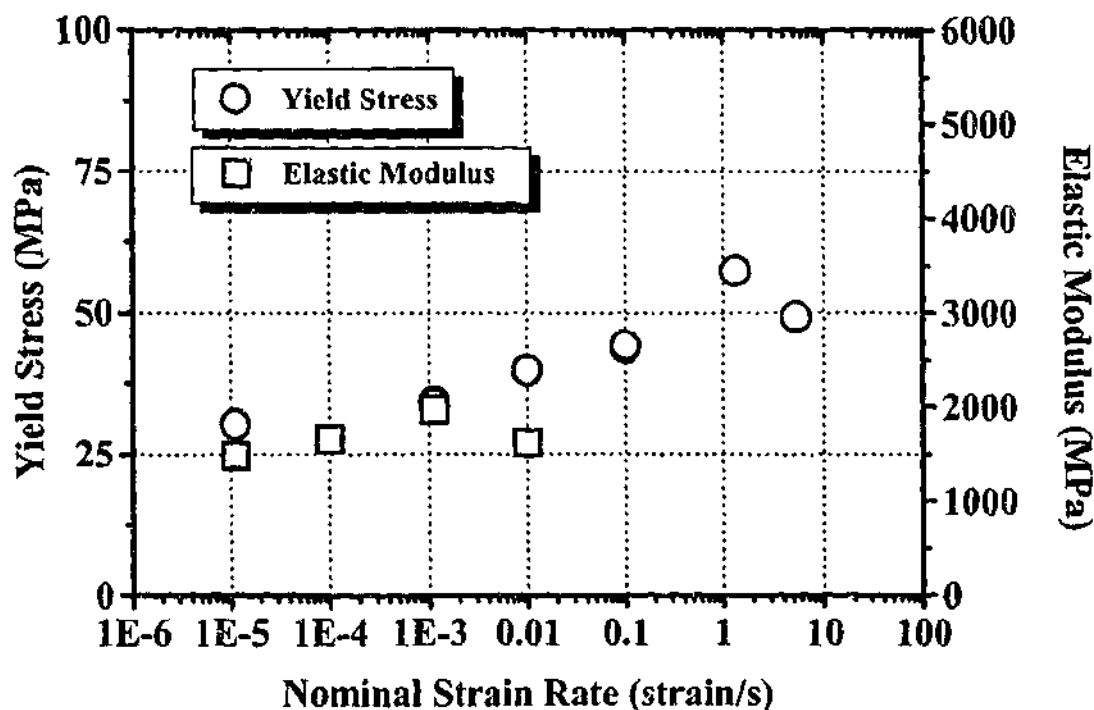


Figure 5.2: Yield stress for PC over a range of strain rates.

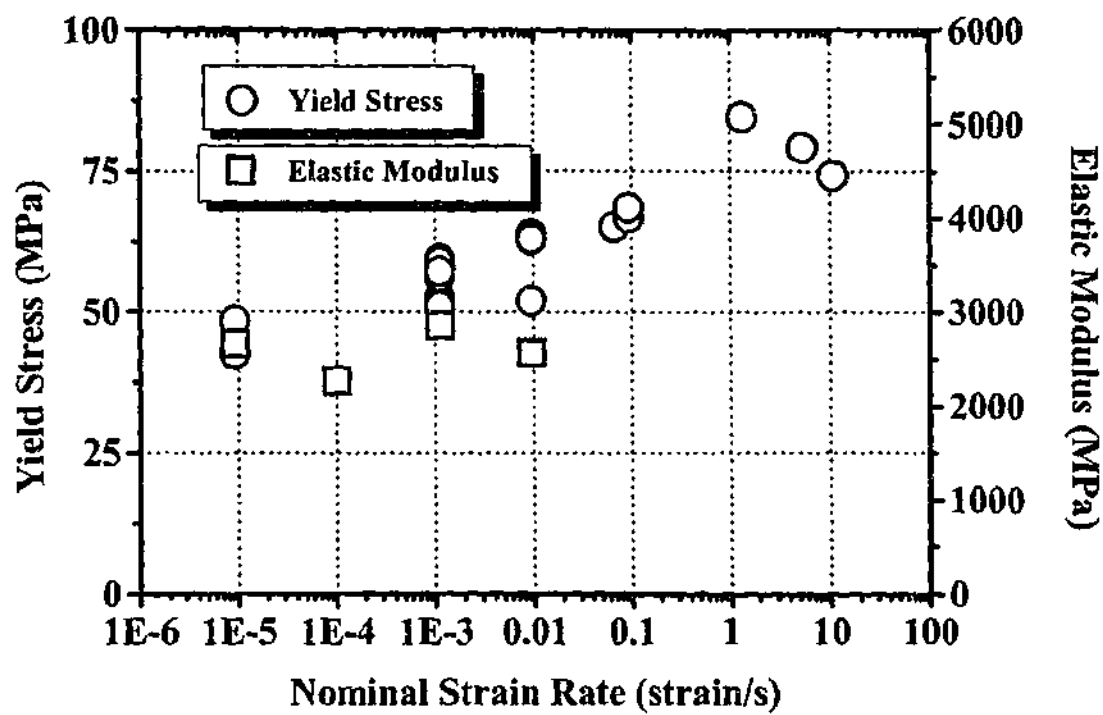


Figure 5.3: Tensile data for PET over a range of strain rates.

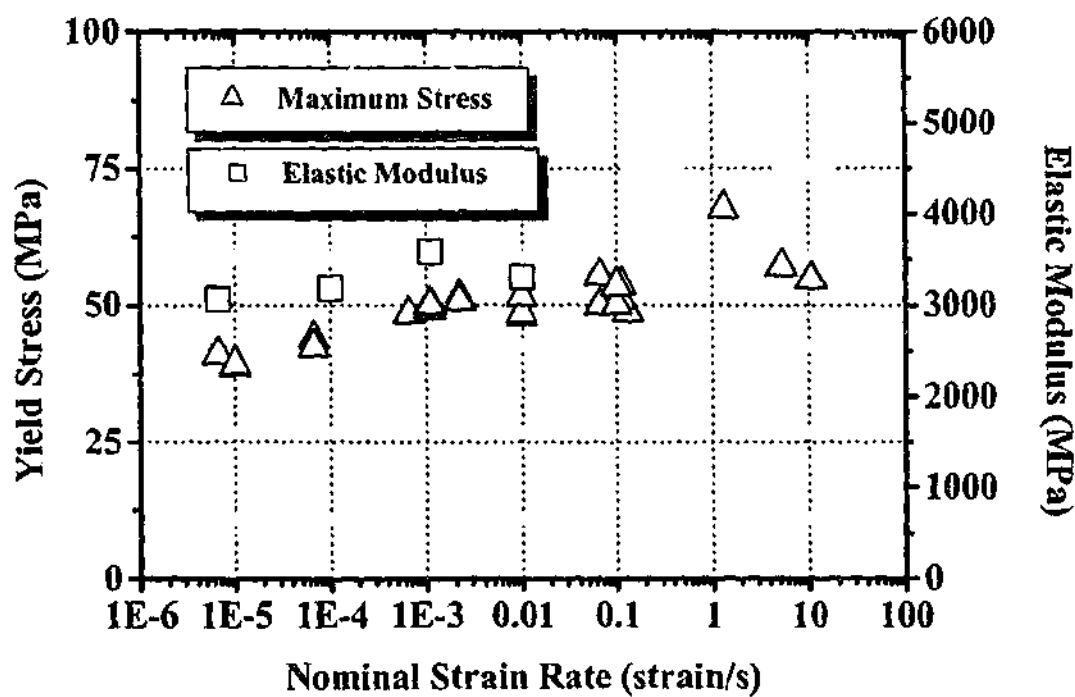


Figure 5.4: Tensile data for PS over a range of strain rates.

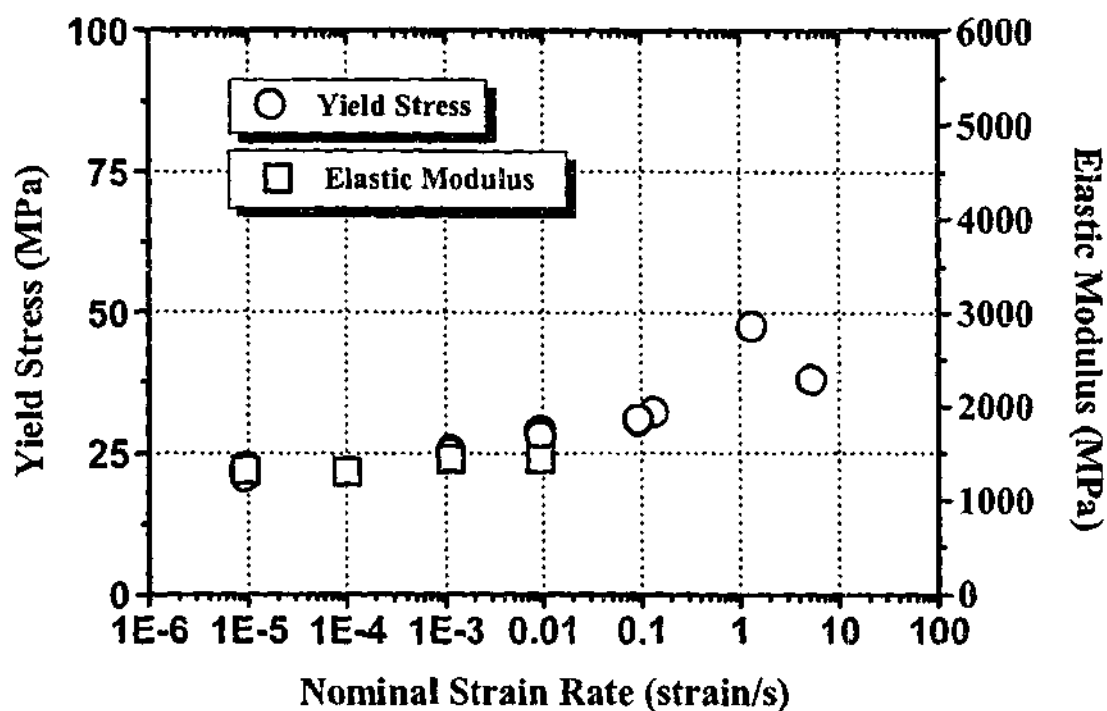


Figure 5.5: Tensile data for CB625 over a range of strain rates.

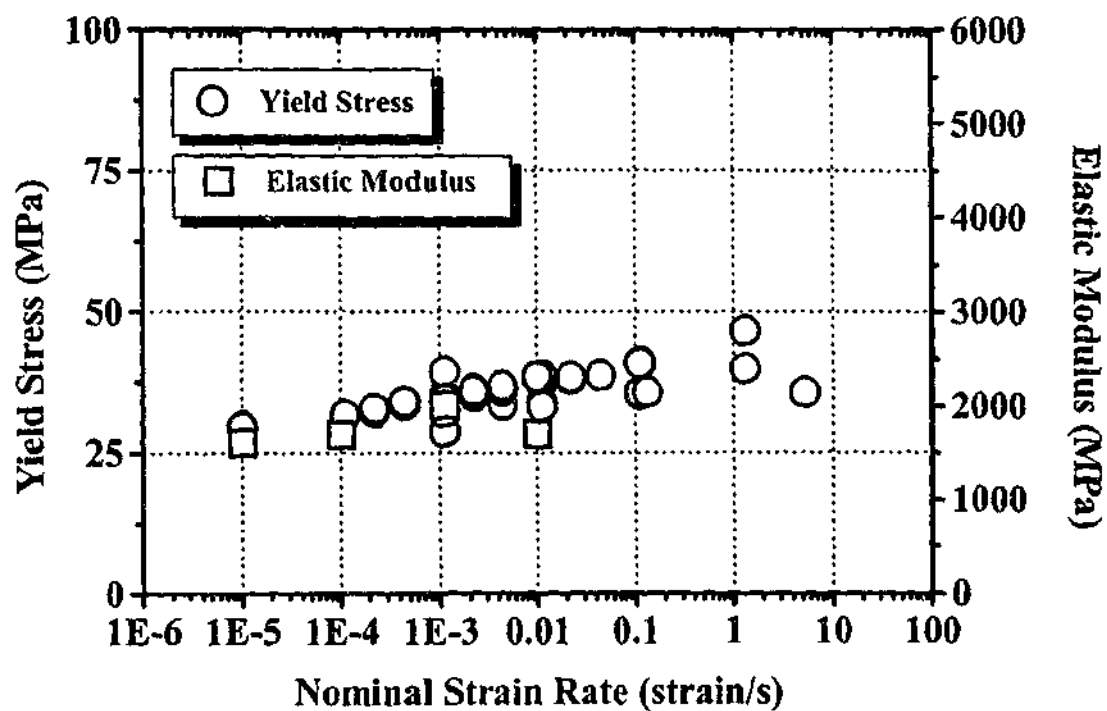


Figure 5.6: Tensile data for Astalac M120 over a range of strain rates.

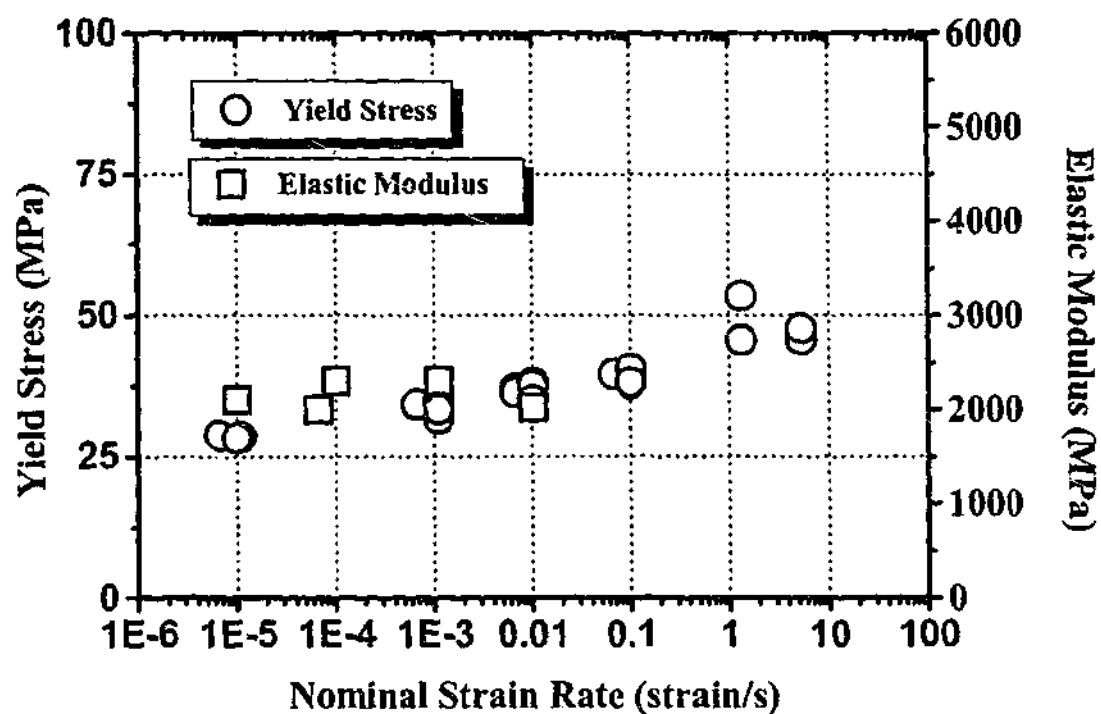


Figure 5.7: Tensile data for Astalac DMT over a range of strain rates.

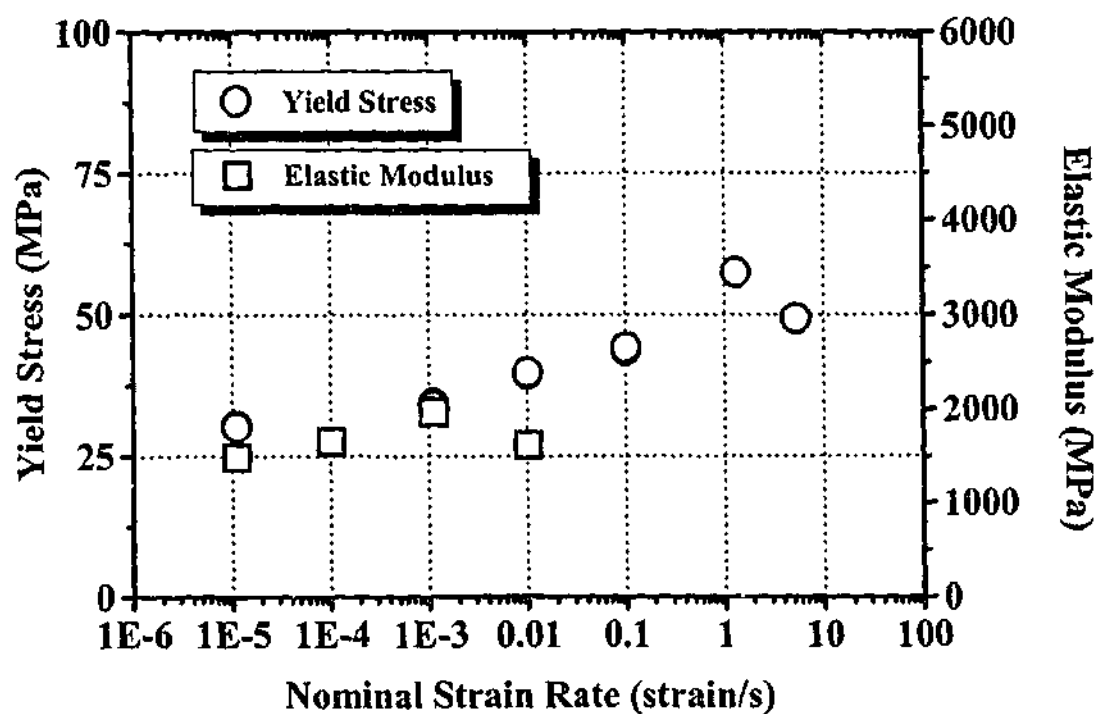


Figure 5.8: Tensile data for ABS/PET over a range of strain rates.

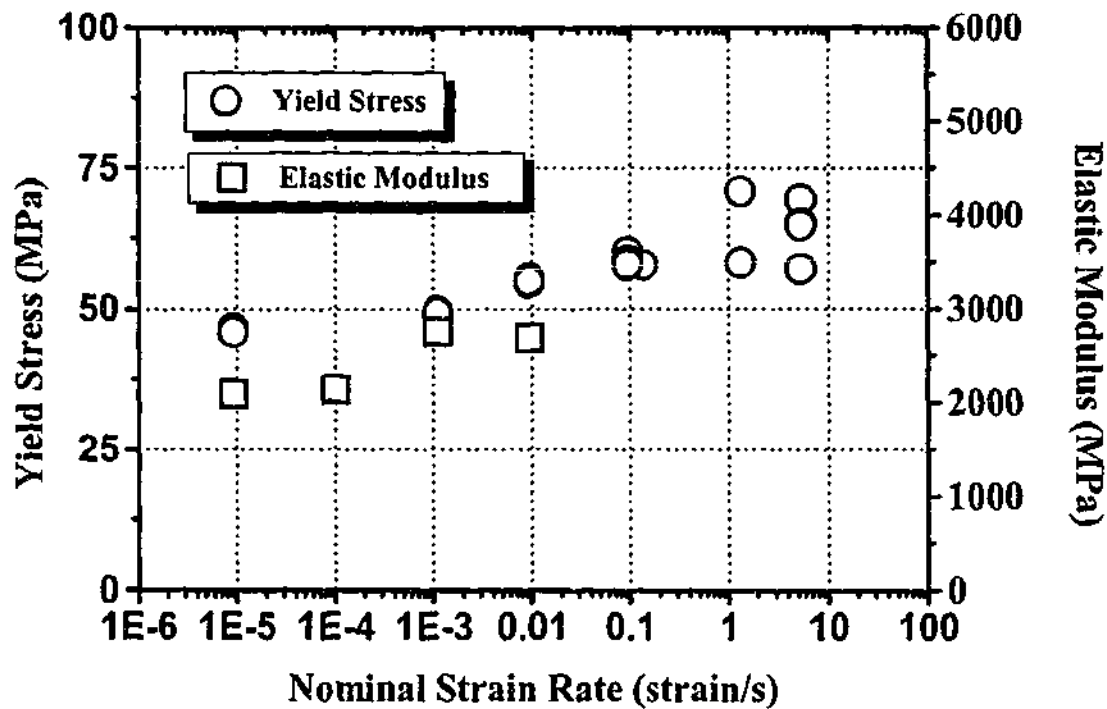


Figure 5.9: Tensile data for ABS/PC over a range of strain rates.

5.2.4 Impact and Izod

The impact energy, as measured using a falling dart test, and Izod values for the materials considered were plotted in order of increasing impact energy - shown by Figure 5.10. The brittle polymer PS absorbed the least energy whilst PC absorbed the greatest amount.

Except for CB625 and PC, the other six materials show an increase in notched Izod energy for increasing impact energy. Referring to Figure 5.10, there is a drop in notched Izod energy for CB625 and PC. This suggests that both these materials exhibit some degree of notch sensitivity.

CB625 is an ABS and the phenomenon of notch sensitivity seems not to be reported in the literature. Cheng (1995) has noted this sensitivity by studying the fracture behaviour of toughened PC with notches of different radius of curvatures. He found that a sharp notch could decrease the fracture strength of toughened PC.

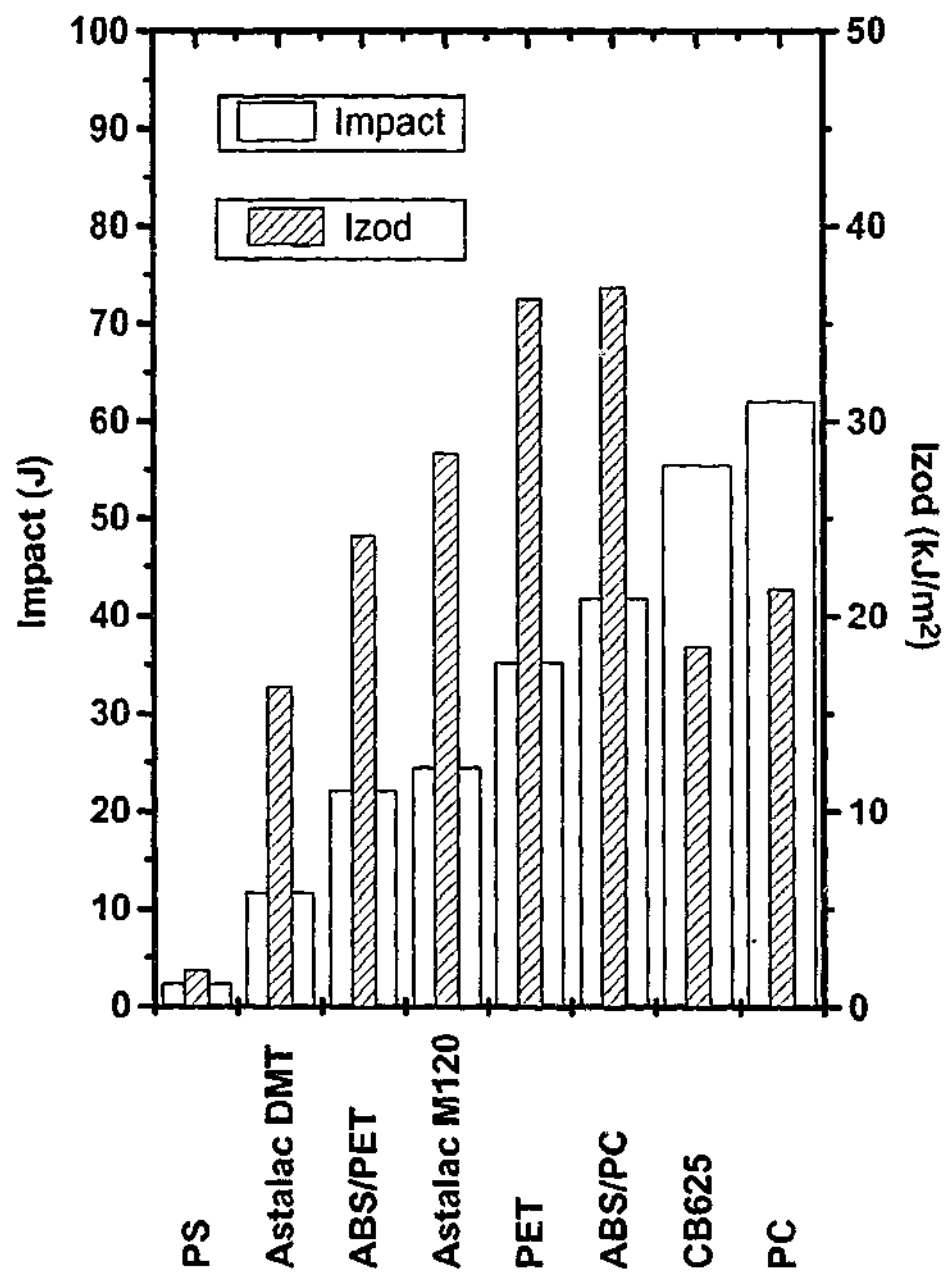


Figure 5.10: Results of impact tests and notched Izod tests for all materials studied.

Chapter 6

Comparison of Experimental and Predicted Failure Loads for Ductile Polymers

6.1 Fracture Toughness Measurement - SENT Specimens

Single edge notched tensile specimens were used to obtain the parameters K_{Ic} and ρ . SENT specimens were chosen because they are easy to manufacture by the injection moulding process. The thickness is also comparable to the majority of articles produced by this manufacturing technique. Plaques were notched to various crack lengths and tested on a tensometer as described in Chapters 4.2.5 and 4.2.6 and the experimental points were plotted. Using LEFM, a curve of best fit was plotted to the data with the equation

$$\sigma_u = \frac{K_{Ic}}{(Y)(\sqrt{W})\sqrt{\pi \frac{a}{W}}} \quad (6.1)$$

where Y is defined by eq. 3.13 and the adjustable parameter was K_{Ic} . The plane strain fracture toughness, for thick specimens, is normally given the label K_{Ic} . In this thesis, K_{Ic} is the nomenclature given to the fracture toughness as measured by the SENT specimens.

For the effective crack tip blunting methodology, the same procedure was followed except the equation used was

$$\sigma_u = \frac{\sigma_y}{\left\{ 1 + 2 \left[\left(\sqrt{\frac{W}{\rho}} \right) \left(\sqrt{\frac{a}{W}} \right) \right] \right\} (Y)} \quad (6.2)$$

where Y is once again defined by eq. 3.13 and the adjustable parameter was ρ .

In order to ensure that K_{Ic} and ρ were parameters that could be used safely in design, the curve fits were subject to the following restrictions. The "usual" curve fitting routine is the minimisation of the error function ξ^2 where

$$\xi^2 = \sum_{i=1}^{I=11} [y(x_i) - y_i]^2 \quad (6.3)$$

and $y(x_i)$ is the value predicted by the function and (x_i, y_i) is the experimental point. In this particular case, the function $y(x_i)$ is given by either eq. 6.1 or 6.2. Each of the equations has one variable parameter (K_{Ic} or ρ respectively) which can alter the value of $y(x_i)$.

A spreadsheet was constructed that summed the error generated between eq. 6.1 or 6.2 using various values of K_{Ic} and ρ and experimental data, for a number of crack lengths (i.e. x_i). An additional constraint was also put on the error comparison procedure which states that if

$$\frac{y(x_i)}{y_i} > T, \quad (6.4)$$

then the "penalty" error generated would be E^* rather than $(y(x_i) - y_i)^2$. In this work T has been chosen to be 0.9 and E^* was 10^6 . Allowing for this additional constraint, K_{Ic} and ρ were iterated, the errors were summed for a range of x_i and the total was minimised. The parameters, K_{Ic} and ρ , obtained by this manner are safe design values because the curve fits are forced to be entirely below the experimental failure loads.

This procedure effectively builds a safety factor into the K_{Ic} and ρ values obtained, so that for subsequent fracture/failure predictions a safety margin is already included.

The curve fitting procedure is also not equivalent to the process of dividing the curve of best fit by a safety factor. Instead, it chooses a curve from a family of K_{Ic} or ρ curves that is below all the experimental data and also minimises the error. In practice, the procedure adopted here is not vastly different to dividing by a safety factor $1/T$, but the method used ensures that the curve passes below all experimental points by a margin of $(1-T)$.

Figures 6.1 to 6.8 show the results of the curve fitting for each material studied, ranked from highest K_{Ic} to lowest K_{Ic} . The failure load as evaluated by net section yielding was also plotted as a comparison. Table 6.1 is a summary of the important material parameters and is also tabulated from highest K_{Ic} to lowest K_{Ic} . The values when compared to Table 2.1 are in the range as reported by literature.

Table 6.1: Material parameters, at a nominal strain rate of 0.08 strains/s, used in predicting failure

Material	σ_y (MPa)	E (MPa)	K_{Ic} (MPa m ^{1/2})	r_p (mm)	ρ (mm)
ABS/PC	49	3756	4.2	1.2	195.8
PET	54	2858	3.5	0.7	18.9
ABS/PET	34	2400	3.4	1.6	109.1
Astalac DMT	34	1863	2.9	1.2	211.2
Astalac M120	35	2009	2.8	1.0	100.2
PC	64	2058	2.7	0.3	3.9
CB625	25	2027	2.4	1.5	194.3
PS*	50	3165	2.0	0.3	2.5

* For cases where the material fails without yielding, the ultimate tensile stress is taken to be the yield stress.

Table 6.1 also includes Irwin's plastic zone size for each material studied, as defined by Eq. 3.4a. They are listed in the second last column. The plastic zone size is important in this comparative study because the crack size is assumed to be longer with the addition of r_p . Therefore the predicted loads are the lowest possible.

The trend represented between the proposed material parameter ρ and the plastic zone size r_p is that materials that are able to accommodate sharp cracks by blunting the end of the crack, tend to exhibit larger values of ρ and r_p when compared to brittle materials.

Importantly Table 6.1 shows that r_p and ρ are not equal. ρ is a theoretical radius of curvature which models the behaviour of cracks formed in ductile polymers due to a variety of mechanisms as opposed to the size of the plastically yielded material in front of the crack as given by r_p .

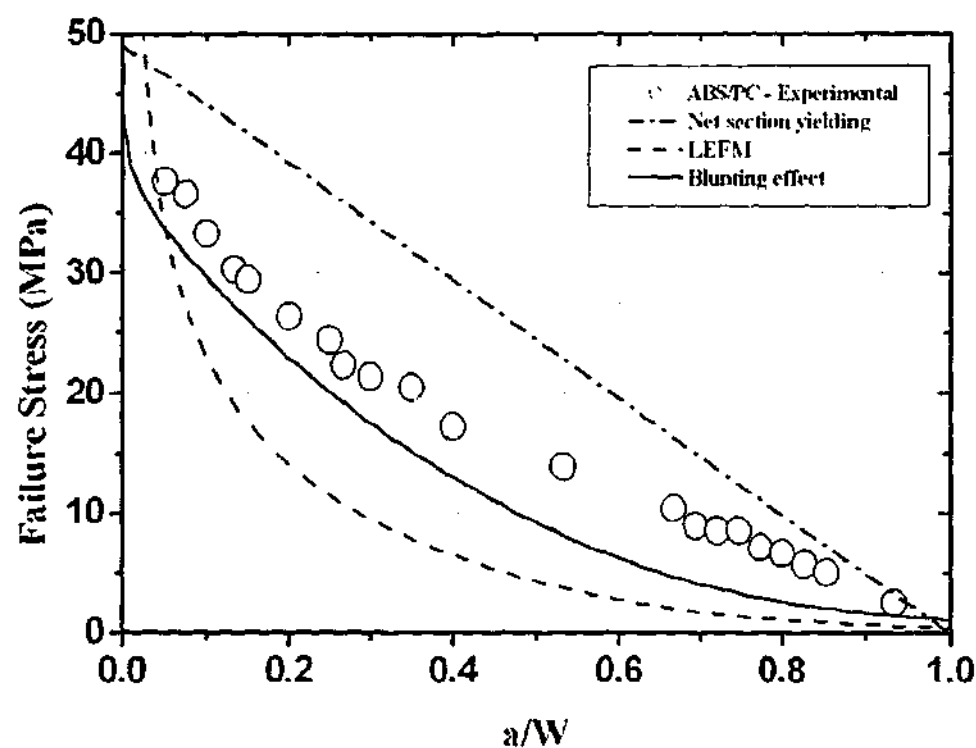


Figure 6.1: Determination of elastic failure parameters for ABS/PC.

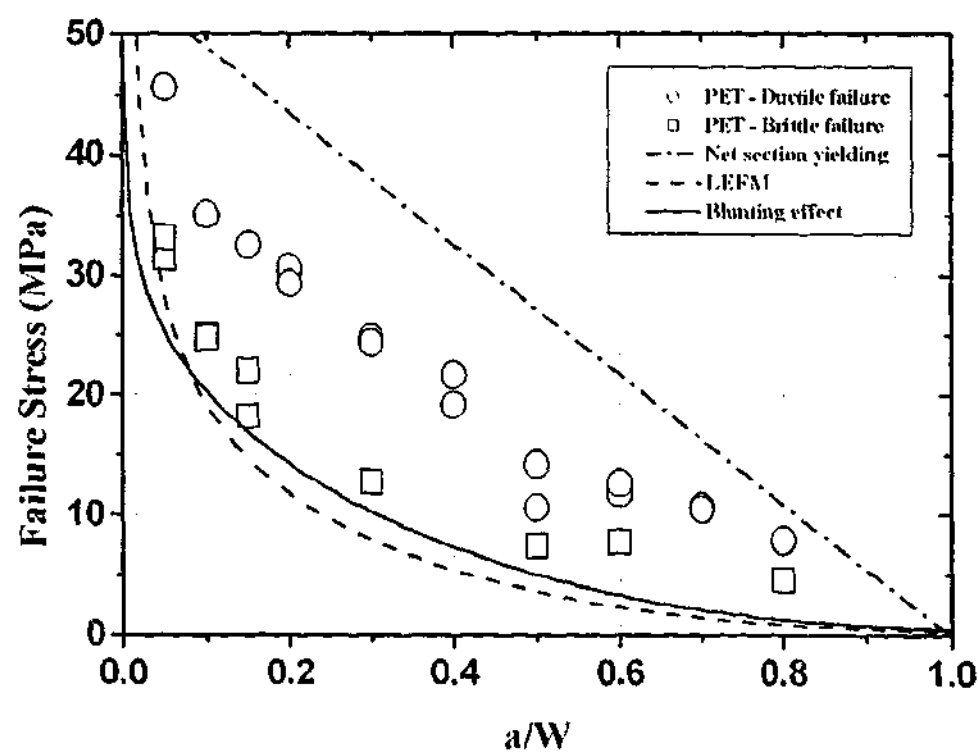


Figure 6.2: Determination of elastic failure parameters for PET.

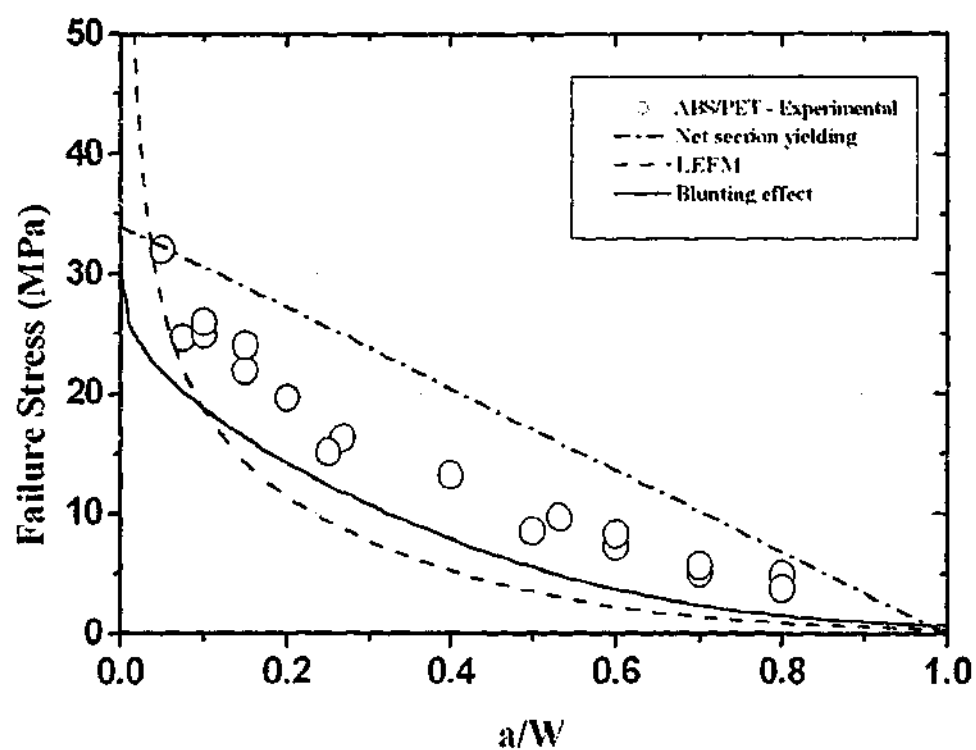


Figure 6.3: Determination of elastic failure parameters for ABS/PET.

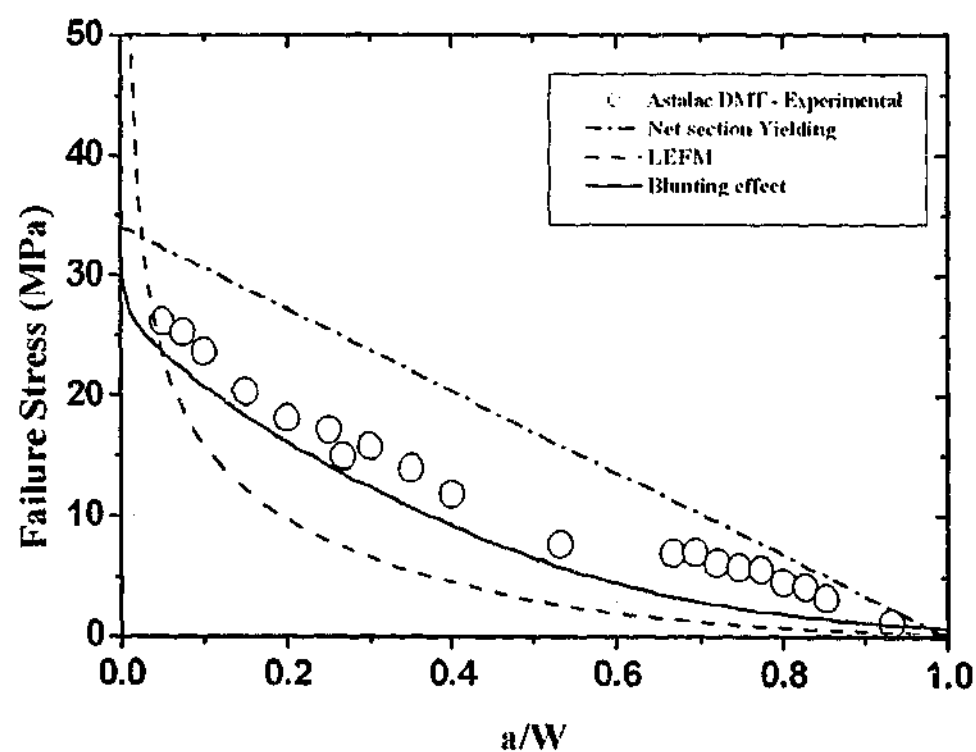


Figure 6.4: Determination of elastic failure parameters for Astalac DMT.

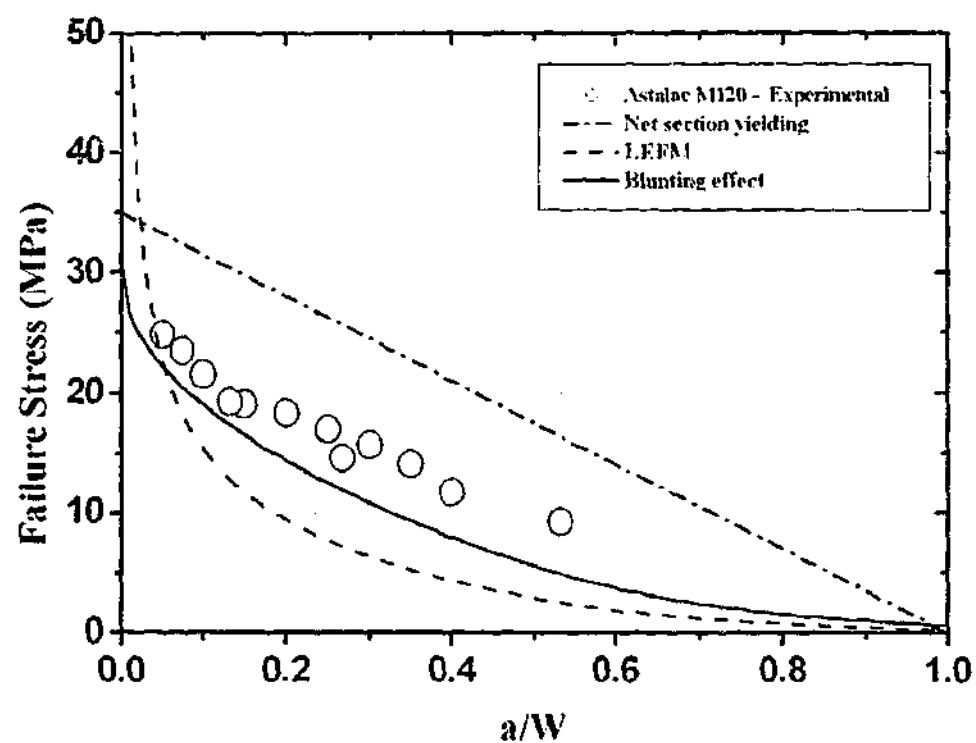


Figure 6.5: Determination of elastic failure parameters for Astalac M120.

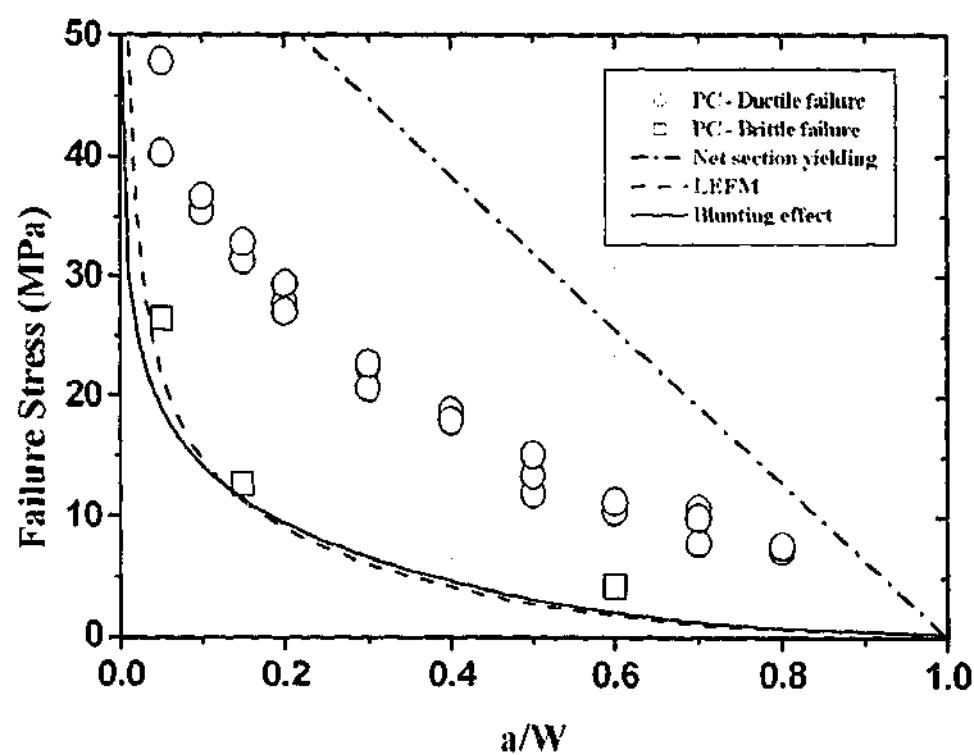


Figure 6.6: Determination of elastic failure parameters for PC.

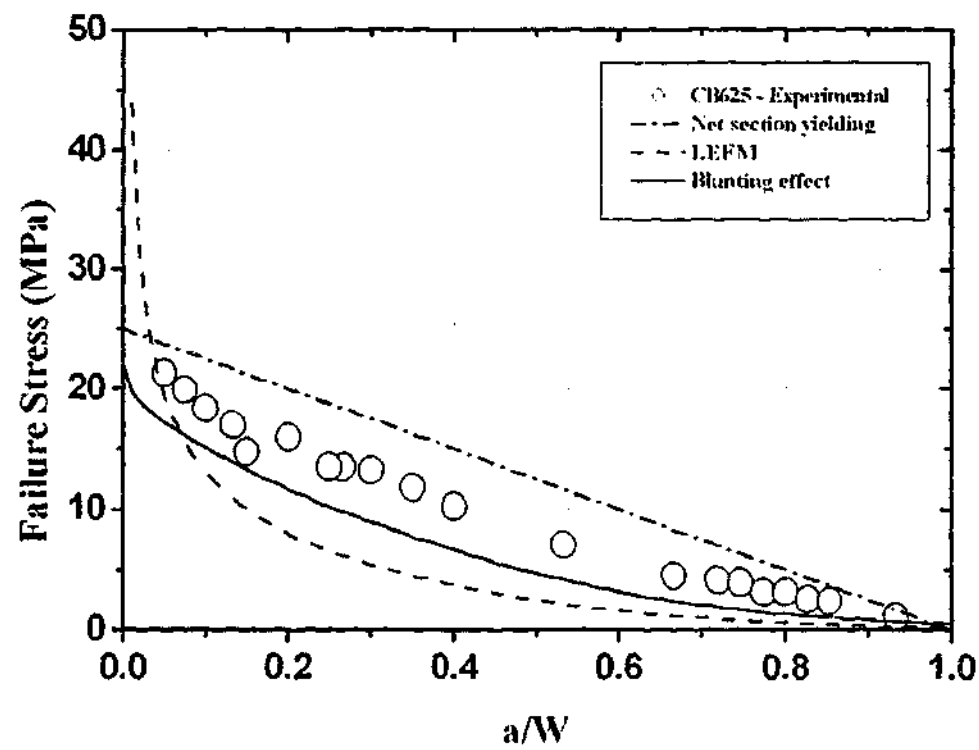


Figure 6.7: Determination of elastic failure parameters for CB625.

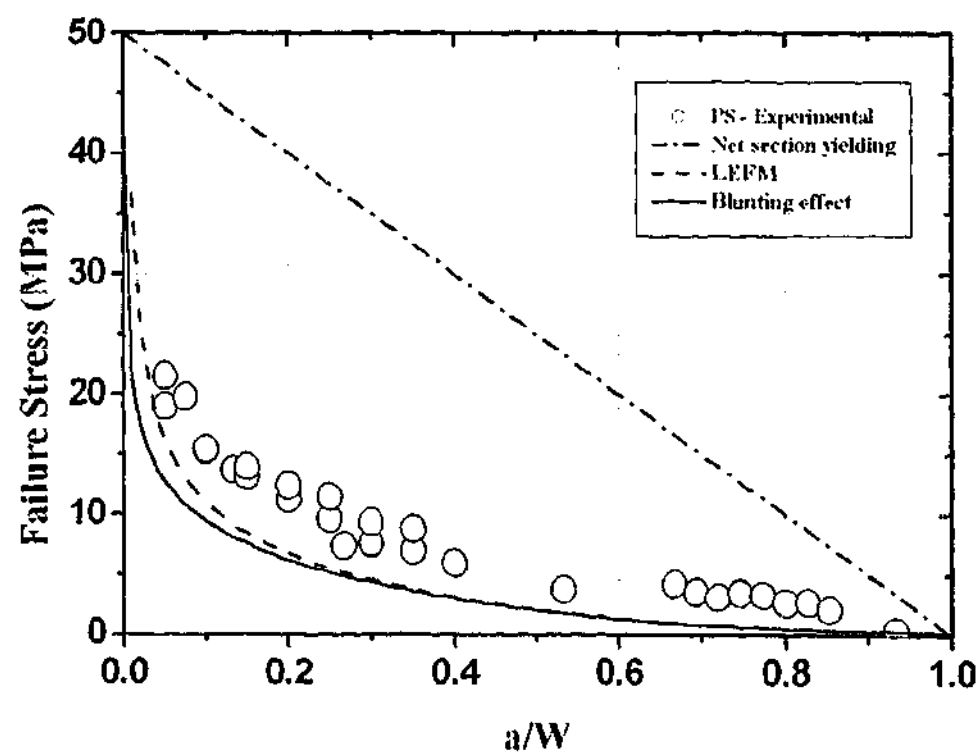


Figure 6.8: Determination of elastic failure parameters for PS.

Importantly for all materials, the curve plotted using the blunting effect methodology provided a good even fit to the experimental data. LEFM also provided a good fit for PET, PC and PS (Figures 6.2, 6.6 and 6.8 respectively) but for the other materials, it predicts much lower loads than the crack blunting method after a/W of 0.1. The net section yielding curve did not follow the experimental data.

Furthermore, PC and PET exhibit brittle failure for some specimens. This is shown by the square shaped data points in Figures 6.2 and 6.4. These few specimens gave lower fracture loads as compared to when they failed in a ductile manner. This in turn lowered the curves of best fit and decreased the adjustable parameters K_{Ic} and ρ .

6.2 Failure Analysis for MHT Specimens

Section 6.1 showed the evaluation of parameters to be used in prediction of more complex injection moulded articles. The values of these parameters are now substituted into the relevant equations to plot prediction curves for MHT specimens. The remote stress required to cause failure by net section yielding is given by Eq. 3.8a used while Eq. 3.12 and 3.16 are used to determine fracture stresses using LEFM and crack tip blunting respectively. The geometric function Y used in Eq. 3.12 and 3.16 is given by Eq. 3.14.

The comparison of predictions by the three methodologies (net section yielding, LEFM and blunting effect) to experimental data are plotted in Figures 6.9 to 6.16.

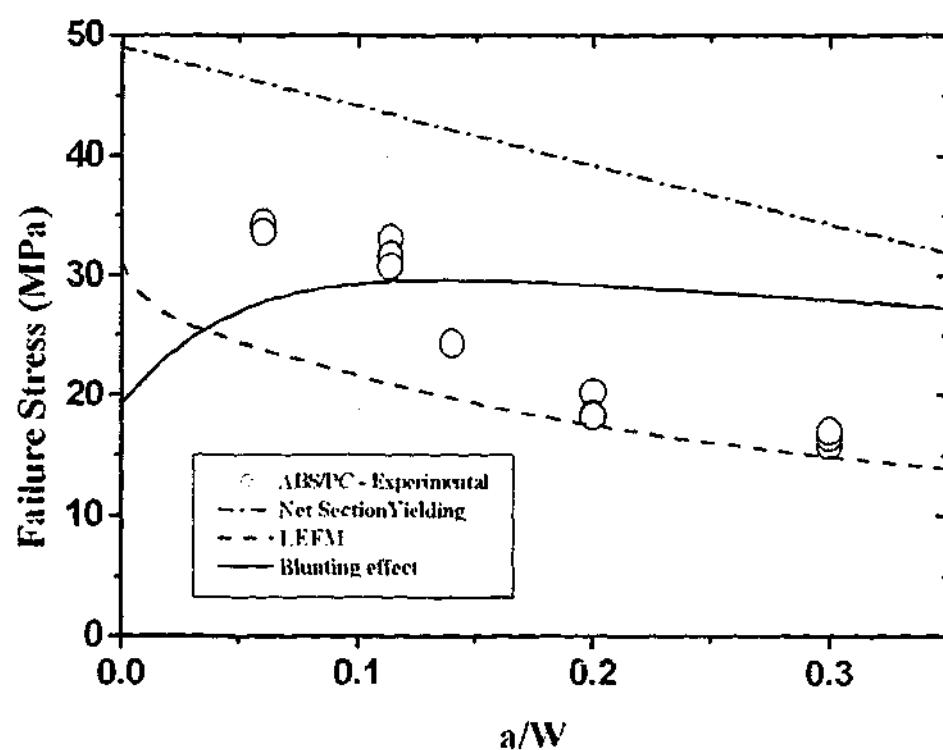


Figure 6.9: Comparison of MHT experimental failure loads and linear elastic predictions for ABS/PC.

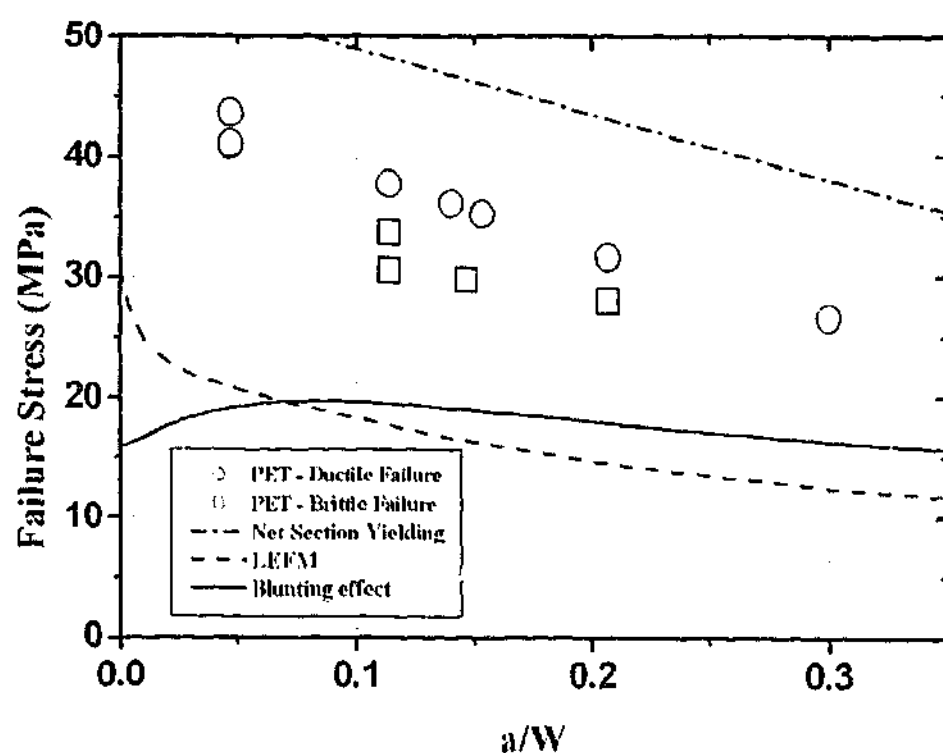


Figure 6.10: Comparison of MHT experimental failure loads and linear elastic predictions for PET.

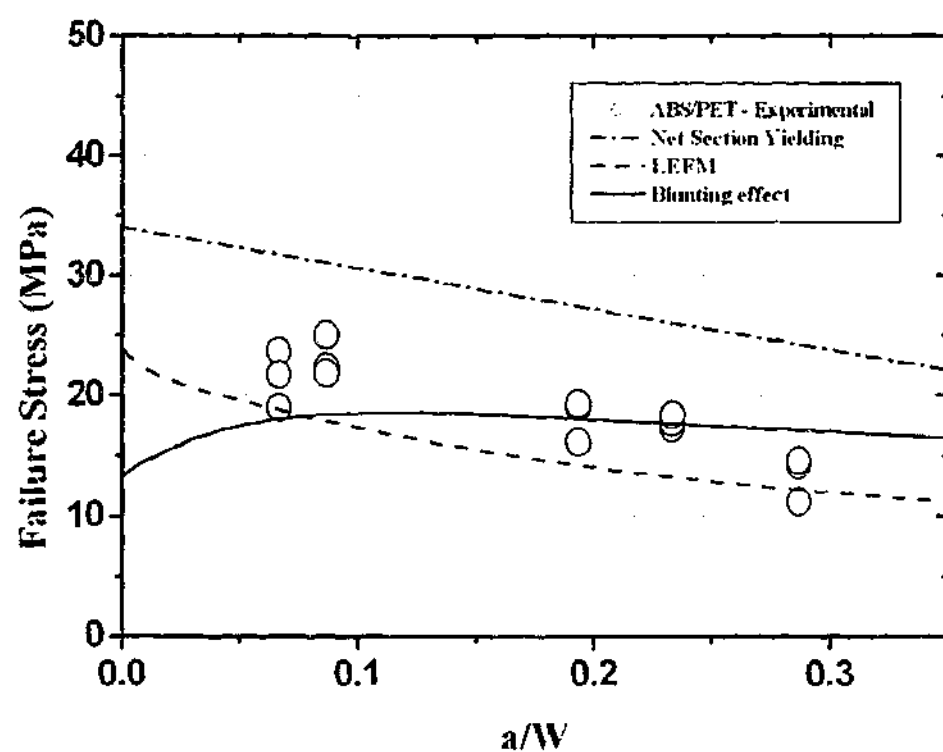


Figure 6.11: Comparison of MHT experimental failure loads and linear elastic predictions for ABS/PET.

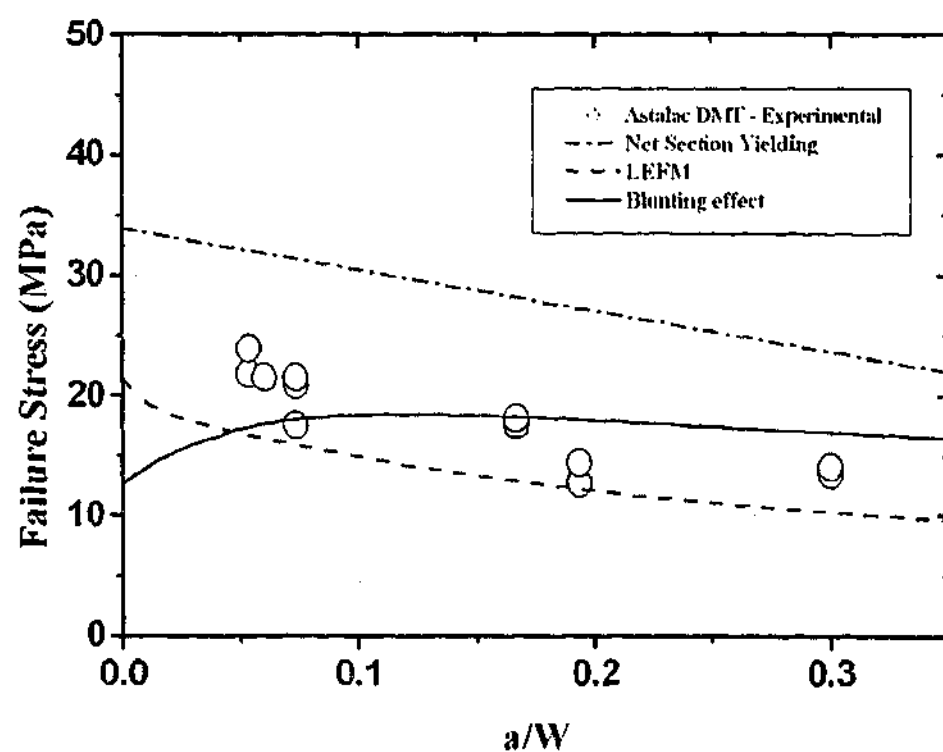


Figure 6.12: Comparison of MHT experimental failure loads and linear elastic predictions for Astalac DMT.

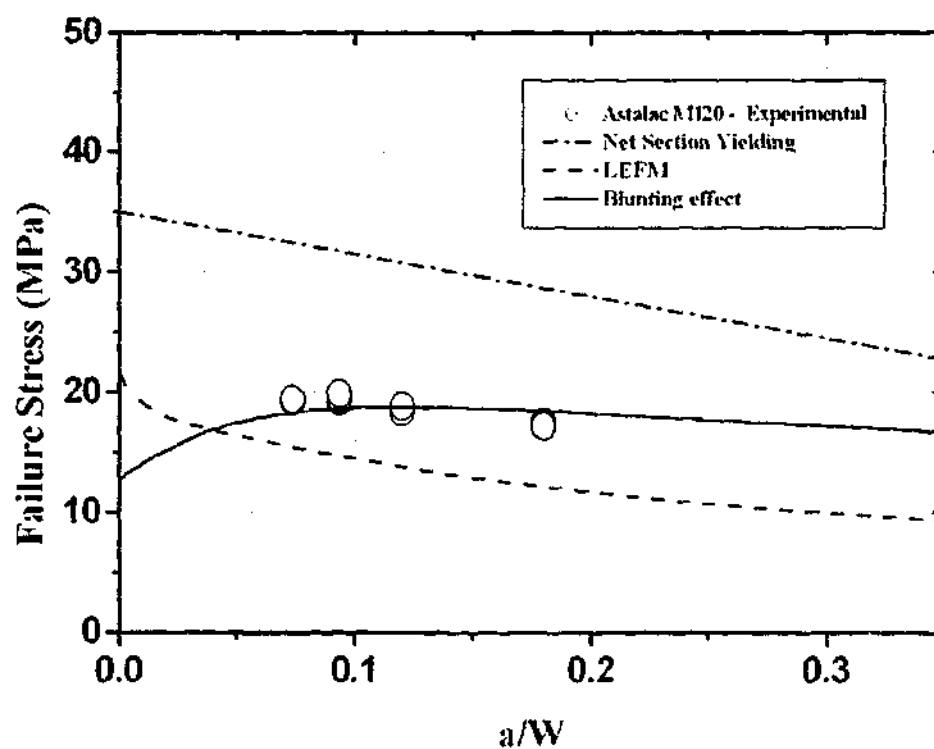


Figure 6.13: Comparison of MHT experimental failure loads and linear elastic predictions for Astalac M120.

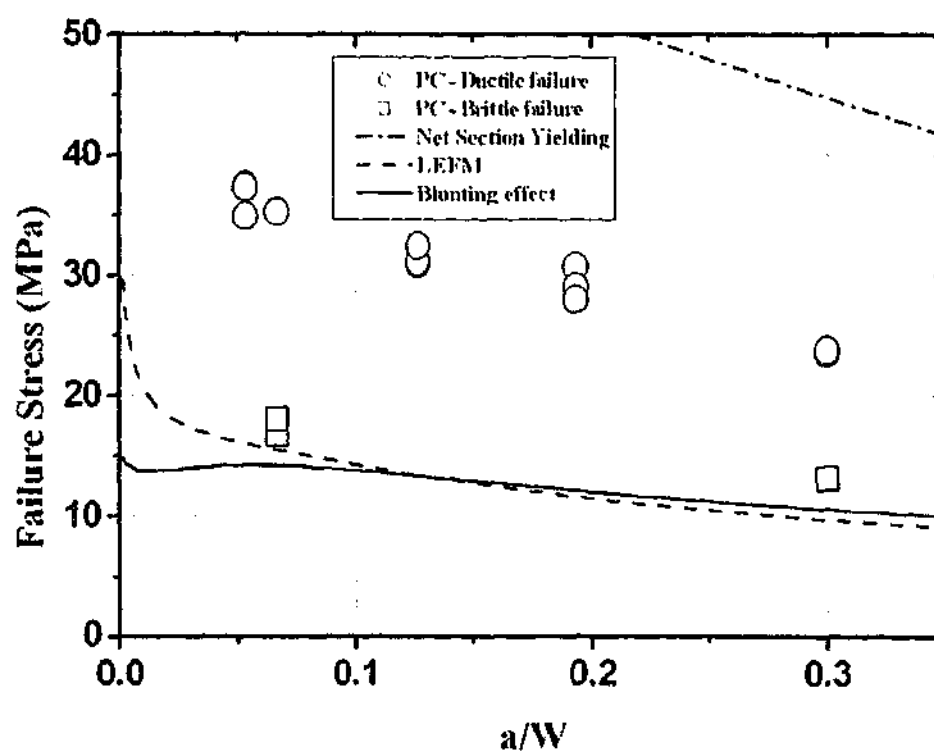


Figure 6.14: Comparison of MHT experimental failure loads and linear elastic predictions for PC.

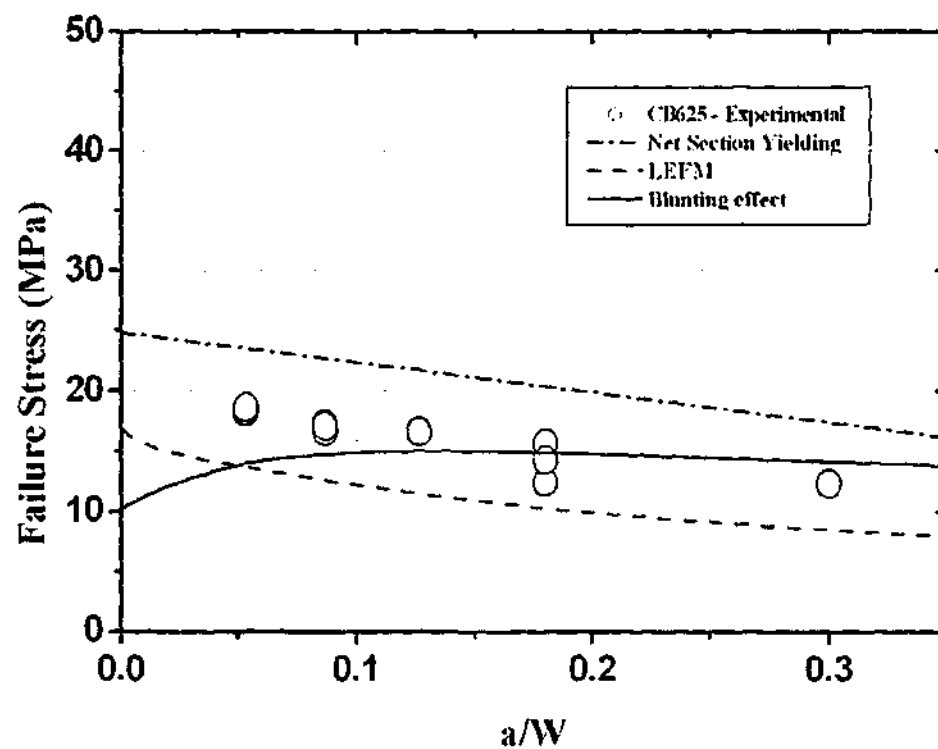


Figure 6.15: Comparison of MHT experimental failure loads and linear elastic predictions for CB625.

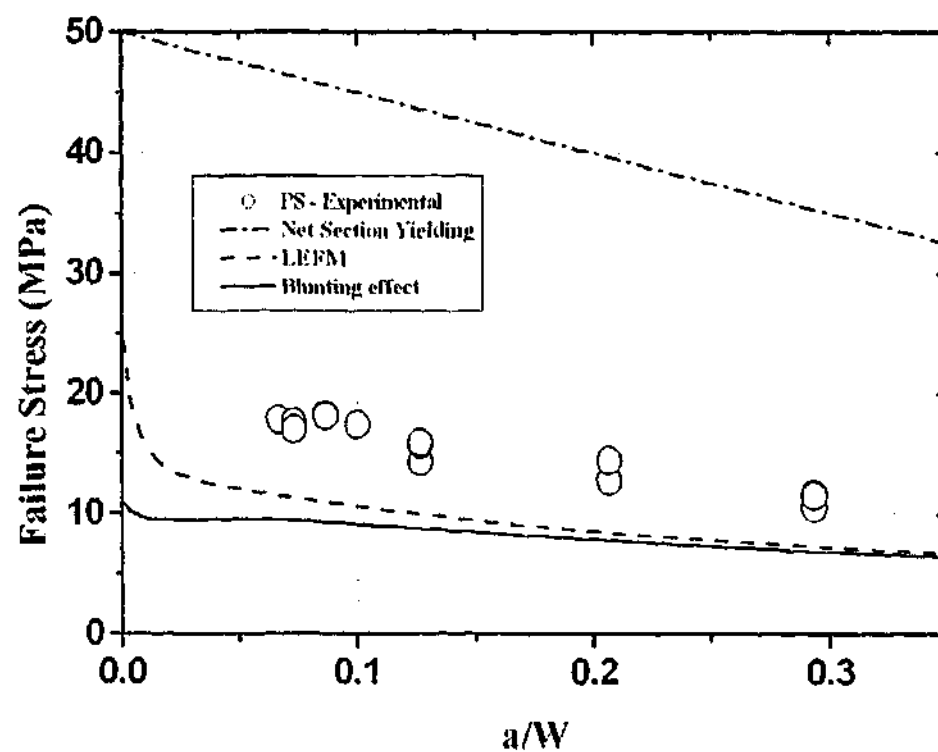


Figure 6.16: Comparison of MHT experimental failure loads and linear elastic predictions for PS.

The MHT results show that for the three grades of ABS, PET and two types of polymer blends, LEFM provides a safe fit for the materials for a/W greater than 0.05. Failure loads predicted by the blunting effect is comparable to LEFM for PC and PS.

Generally, for small crack lengths, the blunting effect provided lower failure loads as compared to LEFM. The results show that by taking the lowest loads evaluated by all three predictive tools, a safe working force can be found for crack lengths up to 20% of its width. Net section yielding predicted loads over experimental data for all four materials.

LEFM and the blunting effect provided a good fit to the MHT data for the three grades of ABS and PS. Once again net section yielding could not be used as a predictive tool because it provided unsafe results.

6.3 Failure Analysis for THT Specimens

The THT specimen is an example where the use of FEA is required. The objective of using finite elements is to analyse the stress distribution within a complicated structure and examine in detail, regions with high stresses. Injected moulded articles are capable of being complex in geometry and an analytical solution may not be possible thus a finite element approach is required.

Figure 6.17 shows the possible mechanisms of failure in a THT specimen. Observations were made on the mode of failure during testing and experimental points in Figures 6.18 to 6.25 indicate the type of failure.

Net section yielding is the first mode of failure to be considered and occurs as mechanism 1 and/or mechanism 3. Prediction of failure using this methodology is discussed in Chapter 3.2.1. In fact, the results from FEA indicates that failure by net section yielding should occur by mechanism 3. Equation 3.10 was chosen as the criterion for yielding except for PS. Polystyrene in tensile tests, had shown brittle behaviour and as a consequence, prediction of failure is calculated by dividing the maximum tensile stress by the maximum principal stress concentration found by FEA.

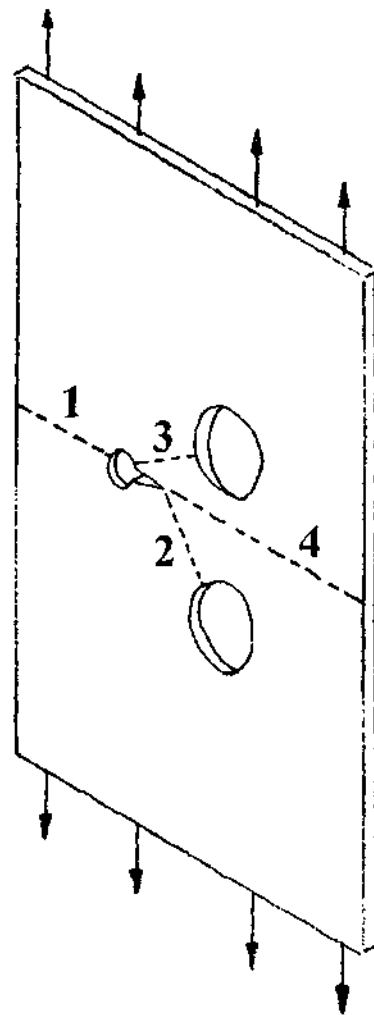


Figure 6.17: Possible process of failure in a THT specimen. 1 – Net section yielding. 2 – Crack extending to larger hole. 3 – Holes linking by yielding and 4 – Crack propagation.

The methodology of applying LEFM and the blunting effect model to THT specimens are described in Chapters 3.2.2 and 3.2.3. Essentially Eqs. 3.12 and 3.16 were used because they include the plastic zone correction and hence would forecast the safest working loads. The geometry parameter Y was found by FEA and is plotted in Figure 3.9. Mechanisms 2 and 4 are possible modes of failure predicted by these two methodologies.

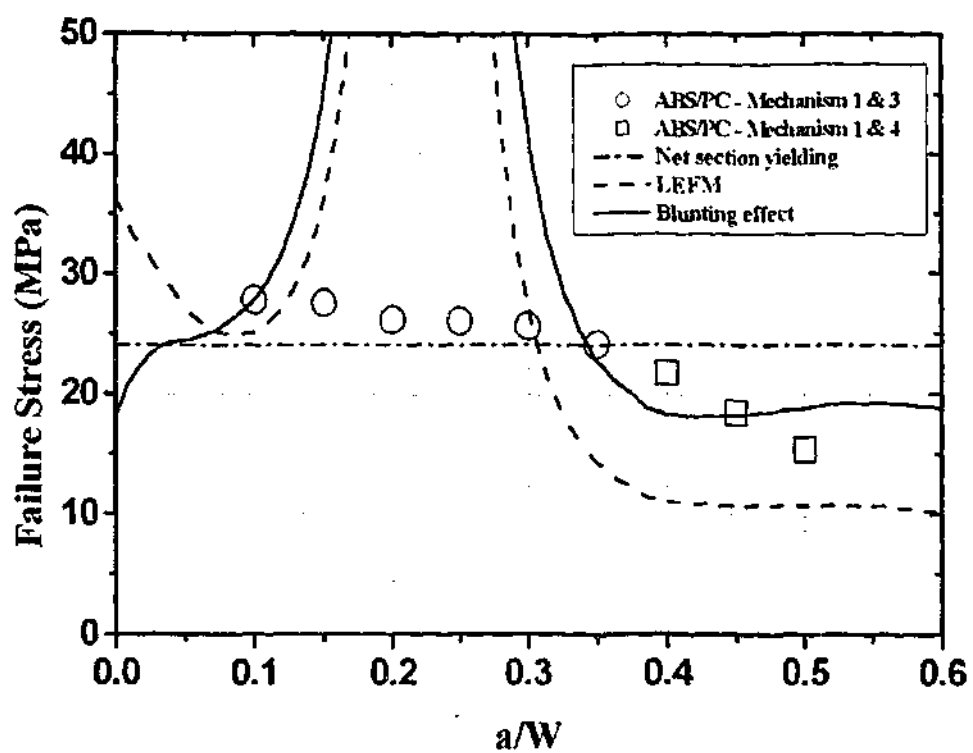


Figure 6.18: THT predicted failure loads versus experimental for ABS/PC.

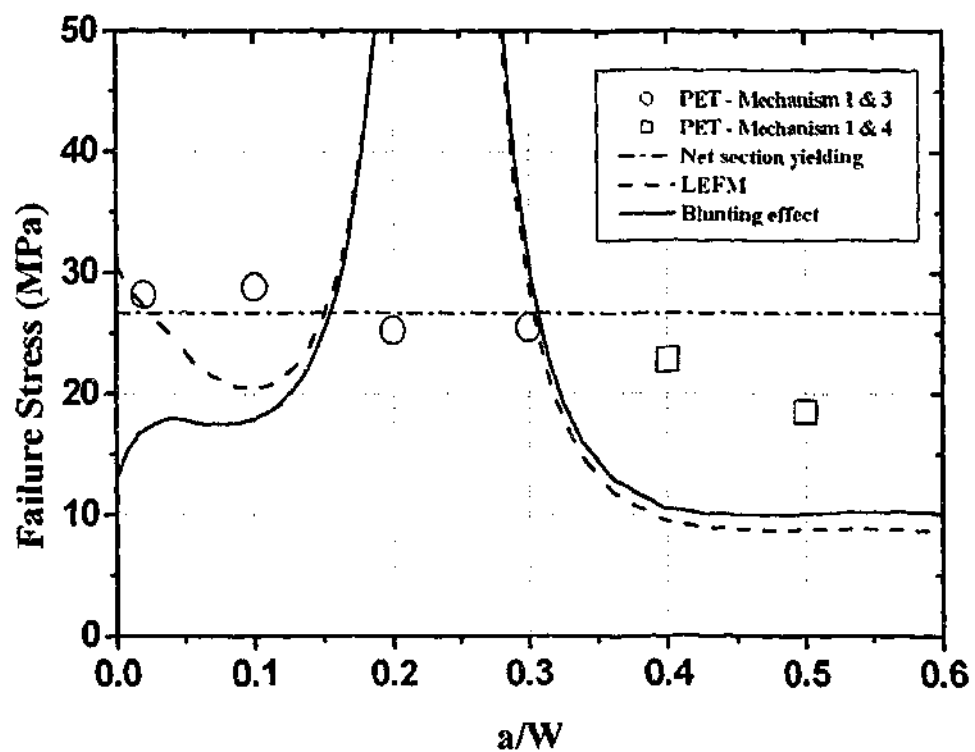


Figure 6.19: THT predicted failure loads versus experimental for PET.

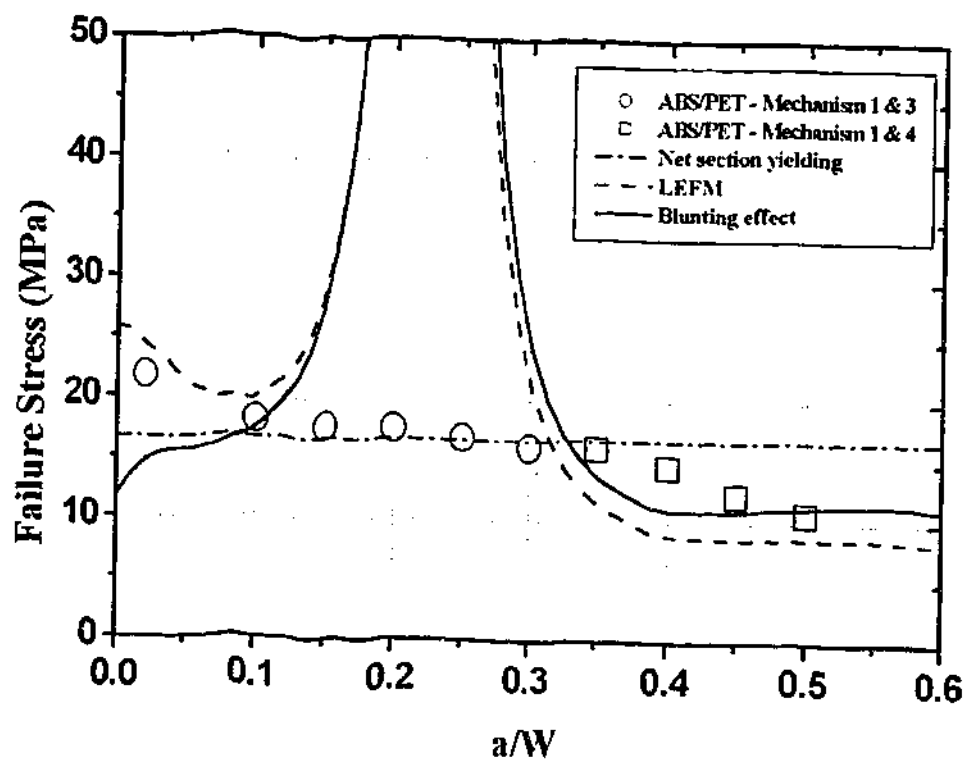


Figure 6.20: THT predicted failure loads versus experimental for ABS/PET.

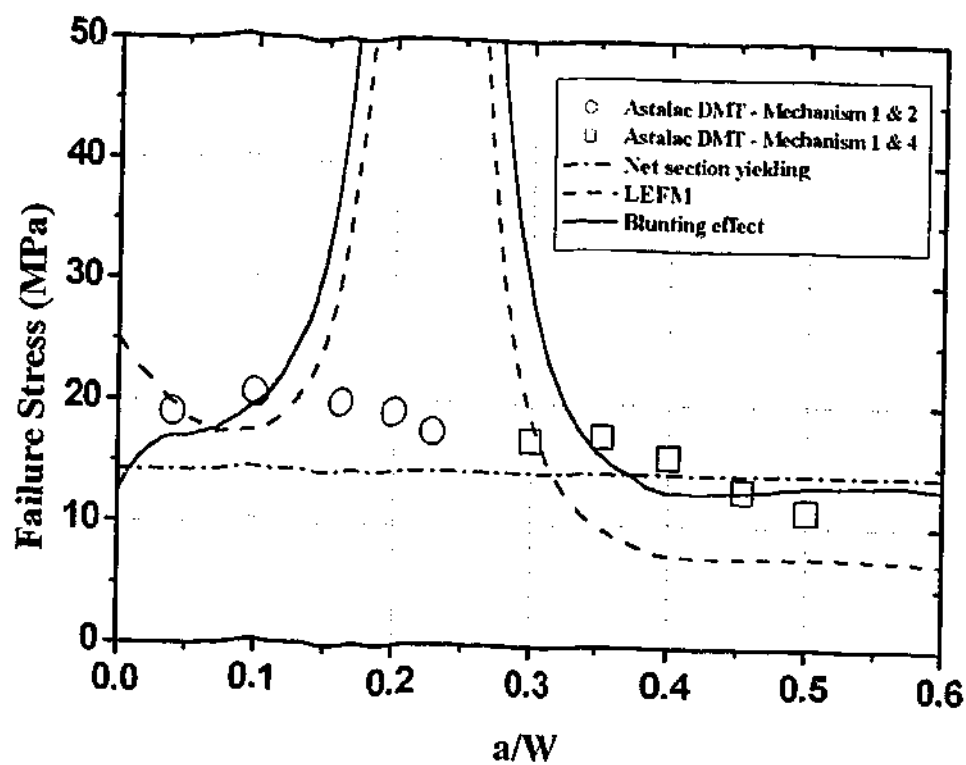


Figure 6.21: THT predicted failure loads versus experimental for Astalac DMT.

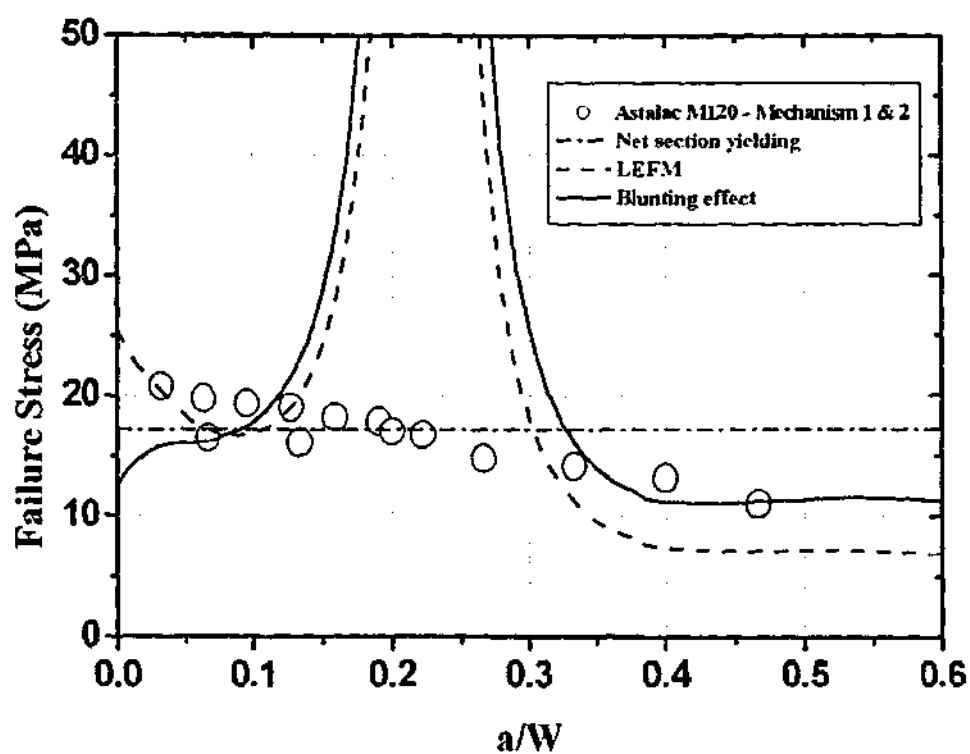


Figure 6.22: THT predicted failure loads versus experimental for Astalac M120.

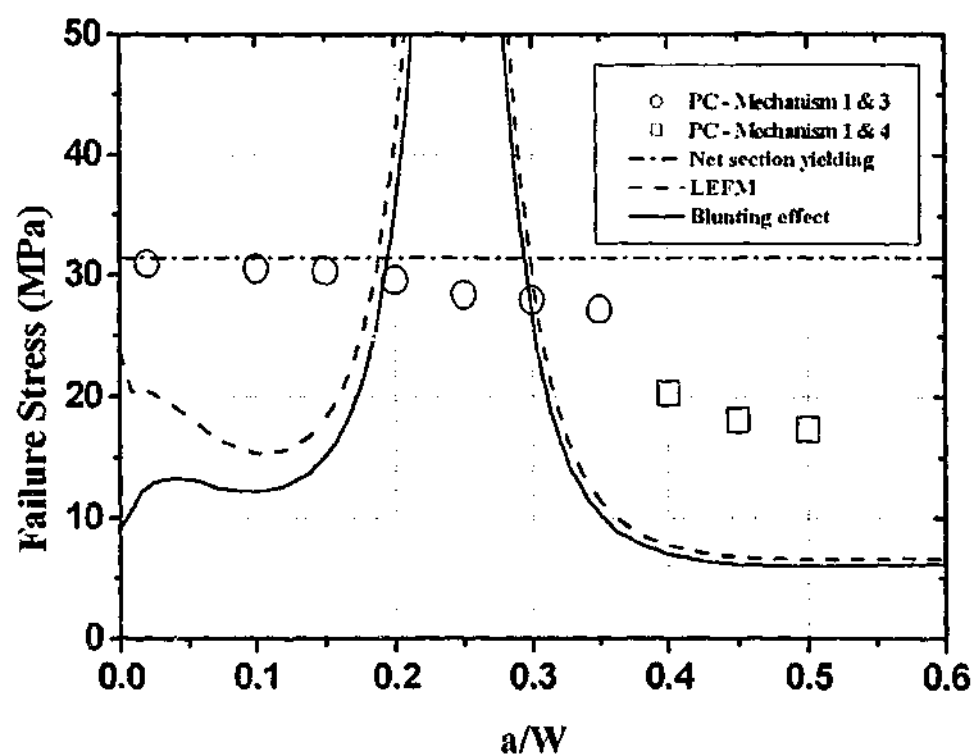


Figure 6.23: THT predicted failure loads versus experimental for PC.

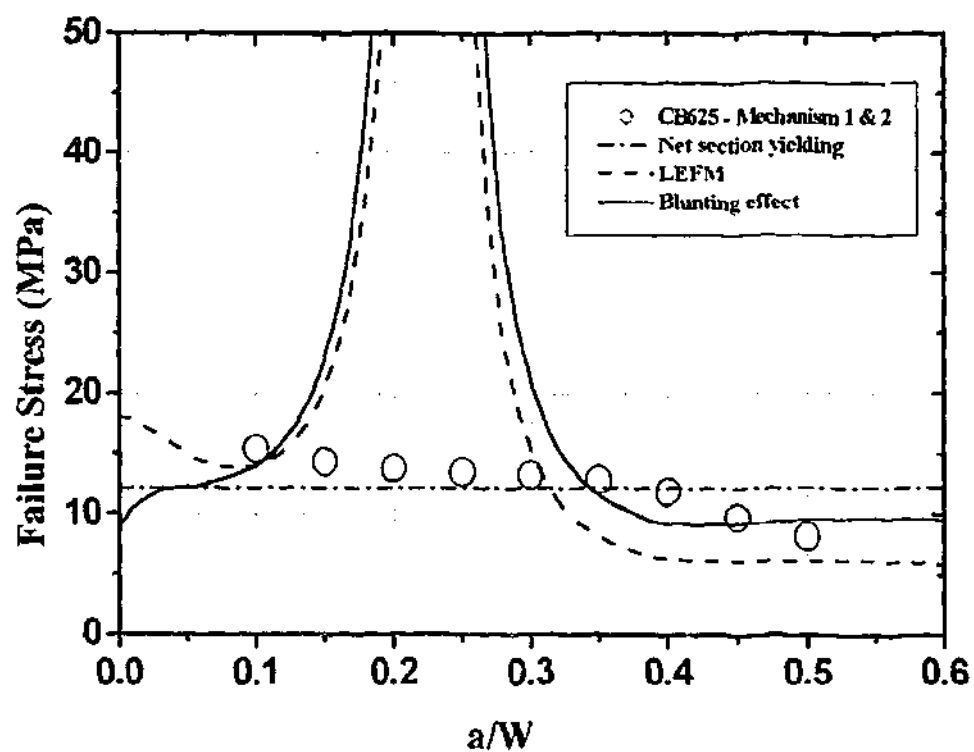


Figure 6.24: THT predicted failure loads versus experimental for CB625.

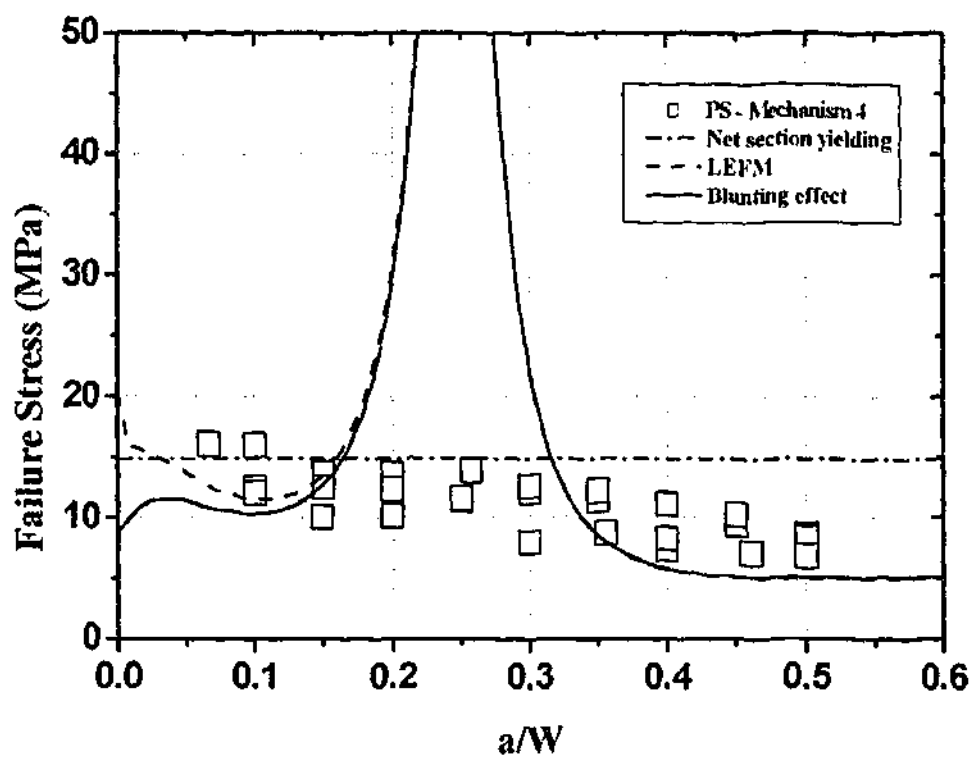


Figure 6.25: THT predicted failure loads versus experimental for PS.

Figures 6.18 to 6.25 show that for tough polymers and polymer blends, the blunting effect consistently gave lower working loads at a/W less than 0.05 when compared to LEFM. Like the MHT specimens, the results show that following the lowest loads as predicted by all three simple predictive tools will give a safe design.

Observations during testing noted that stress whitening occurred simultaneously via mechanisms 1 and 3 for small crack lengths. Stress whitening and necking at the notch was observed even when the crack progressed into the region of lower stresses (i.e. between the two larger holes). In fact, whilst the crack is shielded from the applied stress, predictions made by net section yielding provided a fairly close fit. For longer cracks approaching the edge, stress whitening was found to occur via mechanisms 1 and 4. As the load increased, the crack propagated to the edge.

Figures 6.21, 6.22, 6.24 and 6.25 showed results from experiments and predictions for three grades of ABS and PS respectively. For the ABS materials and at short crack lengths, mechanisms 1 and 2 were the modes of failure. In the case of Astalac DMT, the crack propagated to the edge when the initial crack length was no longer in the area of low stresses whilst fast propagation (mechanism 4) was observed for all crack lengths in PS. Astalac M120 and CB625 showed stress whitening via mechanisms 1 and 2, and for large crack lengths, mechanism 1 was the predominant mode of failure.

Both LEFM and the blunting effect model correlated with experimental data at short crack lengths in areas not shielded by the two larger holes. Predictions by net section yielding were effective in the shielded region for the tough materials whilst PS failure loads were evaluated by dividing the maximum stress found from tensile tests by the maximum principle stress concentration found by FEA.

6.4 Failure Analysis for CT Specimens

In the pin loaded situations (as opposed to uniform loading of the previous three specimens), the blunting effect model is required in predicting failure for crack lengths up till a/W of 0.15. If only net section yielding and LEFM were utilised, failure would occur under the lowest calculated load in PET and ABS/PET (Figures 6.27 and 6.28 respectively).

The predicted curves using LEFM and the effective blunting methodology also show an increase in failure load after $a/W = 0.3$. This cannot be the case in actual fact because as the crack becomes longer, the bending moment effect caused by the load being some distance

away from the tip increases. As a result, the load required for failure should decrease similarly to the net section yielding curve. However the methodology for LEFM and the effective blunting effect was to initially perform a stress analysis on an unnotched specimen. The FE solution (refer to Figure 3.15) shows a decrease in stress concentration away from the loading points because no leveraging effects are present. As stated previously, the consequence for this form of analysis is that it is only valid for short crack lengths

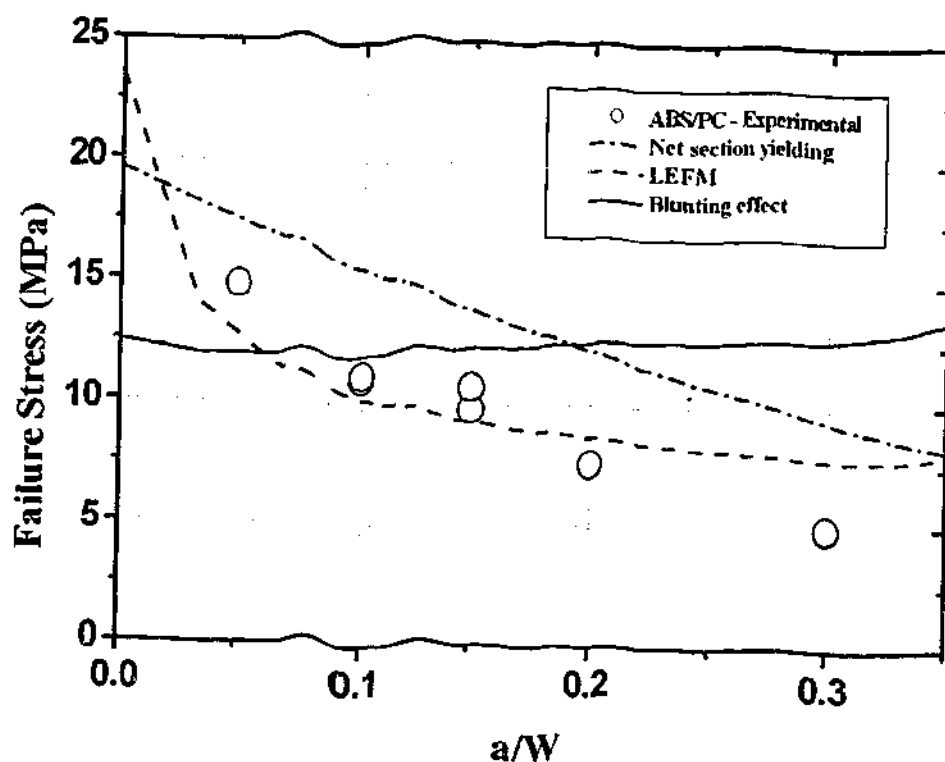


Figure 6.26: Plot of CT predictions versus experimental for ABS/PC.

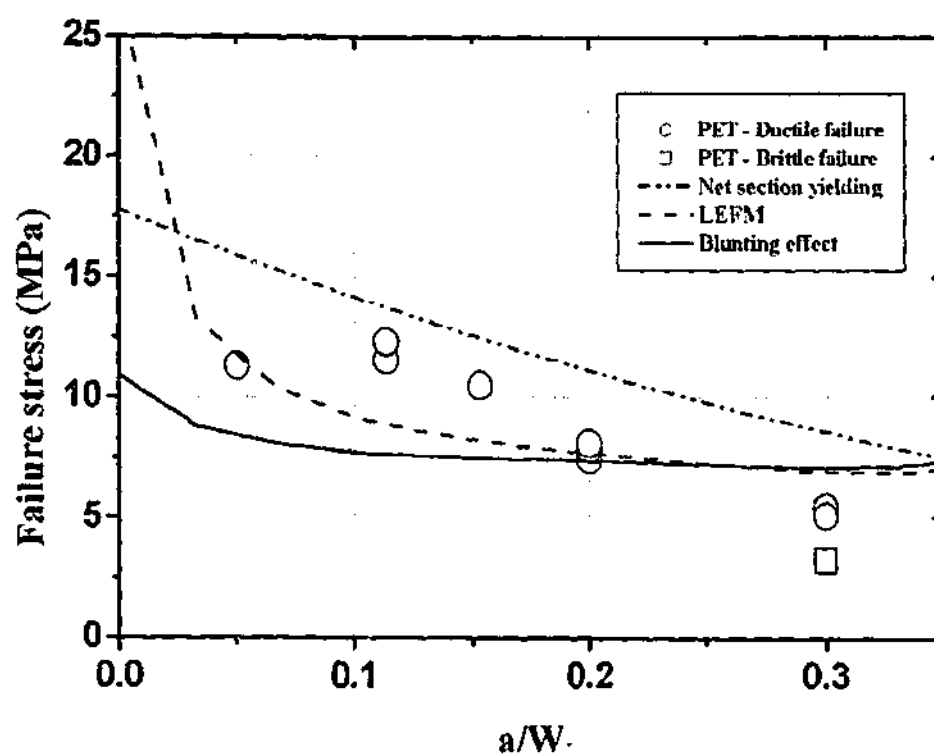


Figure 6.27: Plot of CT predictions versus experimental for PET.

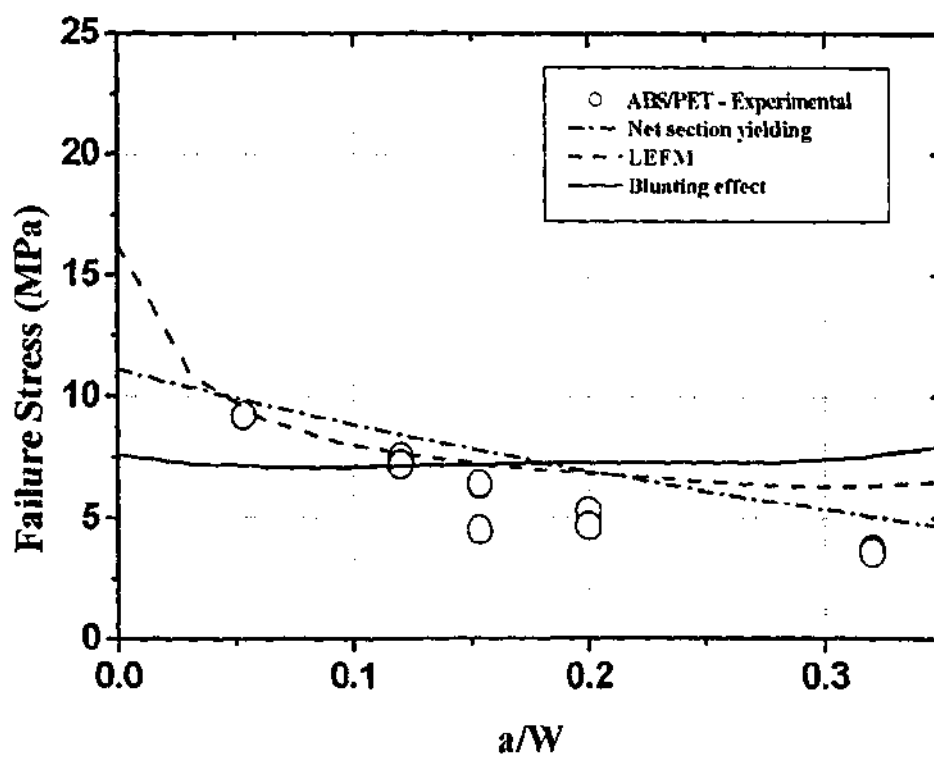


Figure 6.28: Plot of CT predictions versus experimental for ABS/PET.

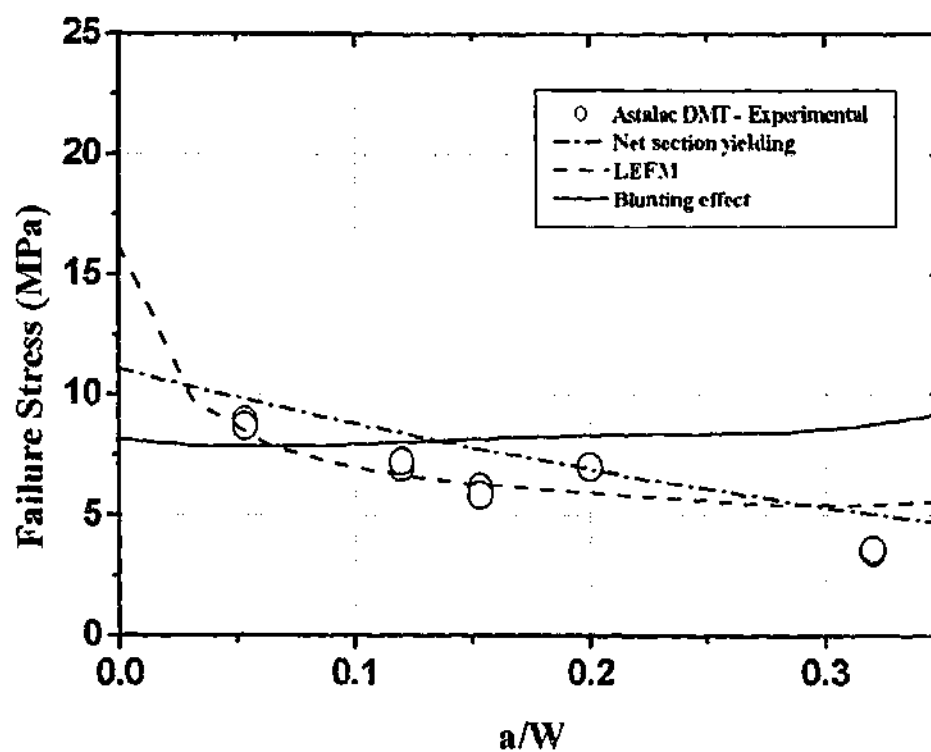


Figure 6.29: Plot of CT predictions versus experimental for Astalac DMT.

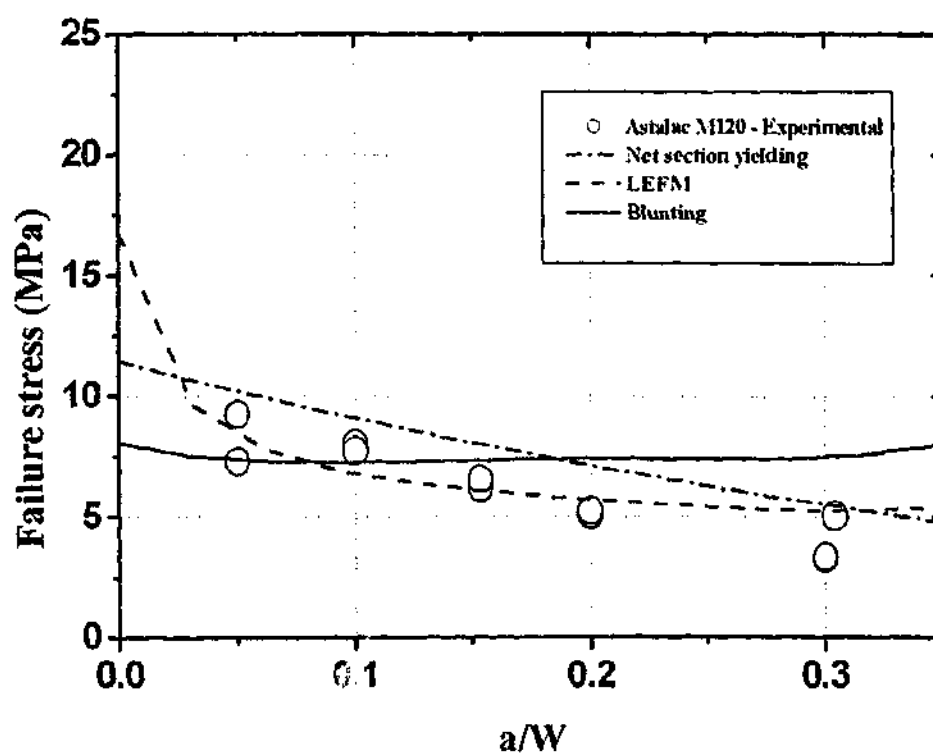


Figure 6.30: Plot of CT predictions versus experimental for Astalac M120.

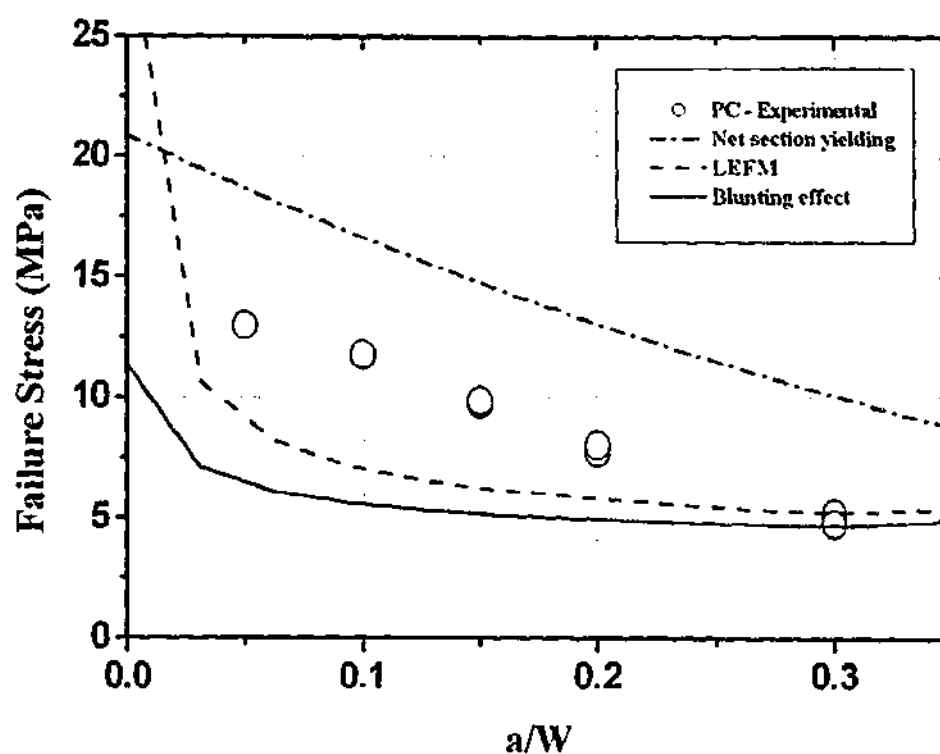


Figure 6.31: Plot of CT predictions versus experimental for PC.

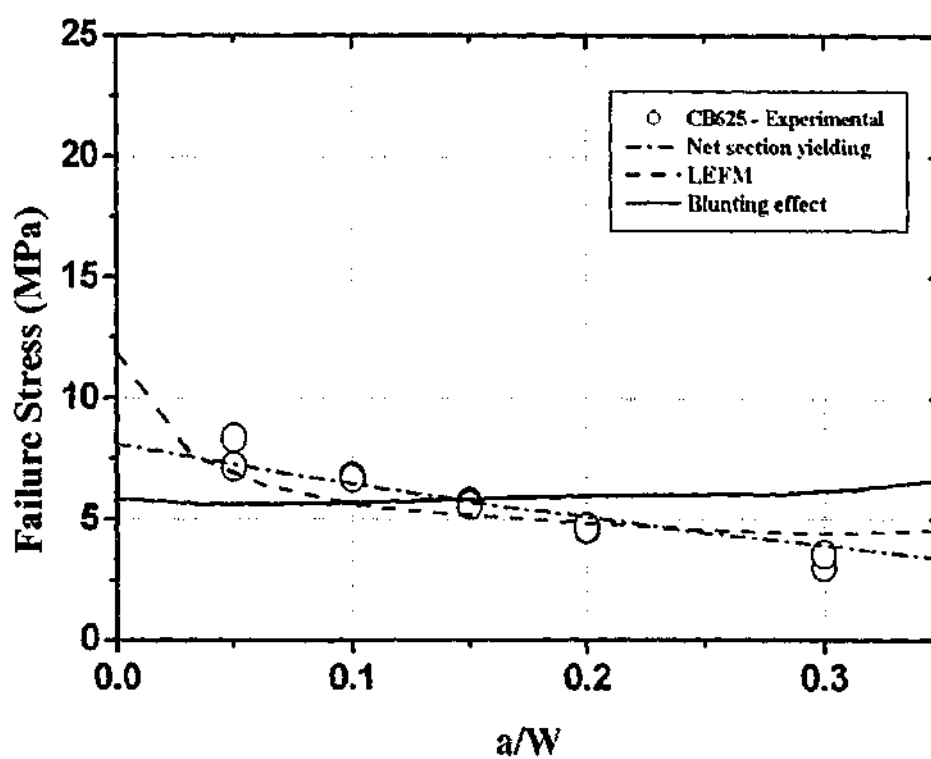


Figure 6.32: Plot of CT predictions versus experimental for CB625.

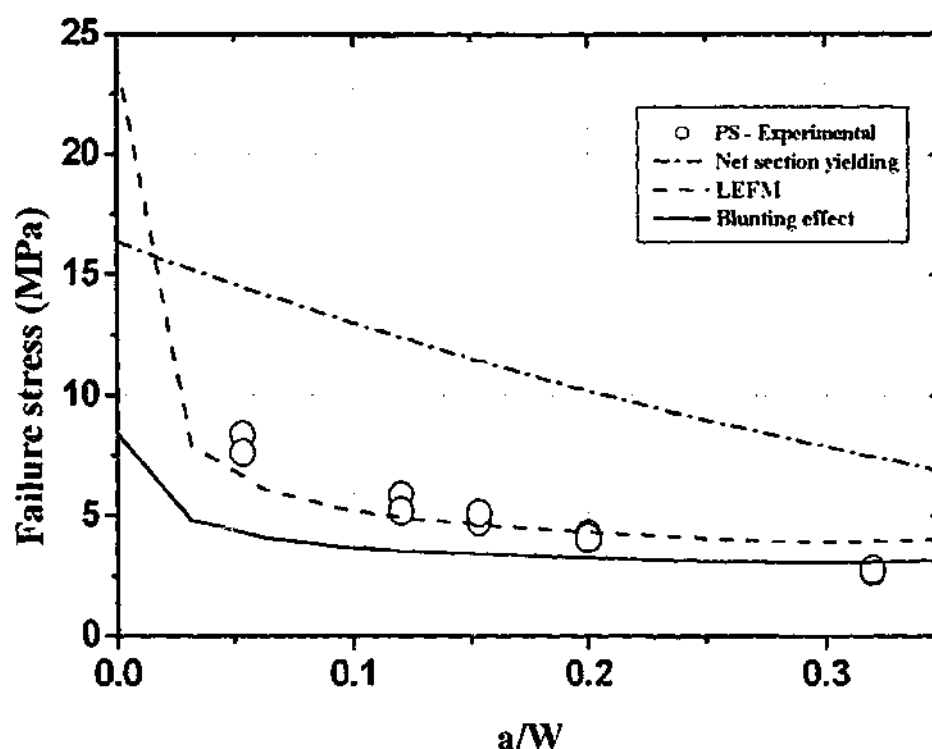


Figure 6.33: Plot of CT predictions versus experimental for PS.

Structures made from these tough ductile materials show failure before reaching the loads predicted by LEFM or net section yielding. The blunting effect provided safe working loads at short crack lengths for even the toughest material, ABS/PC.

Figures 6.29 to 6.33 are plots for materials exhibiting medium toughness to brittle behaviour (Astalac DMT, Astalac M120, PC and PS). Once again only small crack lengths were considered for these three polymers.

The three grades of ABS and PS were materials that reasonably followed the predictions by LEFM in pin loaded situations. However the predictions made by the blunting effect also gave a good fit to the data, even for brittle materials such as PS.

6.5 Failure Analysis for Ribbed Specimens

In the case of ribbed PVC specimens (as in Figure 3.13), three types of specimen were prepared. One had notches placed at the T-intersection whilst another had cracks made 4mm away from the intersection towards the hole and the last had flaws made 8mm away from the intersection towards the hole. Since it was also pin loaded, the analysis used was equivalent to that utilised on CT specimens. Important material properties were found using tensile

specimens and SENT specimens of the PVC. The relevant data are displayed in Table 6.2.

Likened to the THT and CT specimens where the stress state is quite complex, FEA was used to solve the problem. A variety of models were investigated but as Figure 6.34 shows, only the use of a full 3-D solution could predict the stress state at the constraint satisfactorily. The use of 2-D elements and 3-D elements with a lateral constraint at the base provided low stress concentration values. The full 3-D model was also used to find the stress field at a distance 4mm from the constraint and 8mm from the constraint, shown in Figure 6.35. As expected, there is a sharp decrease in stress concentration away from the constraint.

Table 6.2: Material parameters used in predicting failure for PVC.

Material	σ_y	E	K_{Ic}	r_p	ρ
	(MPa)	(MPa)	(MPa m ^{1/2})	(mm)	(mm)
PVC	50.9	3423	3.7	0.8	33
(extrusion grade)					

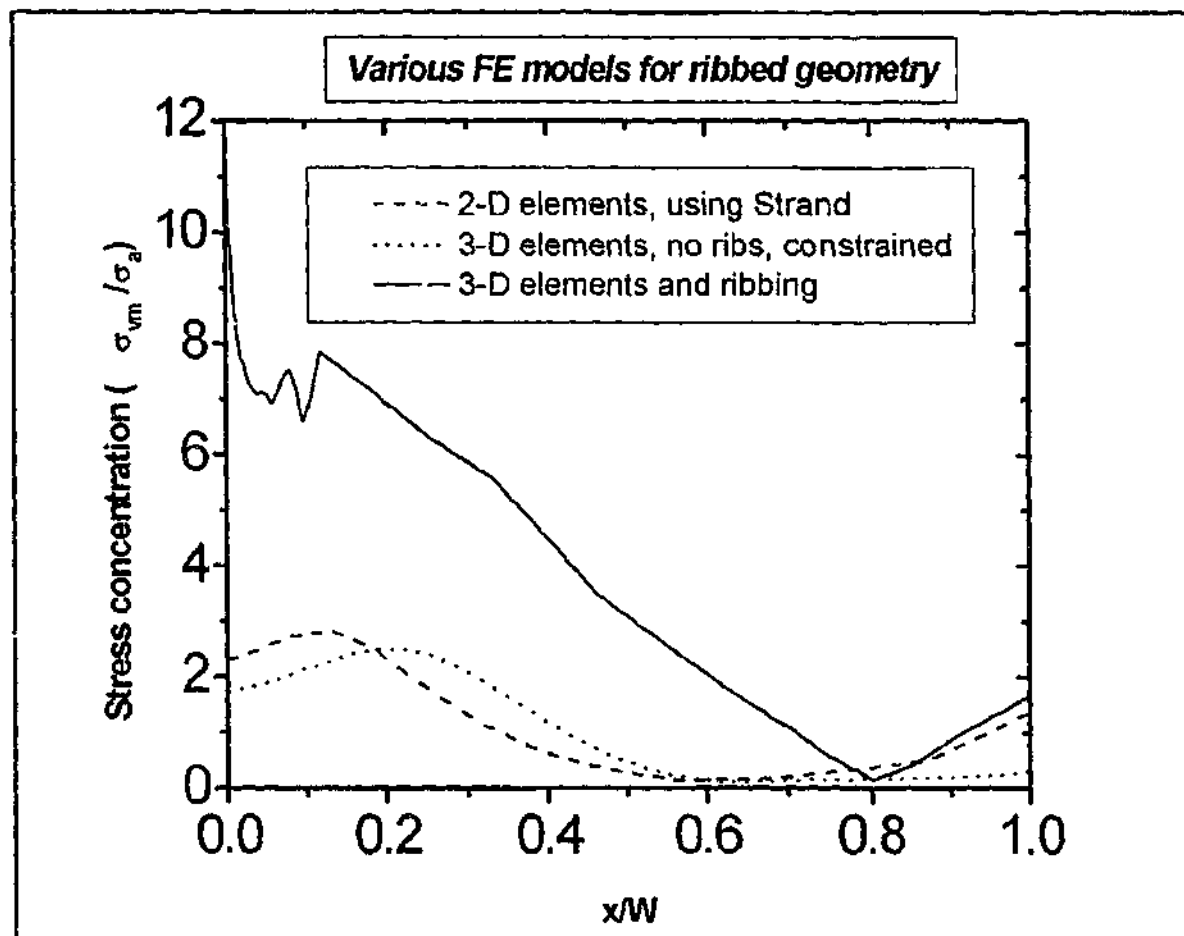


Figure 6.34: Various FEA used to model the plane strain stress field.

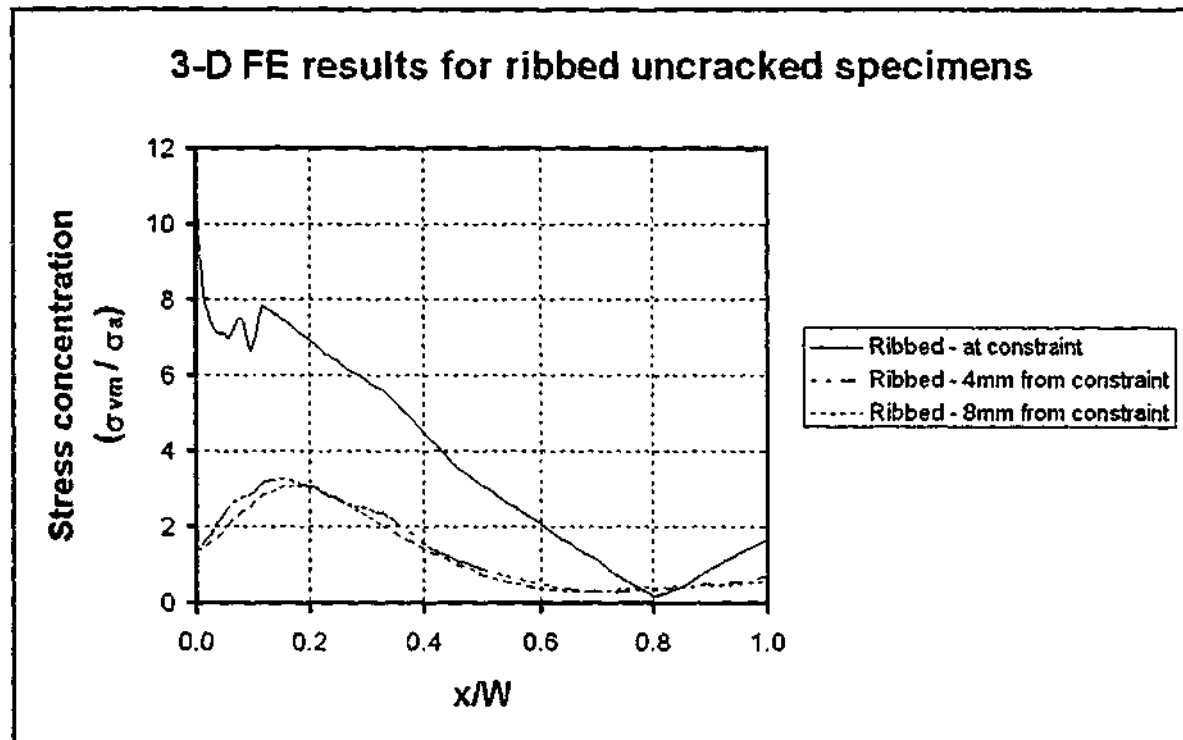


Figure 6.35: Stress states at differing distances from the plane strain constraint using the full 3-D model.

The results of predictions compared to experiments (as shown by Figure 6.36 to 6.38) indicate that when the crack is at the base, and close to a plane strain situation, the failure loads are lower than those of cracks made progressively further away from that area. This effect is most predominant at short crack lengths but the blunting effect methodology predicted safe working loads for cracks experiencing plane strain conditions. At longer crack lengths, all three methodologies provided unsafe results, although the crack lengths had to be greater than 20% of the width for this to occur.

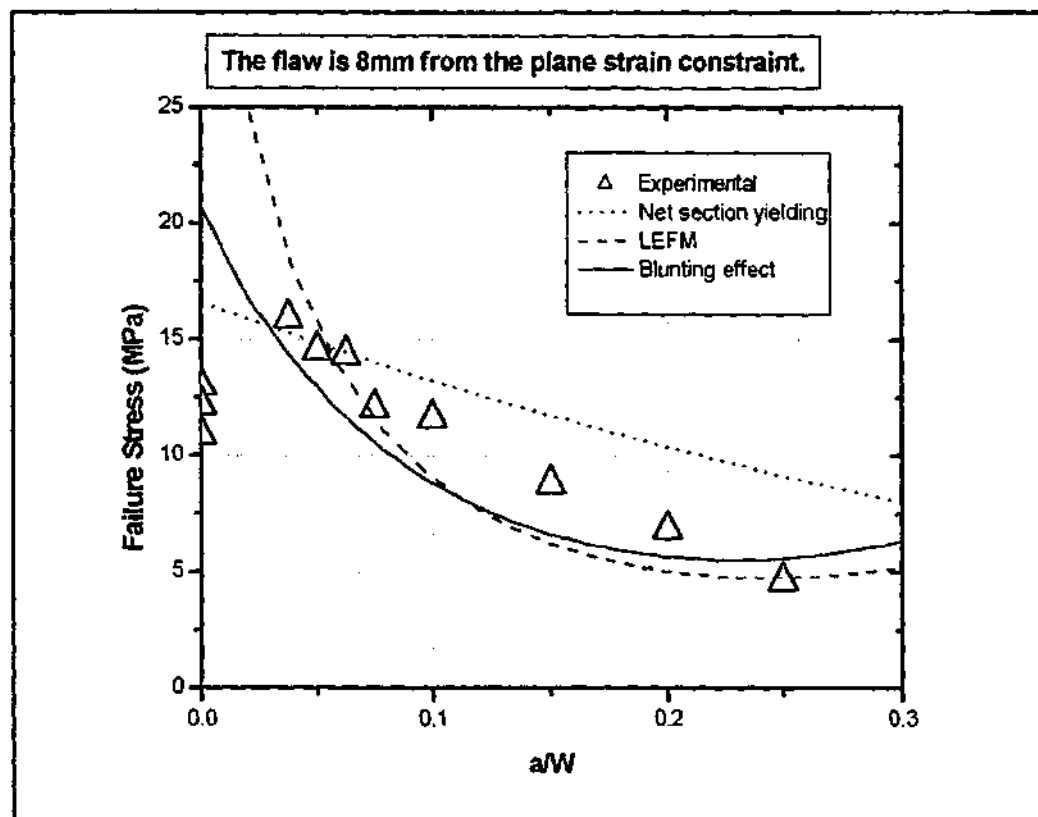


Figure 6.36: Plot of experimental versus predicted for PVC, 8mm from the plane strain constraint.

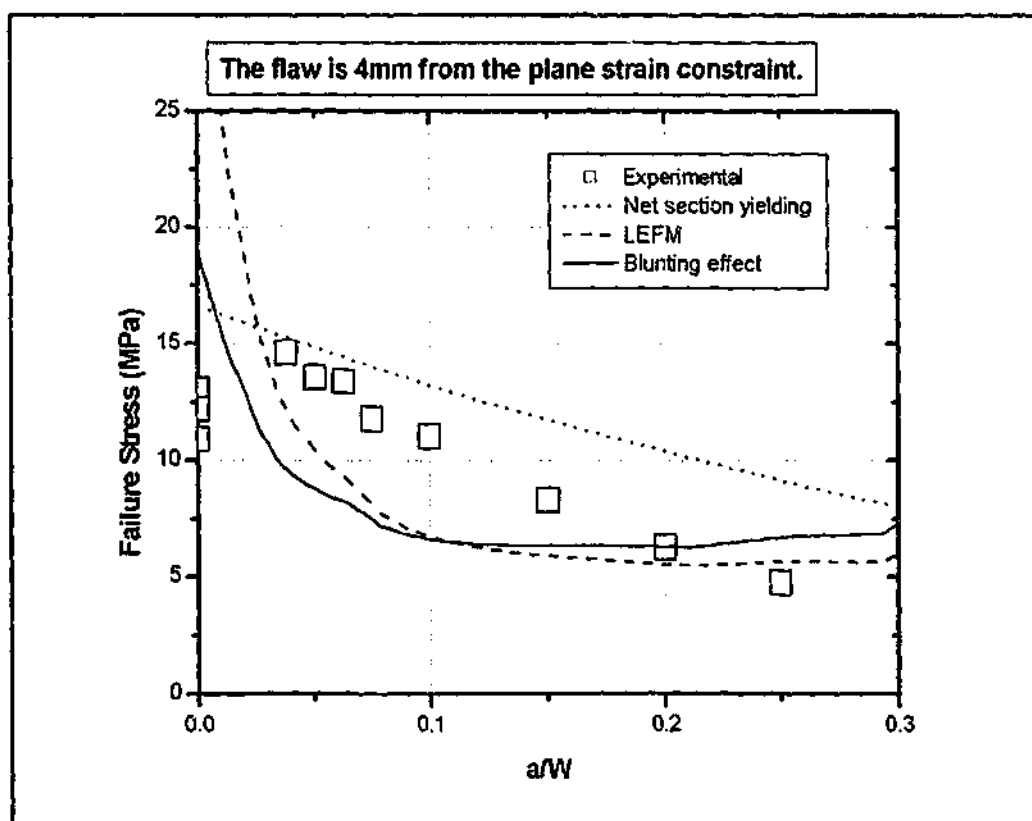


Figure 6.37: Plot of experimental versus predicted for PVC, 4mm from the plane strain constraint.

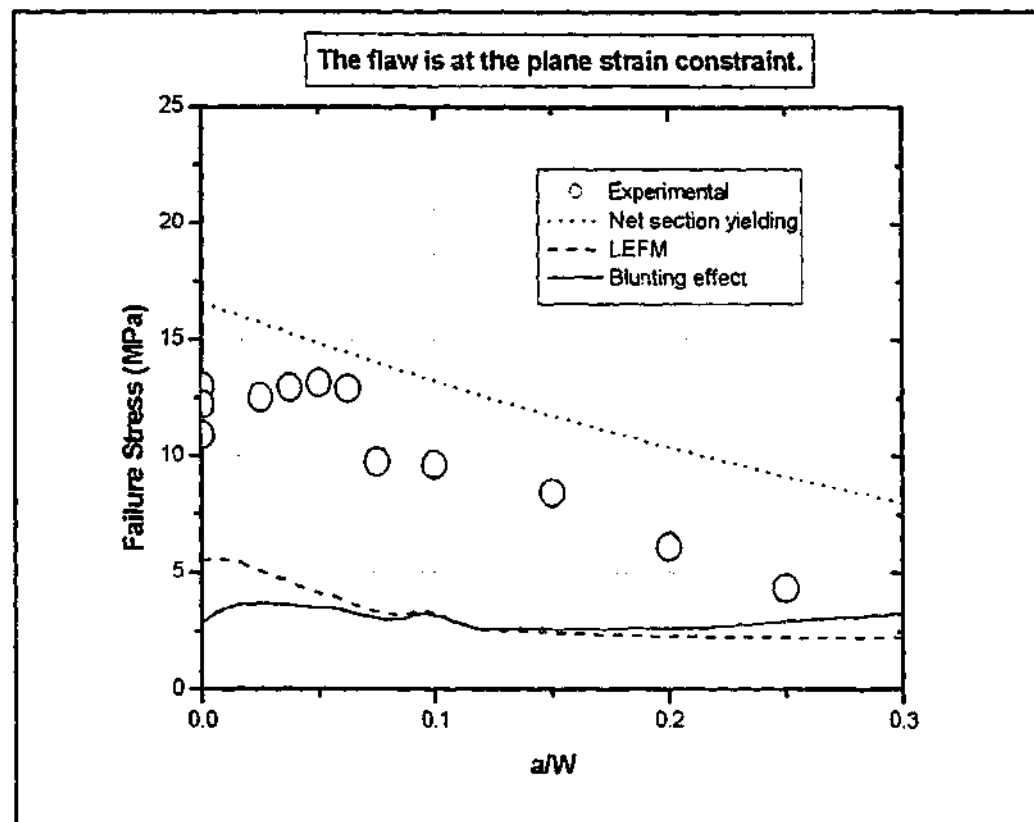


Figure 6.38: Plot of experimental versus predicted for PVC, at the plane strain constraint.

It may be worthwhile to examine the physical meaning of the plane strain effect in order to understand the lower failure loads obtained when cracks are placed at the "T" intersection. Consider a notch in a thick piece of material under a tensile load, as in Figure 6.39(a). Note that in the case of the ribbed specimen (shown in Figure 3.13) the co-ordinate system to be used should be equivalent to that of Figure 6.39. The origin is set at the tip of the crack. X_1 is vertically upwards in the direction of the applied load. X_2 is in the width direction running ahead of the crack. X_3 is in the thickness direction, orthogonal to axis X_1 and X_2 .

The argument for the existence of a triaxial stress state is as follows. A strain ϵ_1 in the X_1 direction close to the tip (i.e. element a in Figure 6.39a) is greater than a strain ϵ_1 which is farther away from the tip (i.e. element b in Figure 6.39a) because of the stress concentration. If an unnotched specimen was considered, and no stress concentrations were involved, then element b would be strained equally to element a in the X_1 direction. Furthermore ϵ_2 and ϵ_3 would be equal to each other, and both equal to $-\nu\epsilon_1$ for elastic deformation, and equal to

$\frac{1}{2} \epsilon_1$ for plastic deformation. That is, ϵ_1, ϵ_2 (equal to ϵ_3) are coupled in a proportionate way.

However with the existence of the notch, strain ϵ_1 near the tip (in the process zone) has been significantly increased. Consequently ϵ_3 is unable to match the extra elongation experienced by elements close to the notch because of the constraint in the thickness direction. As a result, a stress σ_{33} is generated to hold ϵ_2 to a small value consistent with the lateral contraction of the surrounding specimen, remote from the notch (shown by Figure 6.35b). Following the nomenclature of texts on fracture (Nadai 1963; Tetelman and McEvily 1967; Knott 1973),

$$\sigma_{11} > \sigma_{33} > \sigma_{22}.$$

Compare this to a plane stress state where

$$\sigma_1 > \sigma_2,$$

and σ_3 is zero.

Since there are three principal stress components present in the plane strain case, the hydrostatic stress experienced at the tip will be greater when compared to the plane stress situation. As a result, the load required for fracture is lowered.

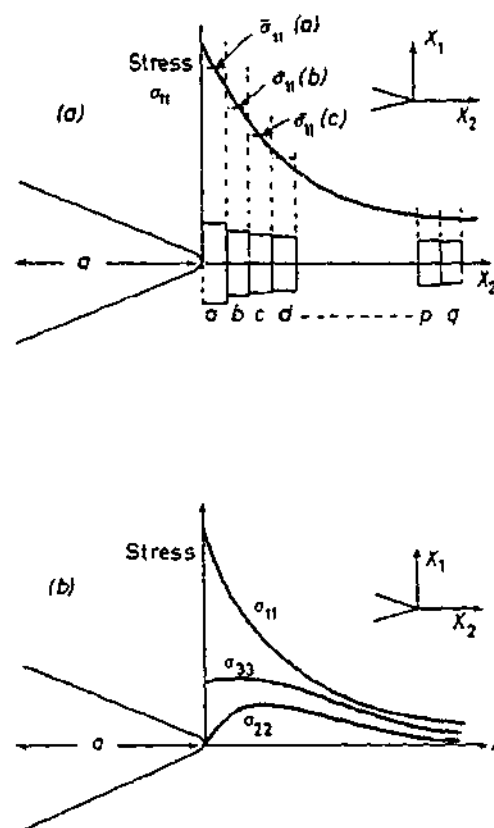


Figure 6.39: (a) Elastically stresses elements ahead of a notch. (b) Distribution of stresses in plane strain (Knott 1973).

6.6 Summary

Chapter 6 showed the experimental results for all five configurations tested and compared them with the predicted curves as defined by the equations in Chapter 3. The definition of failure for these tough materials was the maximum load attained during testing. This is important because up to that point, the material's behaviour is fairly linear and elastic. This validates one of the assumptions used by the three simple methodologies, that is, the material behaves linear elastically.

Also tensile data in Chapter 5 showed little change in yield stress or elastic modulus over a number of decades of strain rates. As a result, material in regions of high strains (near stress concentrators) does not behave too differently to regions under the average strain.

The main conclusion to be drawn from Chapter 6 is that the effective blunting parameter ρ gives a better fit to the experimental data for the single edge notched (SENT) specimen when compared to K_{Ic} . Once these two parameters were characterised, the application of ρ , K_{Ic} and

net section yielding to other components showed that ρ is required to predict safe working loads (for thin walled injection moulded articles with cracks lengths up till 10% of the specimen's width) under all configurations, including the plane strain case. If only linear elastic fracture mechanics (LEFM) and net section were used to predict working loads, experimental data for some articles show that this is insufficient (refer to Figures 6.27, 6.28 and 6.36). Failure can occur below the calculated design loads. The effective blunting methodology should therefore be utilised as a predictive tool for tough and ductile polymers with cracks. It could also be used in the design of complex shaped injection moulded objects to ensure the calculated tolerable crack lengths are within specifications and the article will not fail prematurely under normal service loads.

Chapter 7

Microscopy of Crack Tips

In this section of the work, the materials are grouped into three distinct categories, namely single phase polymers, toughened polymers and polymer blends. Within each category, the polymers are displayed in order of toughest to most brittle. Optical micrographs were taken of the crack tip for each polymer for two cases. The first case was of the polymer prior to being loaded and the second case was when the specimen had been stressed to ninety percent of its failure load. To gain greater depth of field and details of the deformation process in the vicinity of the crack, scanning electron microscopy (SEM) images were also taken. Three cases were considered in the SEM section – unetched specimens, etched specimens prior to being loaded and etched specimens which have been loaded. For all the specimens loaded to 90% of their failure loads, a wedge was used to maintain the crack tip opening displacement (CTOD) and a thermoset was forced into the crack using hydrostatic pressure. This technique is fully described in Chapter 4.2.7.

For all the micrographs shown, the following key points should be noted:

- optical micrographs are for polished sections taken along a crack, normal to the crack tip locus, from the interior of the specimen.
- SEM images can in turn be unetched or etched with a solvent. The section is from the interior of the specimen, normal to the crack tip locus.

7.1 Single Phase Polymers

The first single phase polymer considered, which is the toughest as measured using LEFM, is PC followed by PET and then PS. PC and PET were both etched using a 10%wt solution of potassium hydroxide whilst PS was etched with chloroform.

7.1.1 PC

Figures 7.1 and 7.2 show optical micrographs of the crack tip for PC. Note that from results in Chapter 6 and Table 6.1 that PC is capable of failure in both brittle and ductile modes. Accordingly it has a fairly low value of the material parameter ρ and plastic zone size r_p .

On the left of Figure 7.1, the notch formed by the milling saw can be seen, along with the razor cut used to sharpen the starting crack tip. Notice that no crack propagation has occurred.

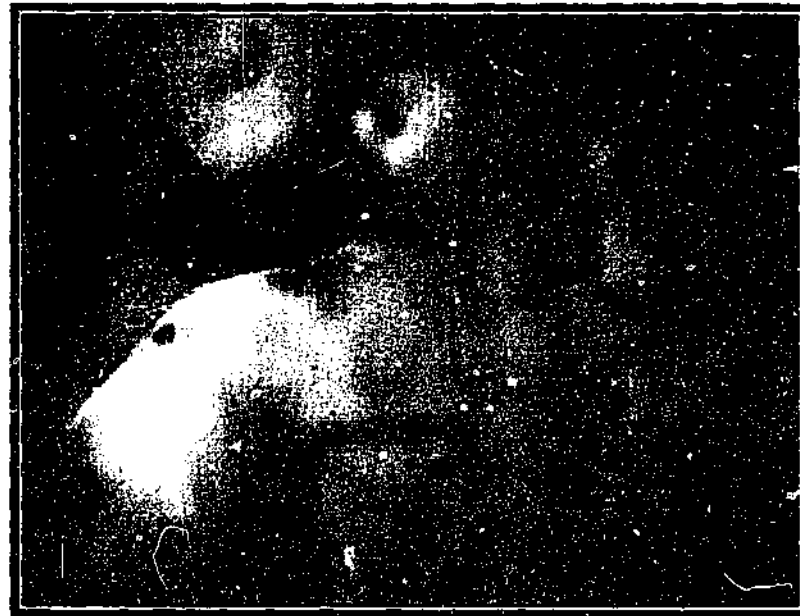


Figure 7.1: Optical microscopy of polished section of PC prior to loading.



Figure 7.2: Optical microscopy of polished section of PC loaded to 90% of failure stress.

Figure 7.2 shows a sharp crack propagating through the PC specimen from the starting notch once it has been loaded. There is also a crack branching away from the main flaw.

Figure 7.3 is a SEM image of an unetched PC specimen. It shows the outline of the crack tip and lines caused by the cutting action of the microtome. As expected, with no relief from preferential etching of the PC over the epoxy, little detail can be seen.



Figure 7.3: SEM – Unetched PC (x220).

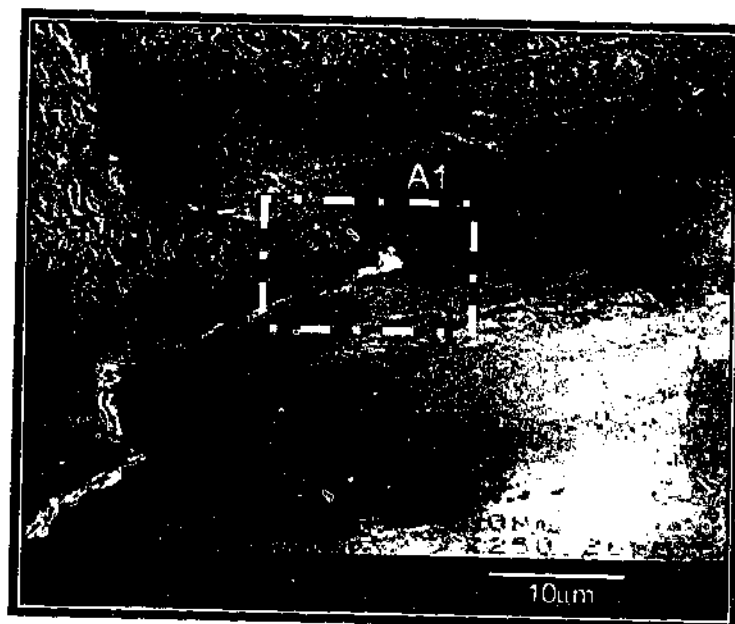


Figure 7.4: SEM – Starting notch and etched PC prior to loading (x250).

Figures 7.4 and 7.5 are micrographs of the etched crack tip in an unloaded case. In both cases no crack branching or microcracking is observable from the sharpened starting notch. Referring to Figure 7.5, the etchant appears to have attacked preferentially the edges of the

epoxy at the crack tip. This is to be expected because the material has been strained in that region from the machining and razor notching process.



Figure 7.5: SEM - Enlarged view of area A1 from Figure 7.4 (x2500).

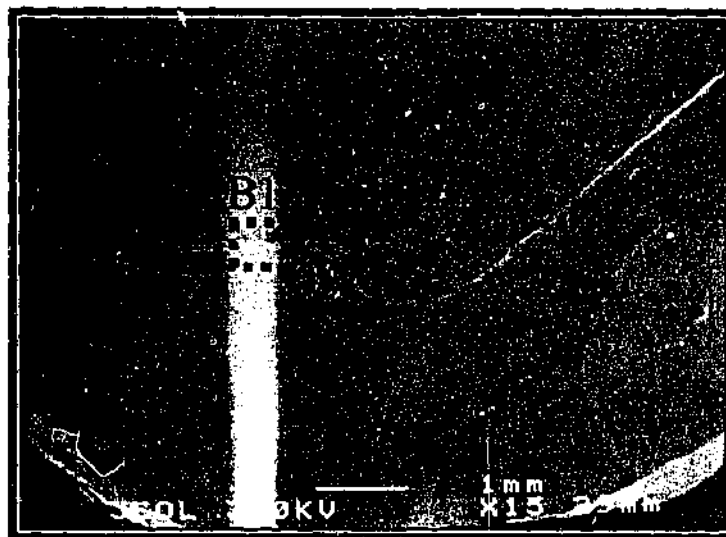


Figure 7.6: SEM - PC loaded to 90% of failure stress (x100).

After being strained to ninety percent of its failure load, the micrograph Figure 7.6 shows a sharp crack appearing in front of the starting notch. Figure 7.7 shows a branched crack from the main flaw. In Figure 7.8, the polycarbonate has been etched away leaving only the impregnated epoxy and some debris. The sharp nature of the main crack tip can be seen in

Figure 7.8. These sharp microcracks could be the reason for PC having a low value of ρ . That is, in spite of having a reasonable plastic zone size, the sharp microcracks could lead to premature crack propagation at low applied loads, particularly if oriented normal to the prevailing tensile stresses.

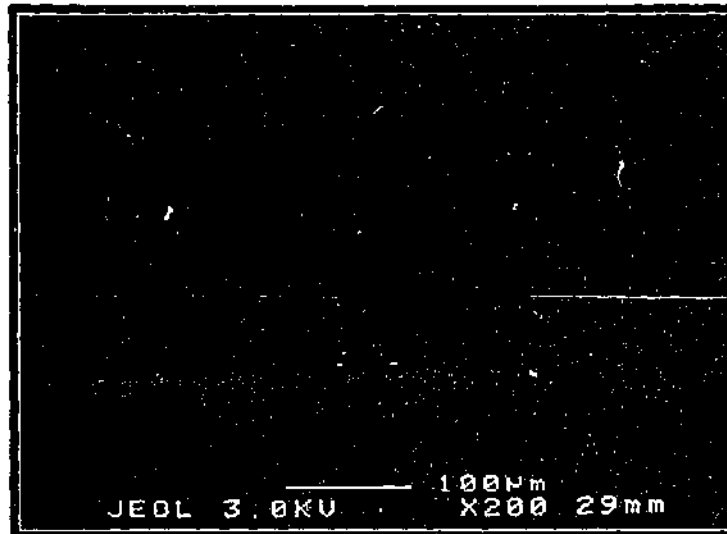


Figure 7.7: SEM - Enlarged view of area B1 from Figure 7.6 (x200).

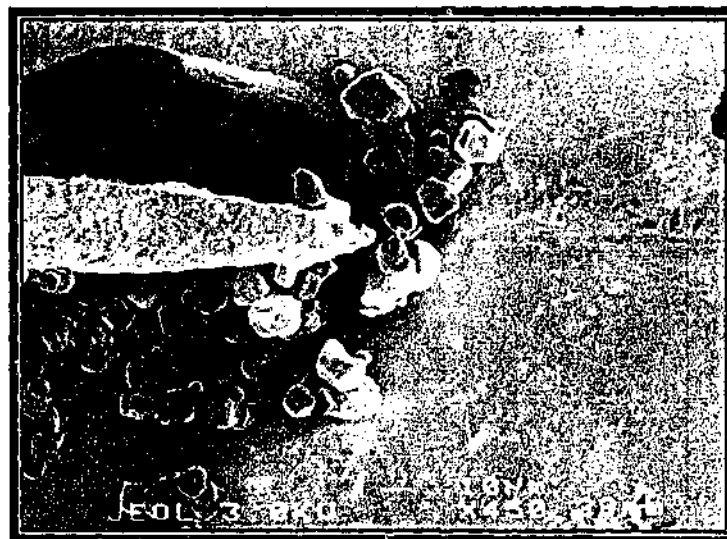


Figure 7.8: SEM - Enlarged view of area B2 from Figure 7.6 (x450).

7.1.2 PET

Like PC, PET is also capable of failing in a brittle manner and has a low value of ρ . The plastic zone size is also comparable to PC. The following optical micrographs show evidence that PET produces a number of cracks in front of a notch once loaded. From observation of ductile failure in PET, the specimens tend to show very little crack propagation. The material in front of the crack yields and thins. This process continues until it reaches the edge and then necking begins, associated with a drop in applied tensile load. Nevertheless, occasionally, PET displays brittle behaviour, possibly when these microcracks are in a suitable configuration.

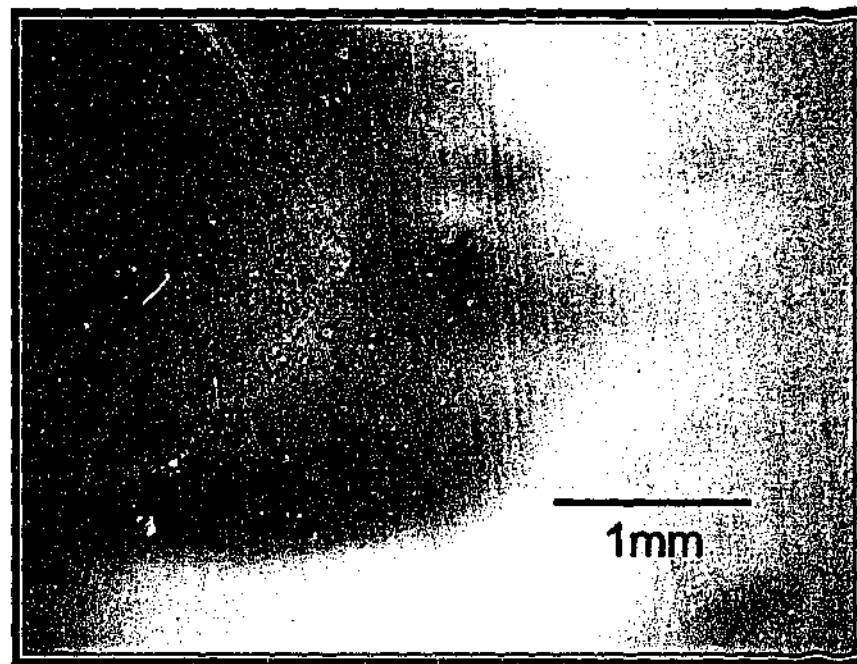


Figure 7.9: Optical microscopy of polished section of PET prior to loading.

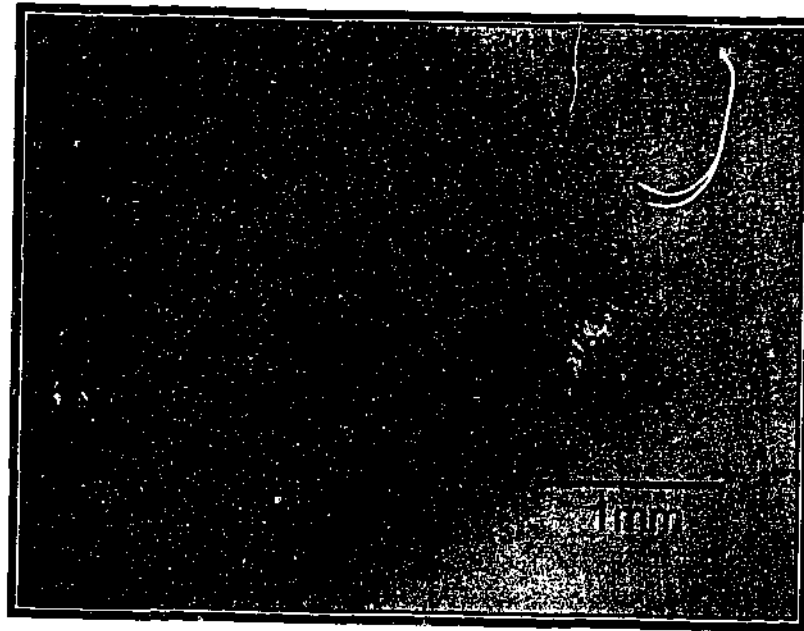


Figure 7.10: Optical microscopy of polished section of PET loaded to 90% of failure stress.

Figure 7.10 show the small advancing cracks which appear in front of the starting notch (compare to Figure 7.9, which shows the notch prior to loading) in PET. Figures 7.11 and 7.12, which are scanning electron micrographs of the starting notch before being loaded show a sharp crack tip (due to the use of a razor blade on the notch). Like PC, they also show preferential etching in front of the crack and around the machined starting notch.

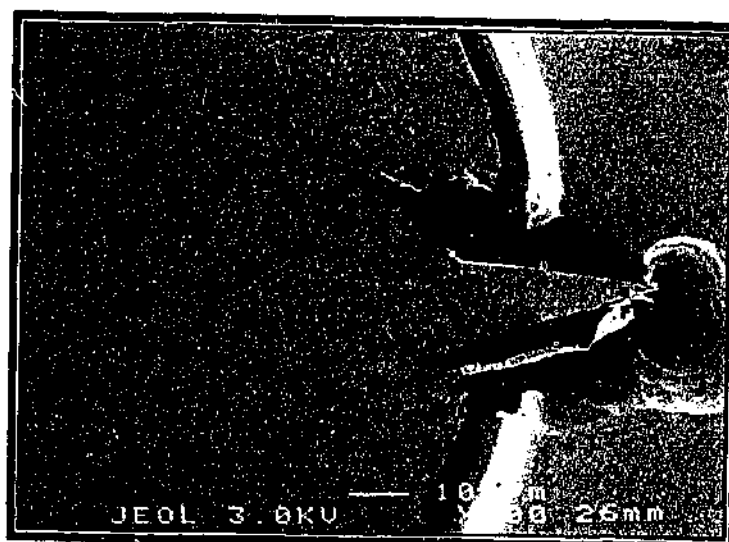


Figure 7.11: SEM – Starting notch and etched PET prior to loading (x100).

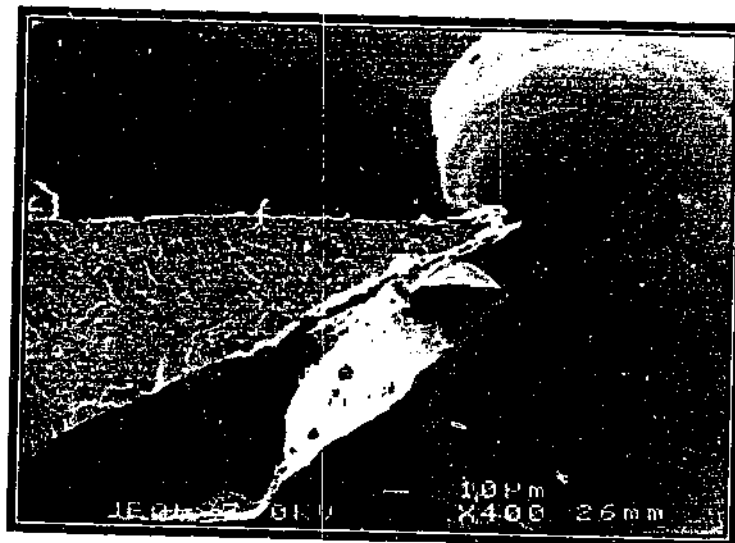


Figure 7.12: SEM – Enlarged view of the square region marked on Figure 7.11 (x400).

Figures 7.13 to 7.15 show the nature of the crack tip once PET has been deformed. In Figure 7.13, the noticeable features are the process zone ahead of the crack and the epoxy being successfully forced into the flaw.

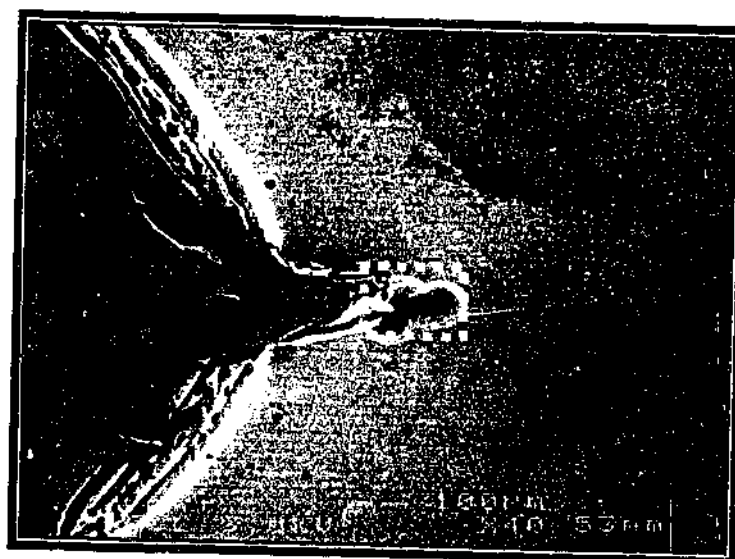


Figure 7.13: SEM – PET loaded to 90% of failure stress (x40).

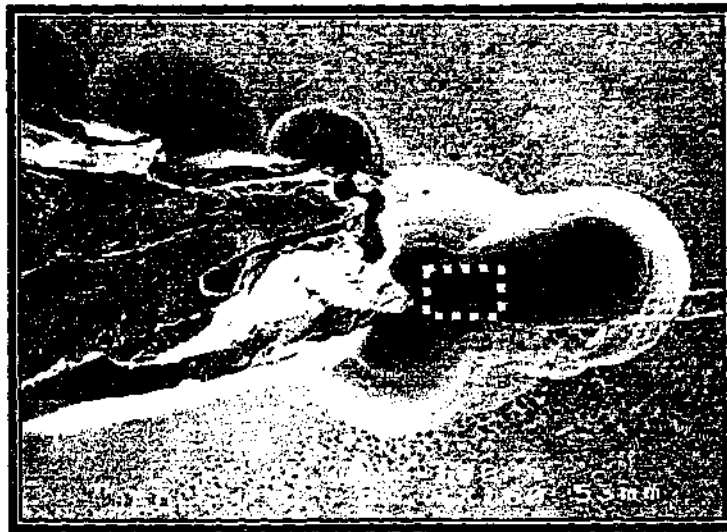


Figure 7.14: SEM – Enlarged view of the square region marked on Figure 7.13 (x160).

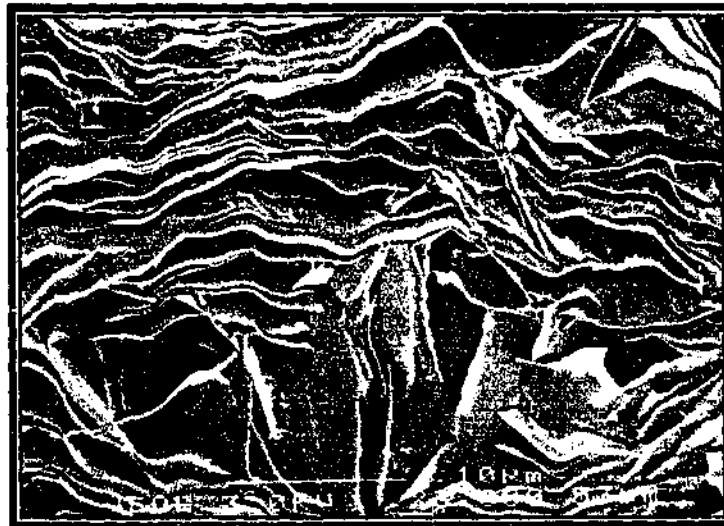


Figure 7.15: SEM – Enlarged view of the square region marked on Figure 7.14 (x3000).

Figure 7.14 shows the crack tip is no longer sharp like Figure 7.12. In Figure 7.15, the process zone is magnified to reveal a laminar type structure. These laminar features are about 200nm in thickness, with larger lateral dimensions. It is possible they are due to the etching out of the amorphous phase between the crystalline regions, but this is at best a tentative explanation (Lin and Argon (1994) have reported the thickness of lamellae to be in the order of 5-25nm for polyethylene).

7.1.1 Polystyrene

PS was the least tough material considered in this thesis. The fracture parameters K_{Ic} , r_p and ρ were the lowest when compared to the other seven materials. Therefore it would be expected that the crack tip would be sharp with little surrounding deformation. The optical micrographs (Figures 7.16 and 7.17) show a singular crack emanating from the starting notch. The starting notch is the dark triangular region on the left in Figure 7.16.



Figure 7.16: Optical microscopy of polished section of PS prior to loading.



Figure 7.17: Optical microscopy of polished section of PS loaded to 90% of failure stress.

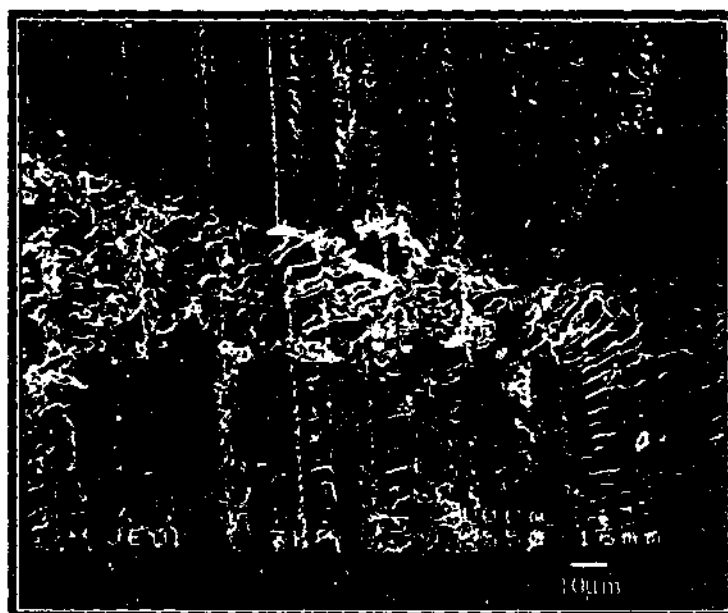


Figure 7.18: SEM – Unetched PS (x550).

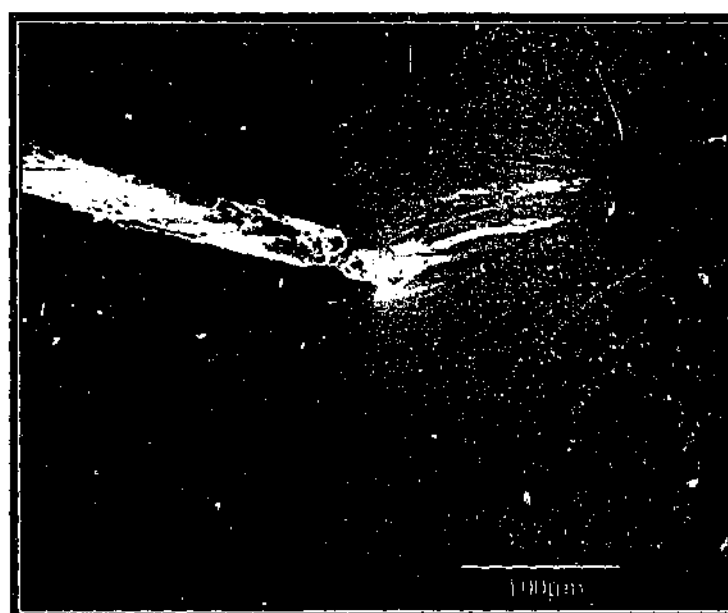


Figure 7.19: SEM – Starting notch and etched PS prior to loading (x270).

Scanning electron micrographs show in greater detail the sharpness of the crack. Figure 7.18 is a SEM image of an unetched specimen. PS was etched with chloroform rather than potassium hydroxide (used on PC and PET). Figure 7.18 indicates that like PC and to a much lesser extent PET, visualisation of the crack tip is difficult without an etchant. Also from Figure 7.19, no larger cracks can be seen from the starting notch for PS which has not

been loaded. However one can see that the impregnation of epoxy resin has reached deep into the starting notch after etching.

For a specimen which has been stressed, the crack tip is certainly observable. Figures 7.20 to 7.22 show a sequence of enlargements of the crack tip and highlight the sharpness of the crack.

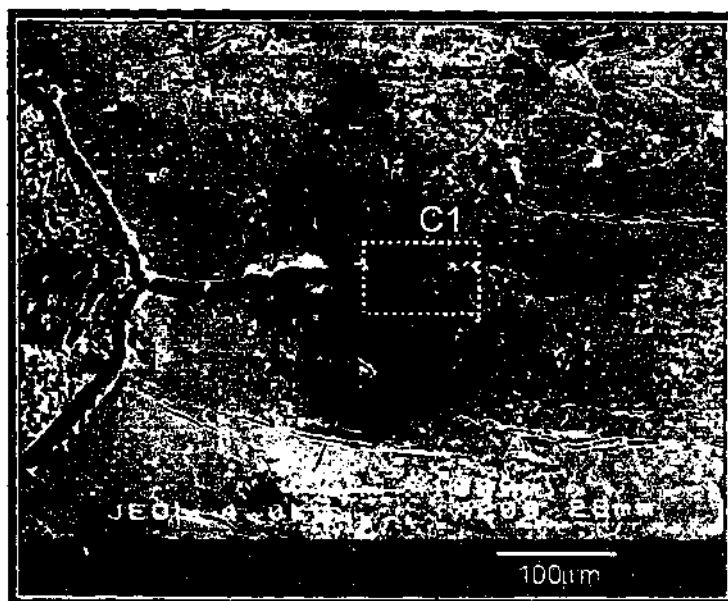


Figure 7.20: SEM – PS loaded to 90% of failure stress (x200).

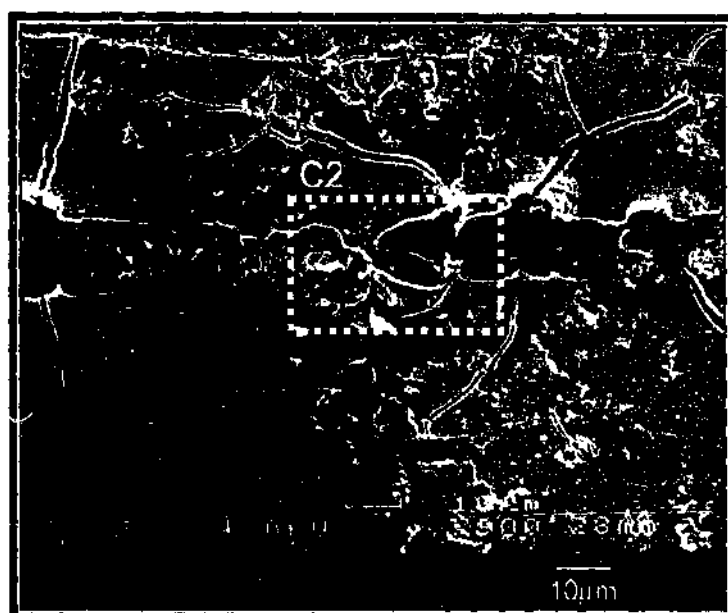


Figure 7.21: SEM - Enlarged view of area C1 from Figure 7.20 (x900).

Even at a magnification of 900 times (Figure 7.21), extensive crazing and microcracking can be observed in PS.



Figure 7.22: SEM - Enlarged view of area C2 from Figure 7.21 ($\times 3000$).

At a magnification of 3000 times, Figure 7.22 shows large scale deformation ahead of the crack. It also shows the epoxy impregnating deep into the tip of the flaw.

7.2 Toughened Polymers – ABS

Observation of deformation in ABS has been extensively performed by transmission electron microscopy [Wood 1992; Frontini 1995; Steenbrink 1997]. Staining of the rubber particles, by reacting a heavy metal with the double bonds, can be achieved using ruthenium tetroxide or osmium tetroxide [Motezinos 1985; Brown 1997]. This technique has shown cavitation and crazing of the particles during deformation. However in this study, only optical and scanning electron microscopy were used. These techniques were chosen simply to give validity to the measured values of the fracture parameters and to investigate the effectiveness of impregnating the crack tip with epoxy under hydrostatic pressures.

7.2.1 ABS – Astalac DMT

For Astalac DMT, a sharp crack develops when it is loaded and there is also stress whitening in front of the notch, as can be seen in Figure 7.24. Figure 7.23 shows no stress whitening but has a sharp crack due to the razor cut into the material.

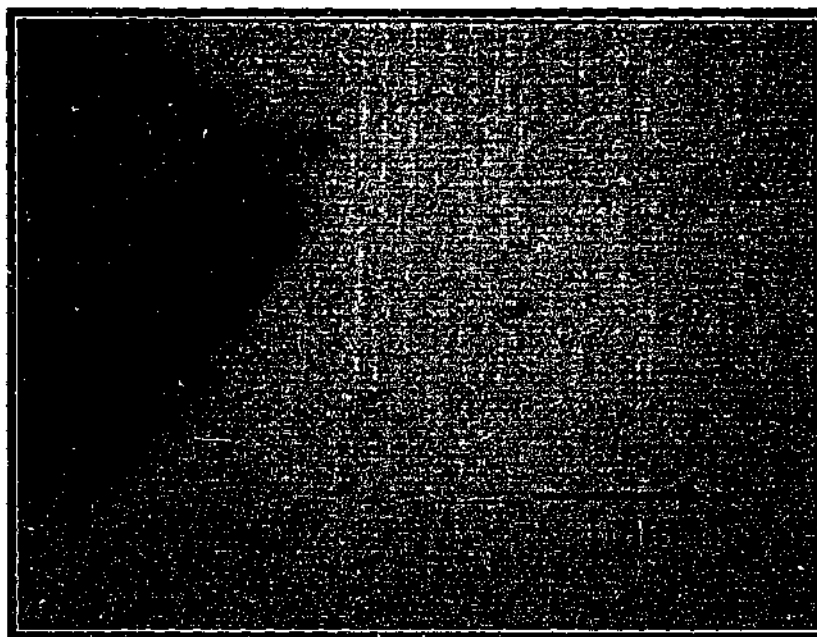


Figure 7.23: Optical microscopy of polished section of Astalac DMT prior to loading.

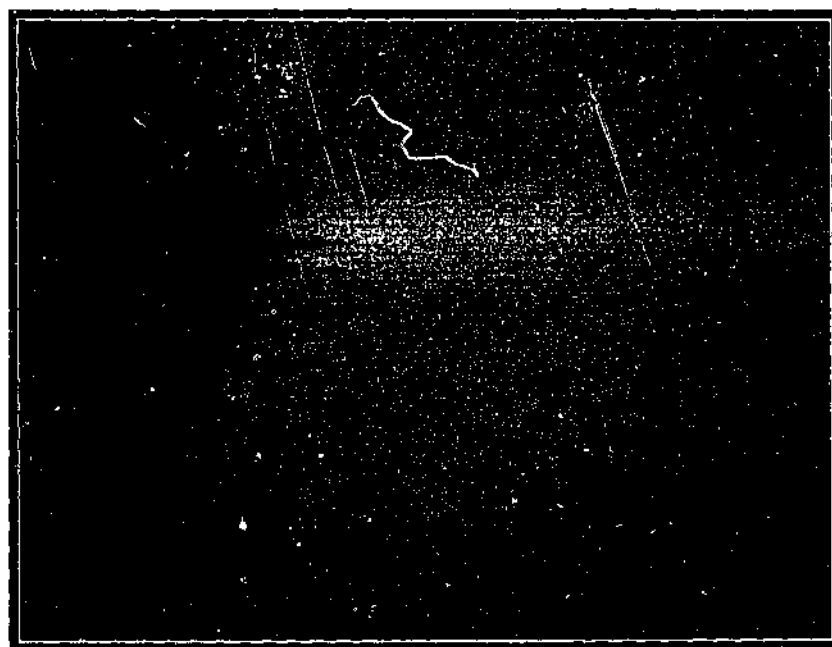


Figure 7.24: Optical microscopy of polished section of Astalac DMT loaded to 90% of failure stress.

The next step is to observe the crack under a SEM. Methyl-Ethyl Ketone (MEK) was the solvent used on the three grades of ABS studied. Without the use of a solvent, no noticeable features were observed (refer to Figures 7.25 and 7.26). If the specimen was etched but not loaded, Astalac DMT showed few details, as shown by Figure 7.27.



Figure 7.25: SEM – Unetched ABS (x100).

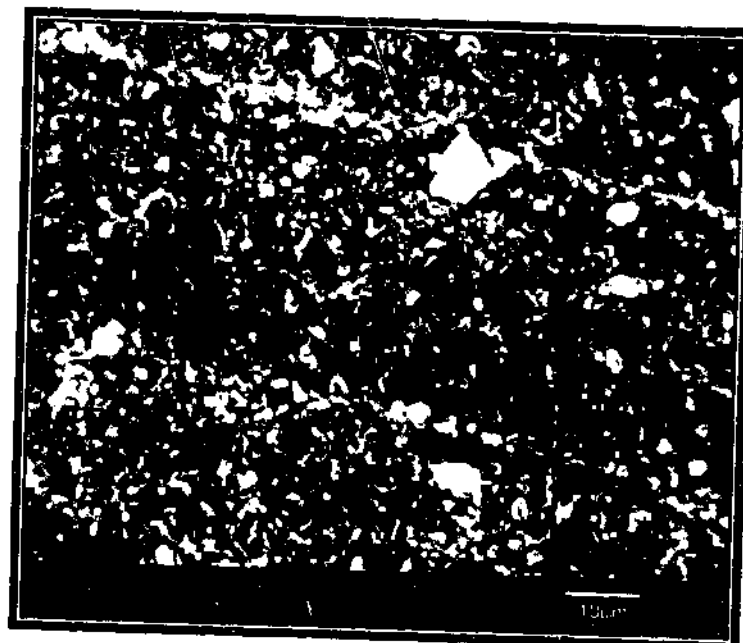


Figure 7.26: SEM - Enlarged view of area D1 from Figure 7.21 (x1200).

The particles which are able to be seen on the specimen in Figure 7.27 are not rubber particles but rather airborne dust. The surface of the ABS becomes extremely adhesive after being etched with the solvent MEK and the unavoidable result is that grit becomes attached to it. All the etched ABS materials show this and the fact that these particles are on the epoxy indicate they are of an extraneous nature.

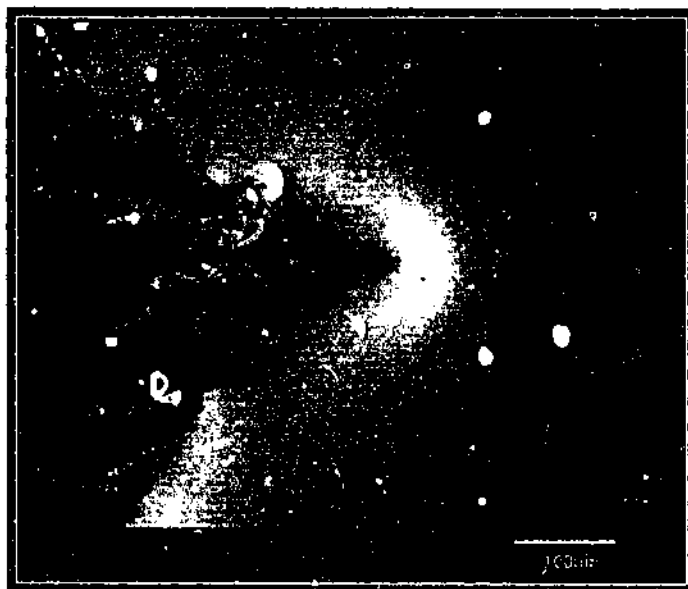


Figure 7.27: SEM – Starting notch and etched Astalac DMT prior to loading (x180).

After being loaded, the crack is able to be seen, but resolution of the crack tip was poor. The crack tip can be seen in Figure 7.28 but at a higher magnification (Figure 7.29), no further detail is evident. The use of a transmission electron microscope (TEM) may be required to observe the deformation processes in this particular grade of ABS.

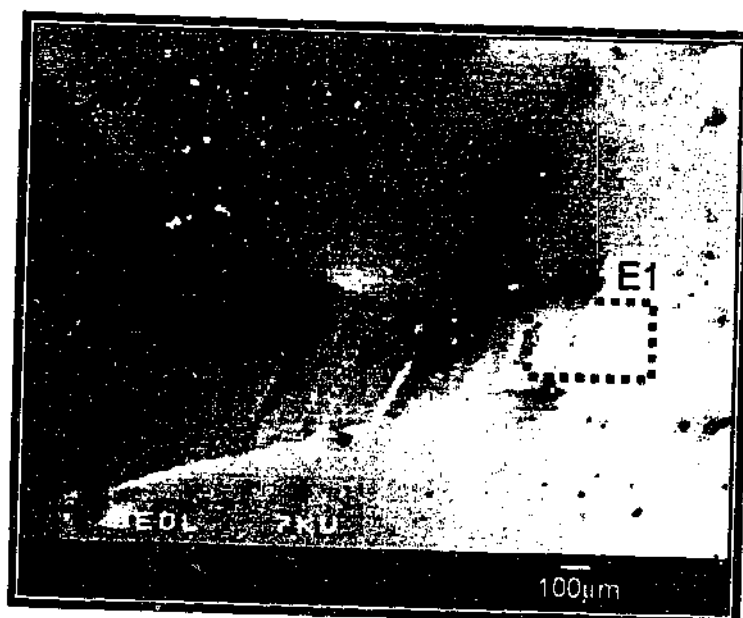


Figure 7.28: SEM – Astalac DMT loaded to 90% of failure stress (x50).

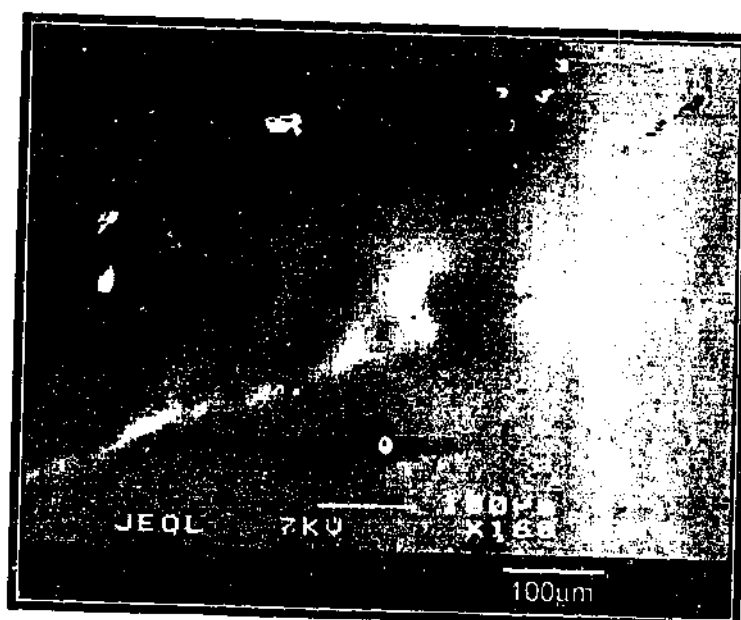


Figure 7.29: SEM - Enlarged view of area E1 from Figure 7.28 (x160).

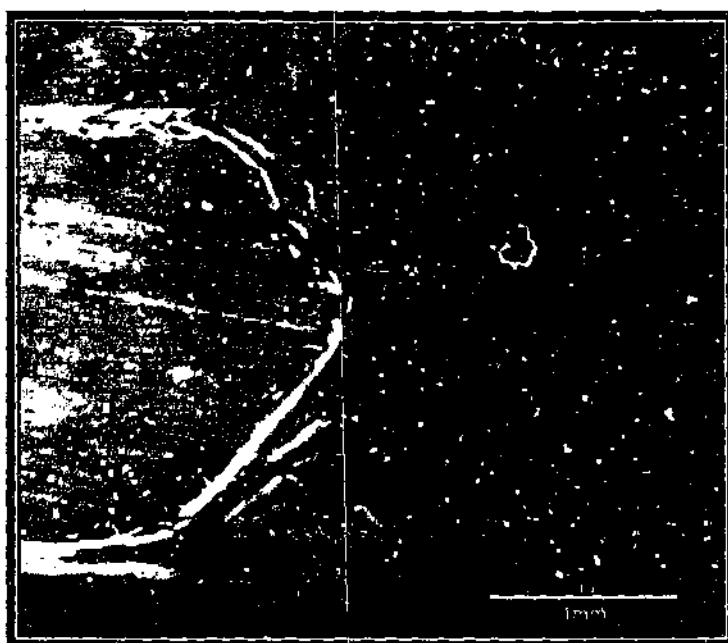


Figure 7.32: SEM – Starting notch and etched Astalac M120 prior to loading (x30).

Like Astalac DMT, Astalac M120 shows stress whitening under load (see Figure 7.31) and as a comparison, Figure 7.30, which is a specimen that has never been loaded, shows no stress whitening. Also an undeformed specimen under SEM shows only the machined notch with little crack propagation (refer to Figure 7.32). A specimen under load (Figure 7.33) provided more detail about the shape of the crack tip.

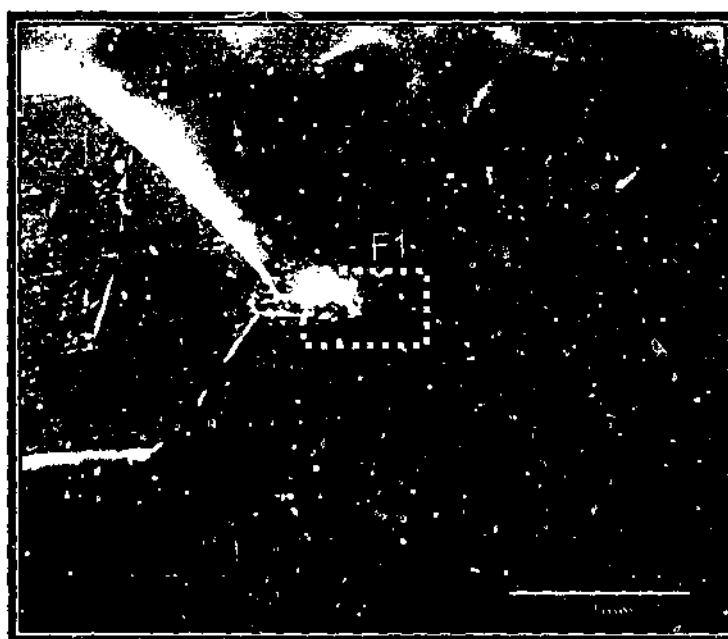


Figure 7.33: SEM – Astalac DMT loaded to 90% of failure stress (x30).

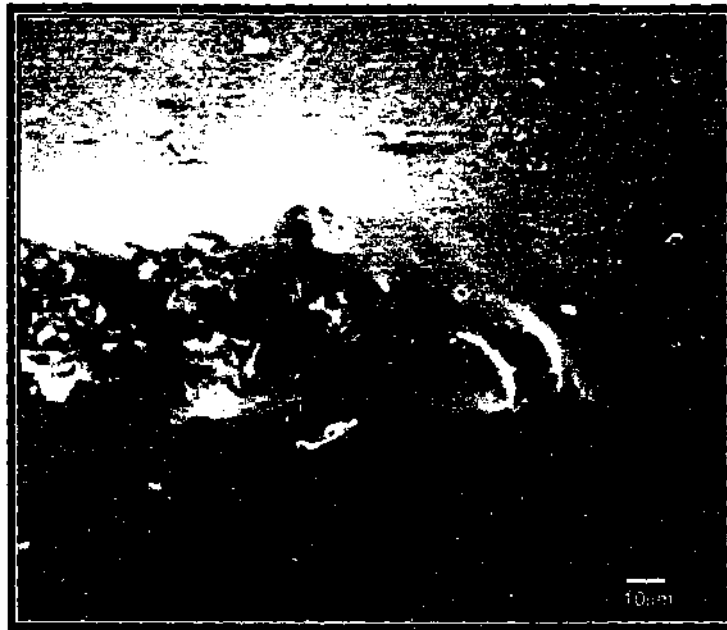


Figure 7.34: SEM - Enlarged view of area F1 from Figure 7.33 (x550).

High magnification of the crack (Figure 7.34) shows good impregnation of the thermoset into the tip and highlights severe blunting at the tip by a combination of cavitation and plasticity. Such blunting leads to the relatively high value of ρ observed for this material.

7.2.3 ABS – CB625

Optical microscopy work on the crack tip of CB625 did not reveal a large amount of detail about the nature of the deformation mechanisms around the crack tip. The loaded material showed a non sharp crack tip but little stress whitening (refer to Figure 7.36) when compared to the other grades of ABS. There was little difference between the profile of the crack tip which was not loaded (Figure 7.35) and one that was under stress.

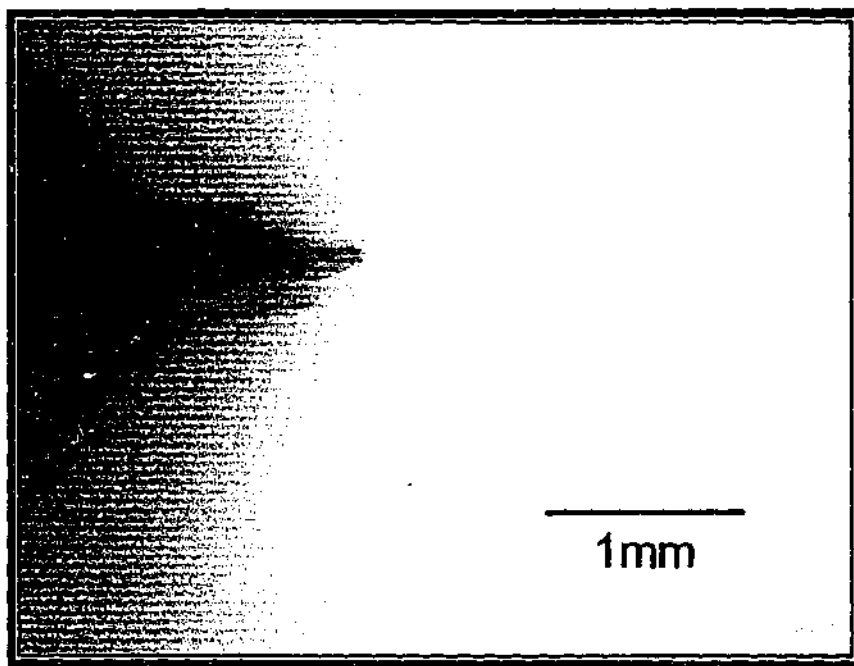


Figure 7.35: Optical microscopy of polished section of CB625 prior to loading.

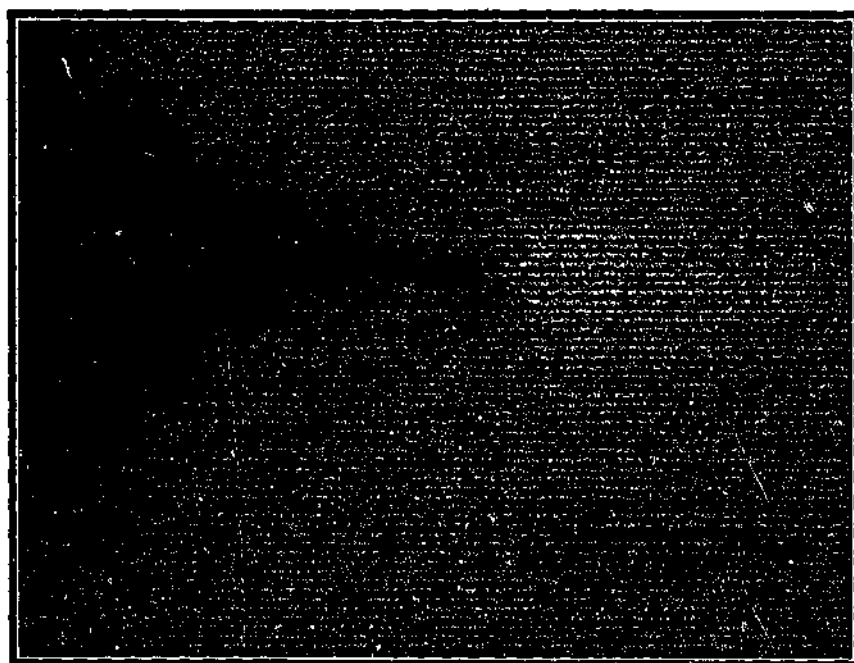


Figure 7.36: Optical microscopy of polished section of CB625 loaded to 90% of failure stress.

Using SEM, the specimen which was etched but not loaded (Figure 7.37), showed that even with the use of a razor blade, the crack tip remains fairly blunt. In fact, after loading, the shape of the crack tip is essentially the same as if it was never loaded (compare Figure 7.38

with Figure 7.37). At a higher magnification, no sharp cracks can be observed in CB25 but in fracture tests, the material showed similar ductile failure behaviour to PET. There was limited crack propagation and thinning of the material in front of the notch was noticeable which was then followed by specimen necking.

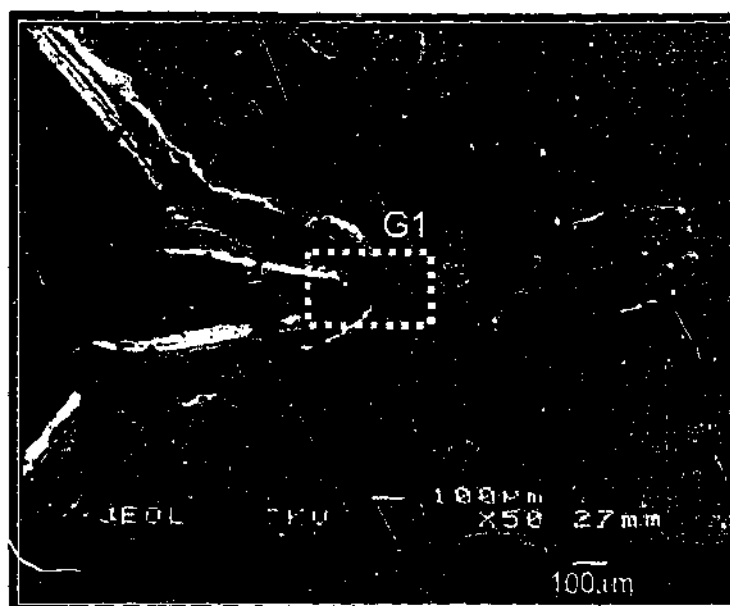


Figure 7.38: SEM – CB625 loaded to 90% of failure stress (x50).



Figure 7.39: SEM - Enlarged view of area G1 from Figure 7.38 (x200).

In terms of the blunting parameter ρ , CB625 had the highest value when compared to Astalac DMT and Astalac M120. It also had the largest plastic zone size and the images of

the crack tip provided by SEM suggest rounding of the crack to be one of the major cause of its high toughness.

7.3 Polymer Blends

As stated in Chapter 2, polymer blending is an inexpensive method of imparting the required properties from one polymer to another which lacks that desired quality. Toughness is one such property and ABS/PET and ABS/PC were the two tough and ductile polymer blends investigated in this study. The etchant used on both these immiscible systems was potassium hydroxide and the phases to be etched out were PET and PC respectively for the two blends.

7.3.1 ABS/PET

The first blend to be considered was ABS/PET. It was also the toughest material considered in this thesis with large values of K_{Ic} , r_p and ρ . Optical micrographs show stress whitening similar to Astalac DMT and Astalac M20 under load (Figure 7.41) compared to the non loaded situation (Figure 7.40).

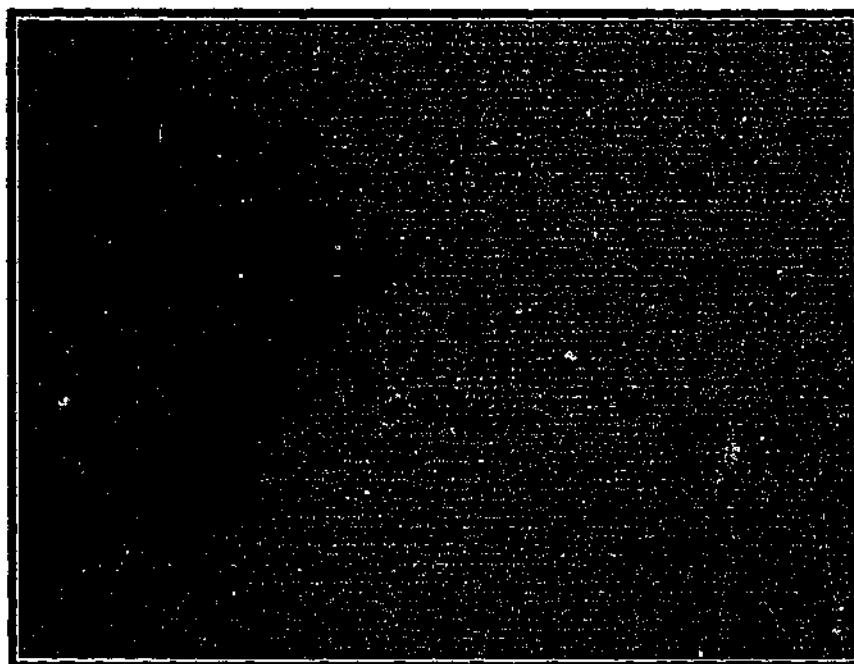


Figure 7.40: Optical microscopy of polished section of ABS/PET prior to loading.

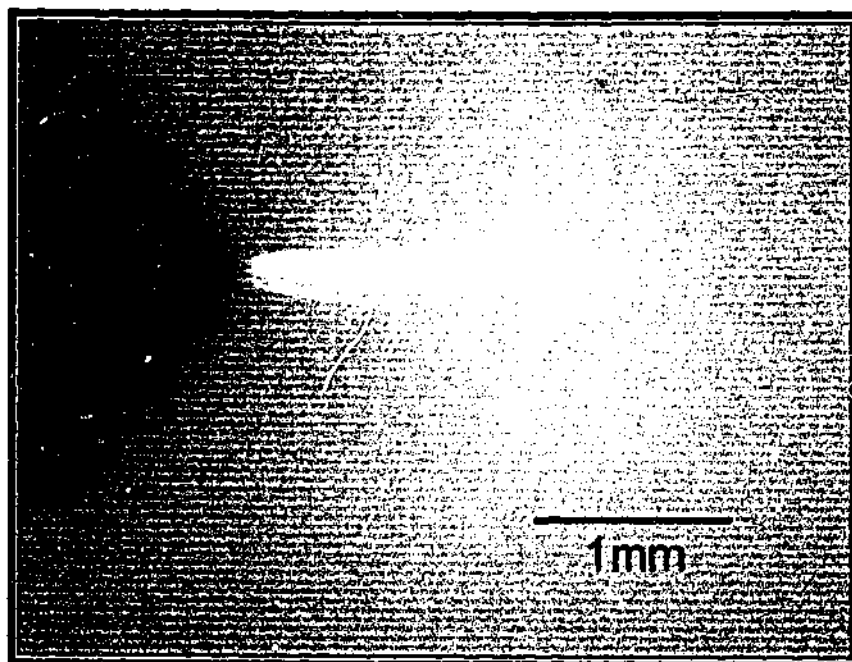


Figure 7.41: Optical microscopy of polished section of ABS/PET loaded to 90% of failure stress.

Figures 7.42 and 7.43 show a low and high magnification SEM image of an unetched ABS/PET material. In Figure 7.43, one can already see a two phase structure with the more ductile phase being drawn out as fibrils during the microtoming process.



Figure 7.42: SEM – Unloaded and unetched ABS/PET (x100).



Figure 7.43: SEM - Enlarged view of unloaded and unetched region (x2000).

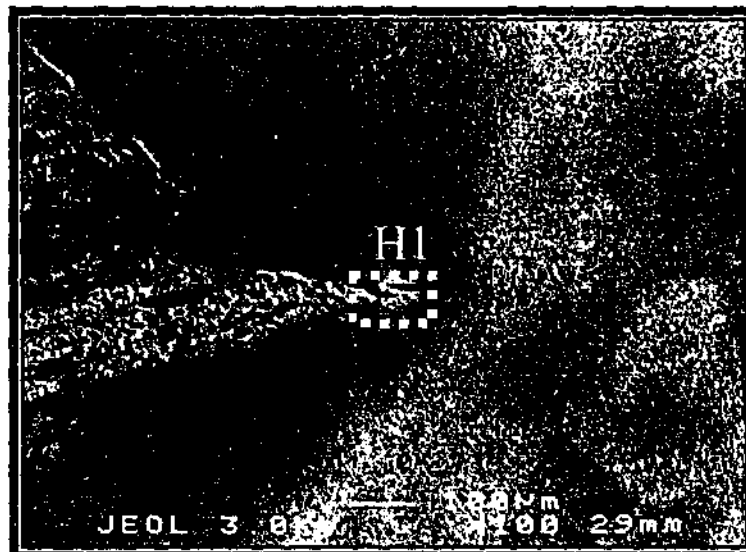


Figure 7.44: SEM – Starting notch and etched ABS/PET prior to loading (x100).

Figure 7.44 shows an etched ABS/PET specimen that has not been loaded. There is evidence that even with the use of a razor blade to provide a sharp crack tip, deformation has occurred in the surrounding material. There are flow lines around the starting notch.

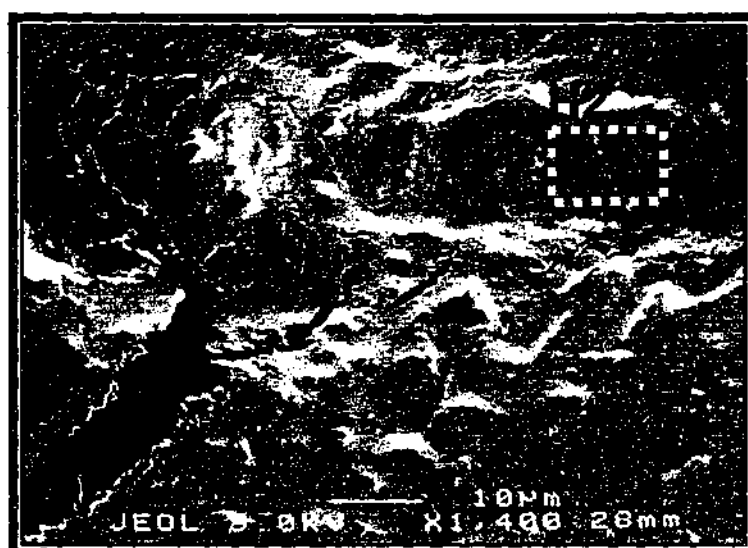


Figure 7.45: SEM - Enlarged view of area H1 from Figure 7.44 (x1400).

However, as expected, at higher magnifications (Figures 7.45 to 7.46) no significant differences could be seen in the structure of the material close to the crack tip (Figure 7.46) compared to an area far away from the flaw (Figure 7.47). Both matrices show an unoriented structure.

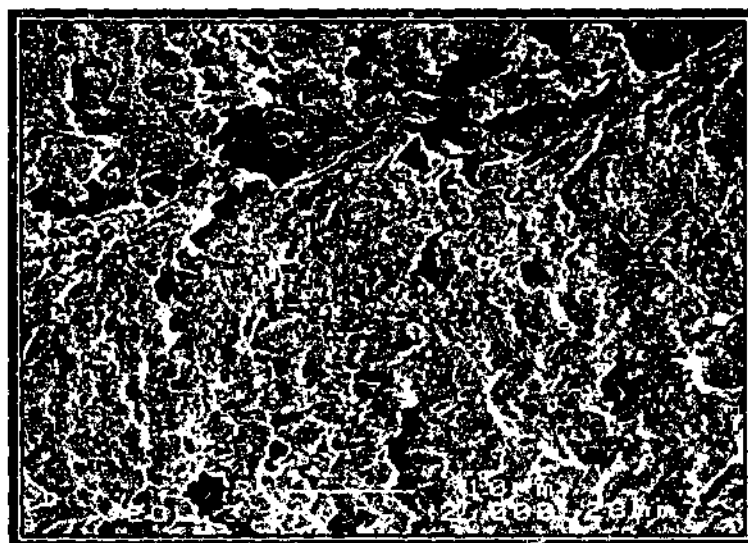


Figure 7.46: SEM - Enlarged view of area H2 from Figure 7.45 (x2000).

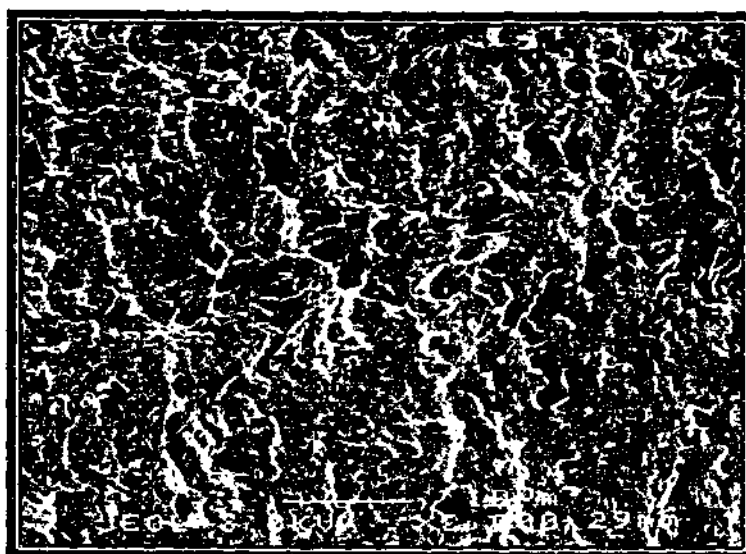


Figure 7.47: SEM - Enlarged view of an area away from the crack (x2000).

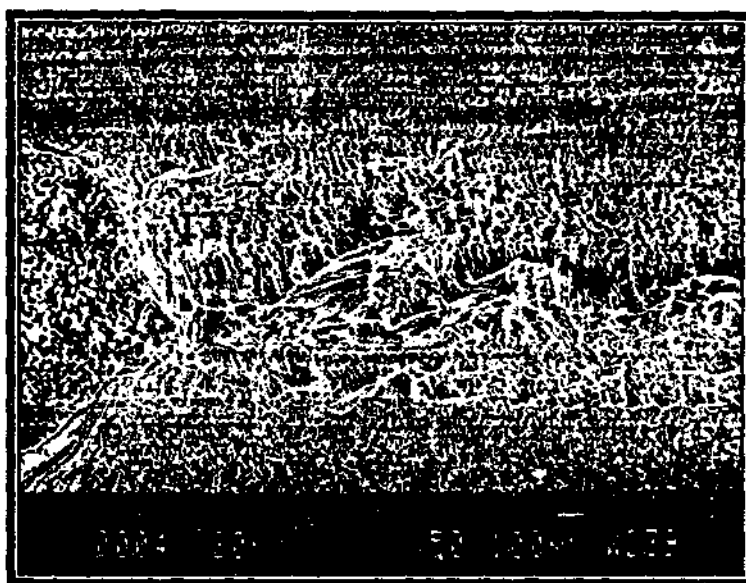


Figure 7.48: SEM – ABS/PET loaded to 90% of failure stress (x50).

In the case when ABS/PET is loaded to ninety percent of its failure stress, intense elongation of the material in front of the crack is observed (refer to Figure 7.48 and Figure 7.49). This is evident when we compare the structure of Figure 7.50 and Figure 7.49. In Figure 7.50, the phase which has not been etched away (in this case it is the ABS phase), shows an unoriented matrix, whereas in Figure 7.49, it is heavily oriented in the tensile direction (which is vertically up and down the page).

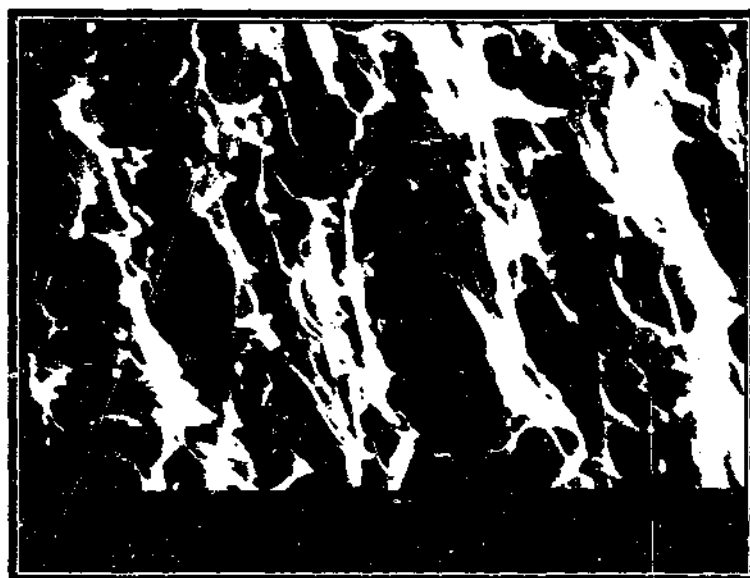


Figure 7.49: SEM - Enlarged view of area II from Figure 7.43 (x2200).

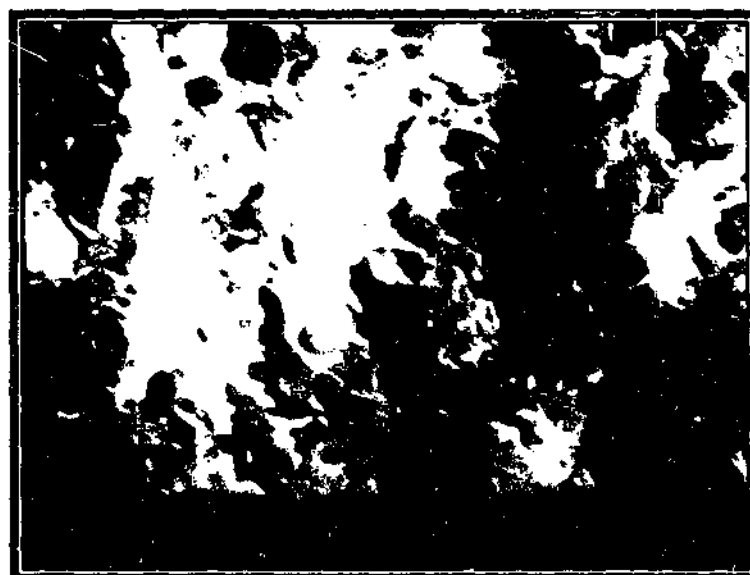


Figure 7.50: SEM - Enlarged view of an area away from the crack (x2700).

7.3.2 ABS/PC

The second polymer blend that was used in this thesis was ABS/PC. It showed similar behaviour to the ABS/PET blend. Once loaded, there was severe stress whitening of the material in front of a sharp crack tip (compare 7.52 to Figure 7.51).

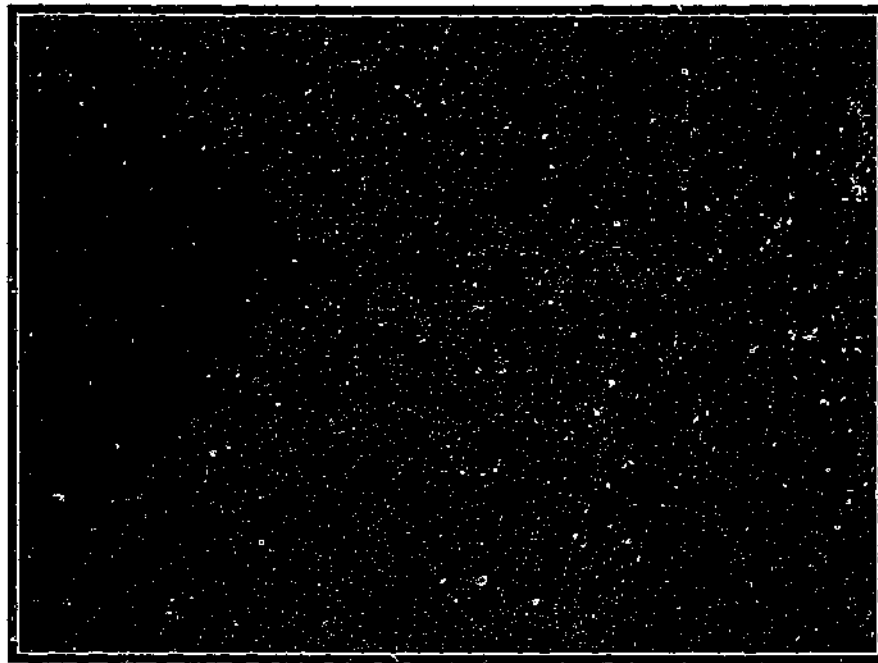


Figure 7.51: Optical microscopy of polished section of ABS/PC prior to loading.

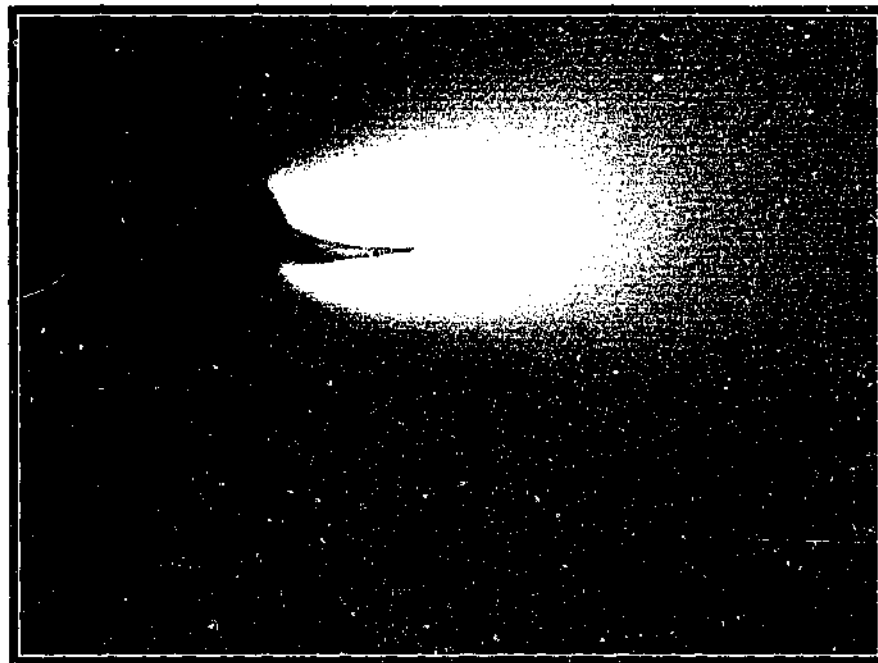


Figure 7.52: Optical microscopy of polished section of ABS/PC loaded to 90% of failure stress.



Figure 7.53: SEM – Starting notch and etched ABS/PC (x120).

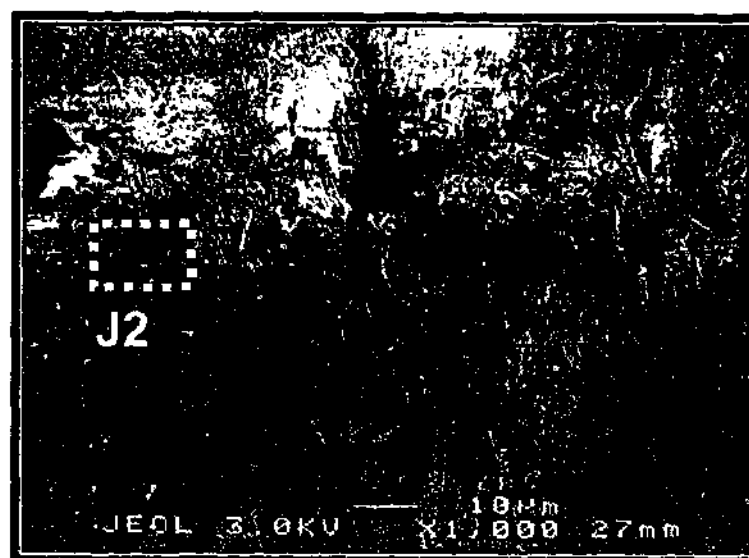


Figure 7.54: Enlarged view of area J1 from Figure 7.53 (x1000).

In Figures 7.53 and 7.54, no significant amount of damage can be seen in an ABS/PC specimen prior to being loaded. Like ABS/PET, at higher magnifications, no differences could be observed between the material close to the crack tip (Figure 7.55) and away from it (Figure 7.56).



Figure 7.55: SEM - Enlarged view of area J2 from Figure 7.54 (x2500).



Figure 7.56: SEM - Enlarged view of an area away from the crack (x2500).

Under a scanning electron microscope, the crack tip can be seen (Figure 7.57 and Figure 7.58). In Figure 7.58, the tip of the crack is well defined and shows the elongation and fracture of material in front of the propagating path. Under smaller magnification (Figure 7.57), the large amount of deformation in front of the crack can be observed.

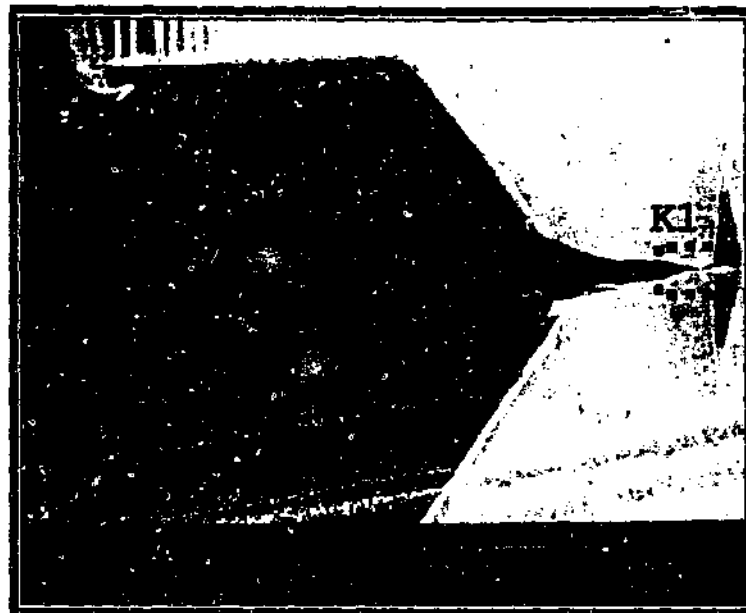


Figure 7.57: SEM – ABS/PC loaded to 90% of failure stress (x30).



Figure 7.58: SEM - Enlarged view of area K1 from Figure 7.57 (x2000).

For the two blends, the large scale extension in the localised area around the crack tip aid in absorbing large amounts of work and effectively blunting the crack, thus giving both blends high values of ρ and K_{Ic} . Using the equivalent magnification as Figure 7.58 but at a distance away from the deformation zone, Figure 7.59 shows the material undergoes little elongation or fracture. The structure is similar to that of a specimen which has not been loaded (refer to Figure 7.56).

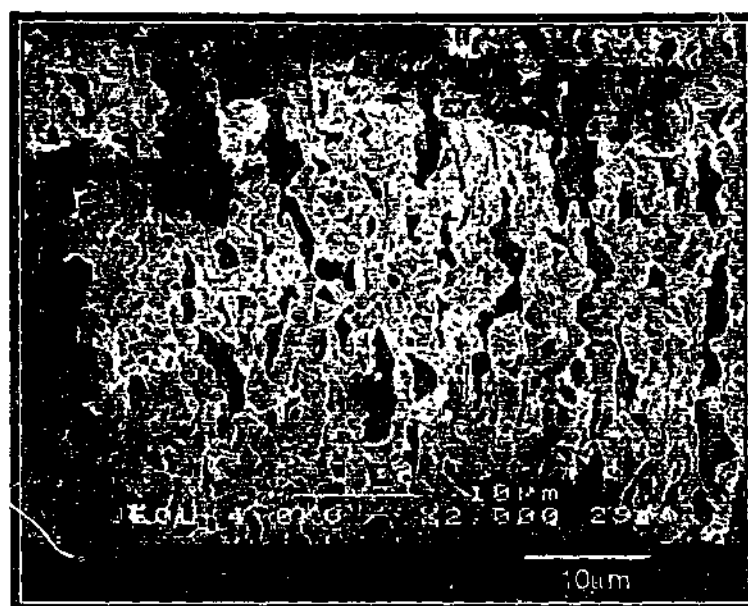


Figure 7.59: SEM - Enlarged view of an area away from the crack (x2000).

7.4 Summary

The microscopy work performed on the eight materials used in this thesis has helped in gaining an understanding of the toughening mechanisms used in a wide variety of polymers to impede crack growth. By using these mechanisms, the polymers effectively blunt the crack to a certain radius of curvature giving validity to the model proposed in this thesis.

In order to slow crack propagation, PC showed crack divergence whilst PET showed multiple crack formation and a large process zone in front of the starting notch. Microcracking and crazing were apparent in PS but these processes are normally associated with fast crack propagation, which is also observed in the fracture of PS. It is therefore no surprise that PS has a low value of ρ compared to the other two single phase polymers.

The three grades of ABS all exhibited similar crack tip deformation behaviour. Astalac DMT and Astalac M120 showed stress whitening in the optical micrographs of polished sections of the materials. With the use of SEM, all three showed severe blunting of the crack tip. In all three cases, not all the deformation could be seen. Cavitation of the rubber particles in ABS has been observed by other workers but that requires the use of a TEM. That technique was not utilised in this thesis.

The tough polymer blends, ABS/PET and ABS/PC, effectively blunt the crack by undergoing severe deformation in front of the crack tip. As observed in the micrographs, large scale extension of the material was observed near the crack tip when compared to a region far away from the crack. The structure of the material away from the crack tip was similar to that of a specimen prior to being loaded. The two materials also showed stress whitening in the optical micrographs. However, not all toughening mechanisms were observed using the two simple microscopy techniques. Once again, TEM would need to be utilised to see cavitation or debonding between phases or other energy absorbing phenomena.

Throughout the microscopy work, the use of an epoxy to impregnate the crack tip was effective. In all cases, the epoxy reached deep into the flaw, arguably freezing the crack propagation process under load. This allows the capturing of images of the deformation processes in all eight materials.

It was also shown how the values of ρ obtained in Chapter 6 coincide with the observed toughening phenomena. It is apparent that tough polymers have a variety of toughening tools to effectively blunt the crack tip allowing them to have large ρ values while brittle polymers do not and therefore had low ρ values.

Chapter 8

Discussion and Conclusion

8.1 Discussion and Concluding Remarks

In the previous chapter, microscopy work has shown that to accommodate sharp cracks, tough polymers undergo various forms of deformation at the crack tip. These energy absorbing processes make it seem like the polymer has effectively blunted the end of the crack to a radius of curvature ρ .

Each material will have a distinct value of ρ and this material property can then be used to predict failure in thin walled polymeric structures. The proposal is that failure occurs when the magnified stresses at the crack tip (due to the effective radius of curvature) reaches the "yield" stress of the material according to Von-Mises criterion. It is also understood that some polymers fail before they reach the stress specified by Von-Mises. For instance, PS and PC craze before the Von-Mises "yield" stress while in ABS the micro cracks coalesce to form a plastic zone. However, the assumption of failure as defined by the Von-Mises "yield" stress is adequate in this work because the actual failure processes of the polymers considered in this thesis is close to the Von-Mises criterion.

The material parameter ρ is not equal to Irwin's plastic zone size r_p , but as the dotted "trendline" in Figure 8.1 shows, the tendency is that small plastic zone sizes results in small values of ρ . Higher values of r_p correspond to larger values of ρ , until about a ρ curvature of about 50mm. ρ then continues to rise but r_p is constant at around 1.5mm. This is because ρ is a modelling parameter that describes the behaviour of cracks in polymers which accounts for all the toughening mechanisms associated with tough polymers - such as cavitation, shear yielding, microcracking, plasticity effects, crazing and others. In this regard, it is also different to the plastic zone size because r_p by definition only accounts for yielding at the crack tip. Failure loads of brittle polymers can also be predicted by ρ , signifying the flexibility of the parameter.

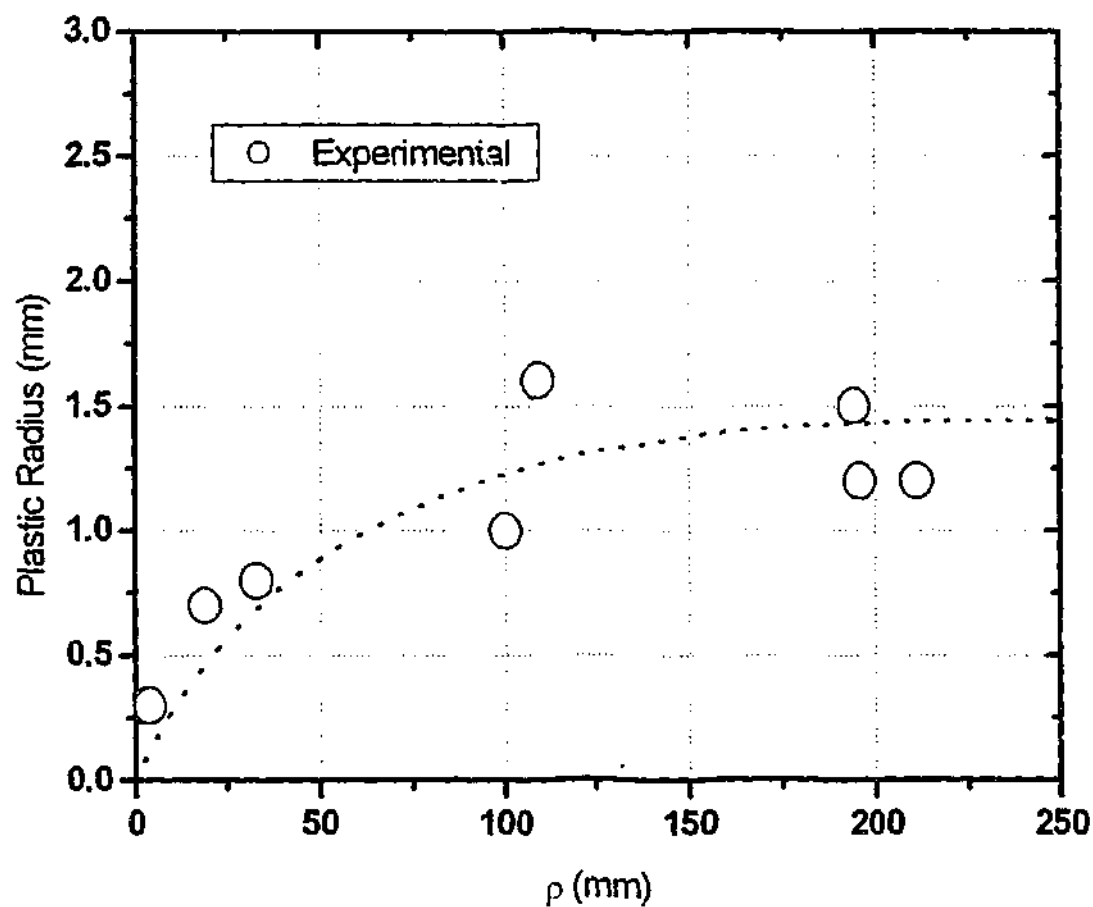


Figure 8.1: Relationship between the parameter ρ and r_p .

Referring to Table 8.1 (ranked from the highest value of ρ to the lowest value), the relationship between ρ and observed deformation at the crack tip is clear. For large values of ρ , there is severe effective blunting of the crack tip. Also stretching and fracturing of material in the path of the propagating crack have been seen in polymer blends. Smaller values of ρ are associated with microcracking, crack branching, crazing and sharp crack tips.

Table 8.1: Showing the relationship between plastic zone size, effective blunting parameter and observed toughening mechanisms.

Material	r_p (mm)	ρ (mm)	Observations from microscopy, macroscopic testing and known mechanisms
Astalac DMT (Injection moulding grade ABS)	1.2	211.2	<ul style="list-style-type: none"> • Blunting of crack tip.^{1,2} • Stress whitening and plastic yielding in front of the crack tip.^{1,2,3} • Cavitation of rubber particles.³
ABS/PC blend (Astaloy 800)	1.2	195.8	<ul style="list-style-type: none"> • Elongation of material in front of the crack.^{1,2} • Stress whitening.^{1,2}
CB625 (General purpose ABS)	1.5	194.3	<ul style="list-style-type: none"> • Blunting of the crack tip.¹ • Cavitation of rubber particles.³
ABS/PET blend	1.6	109.1	<ul style="list-style-type: none"> • Elongation of material in front of the crack.^{1,2} • Stress whitening.^{1,2}
Astalac M120 (Extrusion grade ABS)	1.0	100.2	<ul style="list-style-type: none"> • Blunting of crack tip.¹ • Stress whitening and plastic yielding in front of the crack tip.^{1,2} • Cavitation of rubber particles.³
PET (Blow moulding grade)	0.7	18.9	<ul style="list-style-type: none"> • Microcracks appearing in front of the starting notch.¹
PC (General purpose grade)	0.3	3.9	<ul style="list-style-type: none"> • Crack branching.¹
PS (General purpose grade)	0.3	2.5	<ul style="list-style-type: none"> • Microcracks and crazing around the specimen.¹ • Sharp crack tip.¹

¹ Observations from microscopy² Macroscopic testing³ Known mechanisms

A few other main conclusions can also be drawn from this body of work. Firstly, a range of polymeric materials were tested, ranging from tough and ductile polymers and blends to brittle thermoplastics. Furthermore, these polymers were tested under numerous loading situations. They included plane stress to plane strain specimens and uniform loading to pin loading conditions. In Chapter 6, it was shown that in all these cases, the novel and simple blunting effect methodology proposed in this thesis provided predictions which were consistently safe for short crack lengths. LEFM and net section yielding methodologies were inadequate in some cases by forecasting working loads which were higher than experimental data.

Secondly, because the effective blunting method seems to predict safe working loads for a wide range of materials and stress states, it can also be utilised as a design parameter. In summary, it can be said that once the stress state of the article is well known and areas of high stresses identified, the allowable crack length can be determined. If one uses the effective blunting method, the calculated allowable crack length will always be tolerable. Chapter 3.4 provides a full description of the procedure for utilising ρ as a design tool.

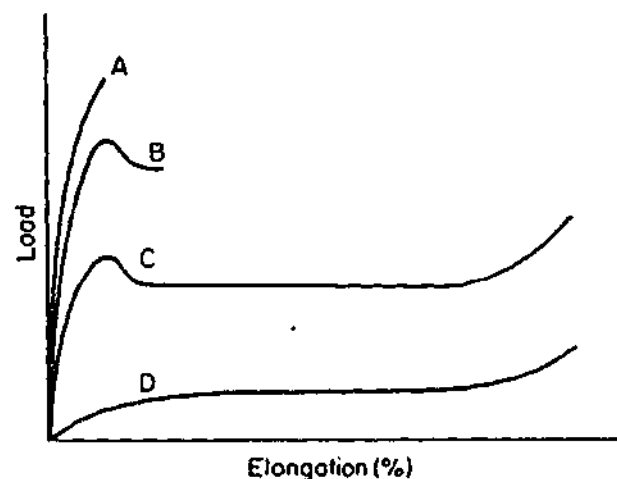


Figure 8.2: Tensile behaviour of polymers under a variety of strain rates. The curve A represents a fast rate of testing whilst curve D is a slow rate of testing [Ward 1986].

The conclusions given above may give the impression that the model is complete but this is not the case. In fact, one of the main problems with the parameter ρ is its simplicity. It does

not take into account the time-dependence nature of polymers. Polymers are visco-elastic materials and as Figure 8.2 shows, they are capable of exhibiting a range of behaviour depending on the rate of loading. Perhaps the only counter to this argument is that changes in the material properties occur over many decades (as shown by Figures 5.2 to 5.9).

Another flaw in the modelling of failure loads using the various simple methodologies in this study are their lack of account of plasticity effects. However Chapter 3.3 shows that solutions using elastic-plastic fracture mechanics is fairly complicated and furthermore the stress-strain behaviour of these materials at the testing rates considered do not follow the simple elastic-plastic governing equations.

8.2 Recommendations for Future Work

There is certainly a large amount of work to be done in this field. One must address all the issues discussed previously such as time dependency and plasticity effects. Future workers could use a simple elastic-plastic fracture mechanics approach and assume an elastic-plastic stress-strain relationship for the polymer and compare its effectiveness to the elastic methodologies.

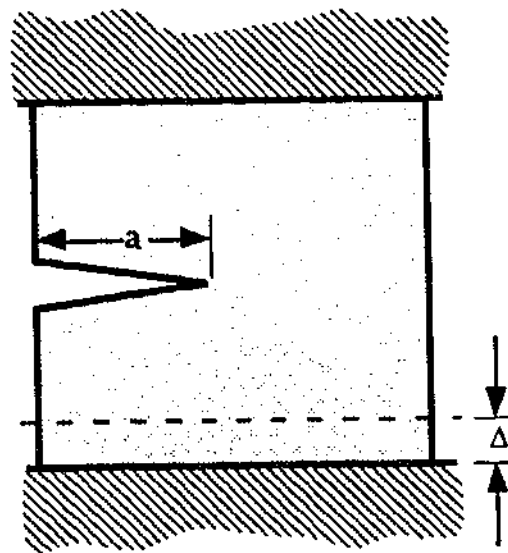


Figure 8.3: Schematic of a constant displacement condition [Anderson 1995].

Specimens should also be tested under different extension rates to check for deviations between experimental data and the simple failure prediction methodologies used in this thesis which does not take into account the visco-elastic nature of polymers. In engineering circumstances, the extension rates will obviously be different to those used in this work, indicating a need to better understand the effect of time on these materials.

Another imperative for the next worker in this field is the use of engineering loading situations to characterise failure. The two other modes of loading as compared to constant velocity are constant displacement and constant load (shown by Figures 8.3 and 8.4 respectively).

Constant displacement is probably not as severe as the case of constant load, especially for polymers. Polymers have the capacity to relax over time and if a constant displacement was applied, the chains in the polymer will accommodate the extra strain by disentangling.

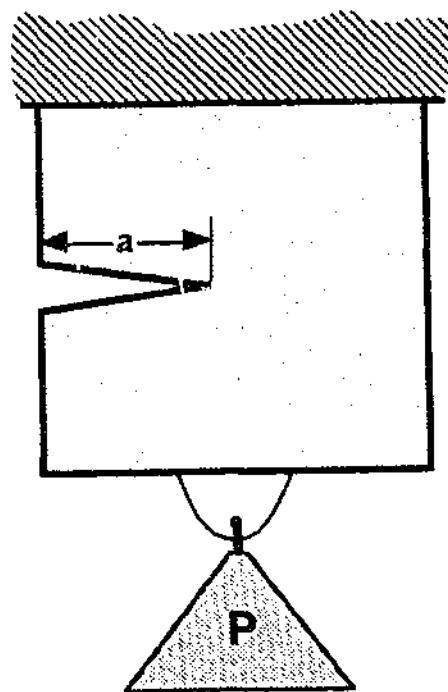


Figure 8.4: Schematic of a constant load condition [Anderson 1995].

The technique of impregnating the crack tip with a thermoset using hydrostatic pressure should be employed in future microscopy work. It was shown in Chapter 7 that this simple

technique was capable of freezing the crack just before propagation. At present, the microscopy work has concentrated on one plane of the crack tip. The shape of the crack tip in these tough ductile polymeric materials captured under load would be more complete if photos were taken from the other two planes. This would give a three-dimensional view of the crack tip. The effects from environmental stress cracking (ESC) should also be avoided. Usage of low exothermic thermosets and "gentle" etchants, such as those employed in this work and by other workers, will minimise this problem. This procedure will also lower the number of artefacts in the micrographs. Transmission electron microscopy (TEM) should also be employed to give a higher magnification of the deformation. A failure model could then be proposed relating the microstructure to the macro behaviour.

Lastly and most importantly, there needs to be a facile method of applying the essential work of fracture (EWF) to predict failure in tough ductile injection moulded polymeric articles. EWF has predominantly been utilised as a characterisation tool. It has shown to be a simple and effective means of measuring toughness. Therefore, the author's recommendation is to develop a model which will encapsulate the fundamentals of EWF and allow it to be used in engineering situations.

References

- Anderson T.L., (1995), *Fracture Mechanics, Fundamentals and Applications*, CRC Press Inc., Boca Raton, Florida.
- Ansafori, A. and Andrews, E.H., (1993), *J. Mater. Sci.*, **28**, p.3564.
- Argon, A.S., Cohen, R.E. and Mower, T.M., (1994), *Mater. Sci. Eng.*, **A176**, p.79.
- ASTM 638.98, (1999), *Annual Book of ASTM Standards*, **08.01**, American Society for Testing and Materials, Philadelphia, p.45.
- ASTM D256-97, (1999), *Annual Book of ASTM Standards*, **03.01**, American Society for Testing and Materials, Philadelphia, p.1.
- ASTM E813-89, (1990), *Annual Book of ASTM Standards*, **03.01**, American Society for Testing and Materials, Philadelphia, p.700.
- Ashby, M.F. and Jones D.R.H., (1996), *Engineering Materials 1: An Introduction to their Properties and Applications*, Butterworth-Heinemann, Boston.
- Atkins, A.G. and Mai, Y.W., (1985), *Elastic and Plastic Fracture: metals, polymers, ceramics, composites, biological materials*, Ellis Horwood, Chichester, UK.
- Bacoffen, W.A., (1972), *Deformation Processing*, Addison-Wesley Publishing Company Inc., Sydney.
- Beahan, P., Bevis, M. and Hull, D., (1975), *Proc. Royal Soc. Lond. Series A*, **343**, p.525.
- Bhowmick, A.K. and De, S.K., eds., (1991), *Fractography of Rubbery Materials*, Elsevier Science Publishers Ltd., Essex.
- Billmeyer Jr., F.W., (1971), *Textbook of Polymer Science*, Wiley-Interscience, New York.
- Broberg, K.B., (1968), *Inter. J. Fract. Mech.*, **4**, p.11.
- Broberg K.B., (1975), *J. Mech. Phys. Solids*, **23**, p.215.
- Broek, D., (1986), *Elementary Fracture Mechanics, 4th Edition*, Kluwer Academic Publishers, Dordrecht.

- Broek, D., (1989), *The Practical Use of Fracture Mechanics*, Kluwer Academic Publishers, Dordrecht.
- Brown, G.M. and Butler J.H., (1997), *Polymer*, **38**, p.3937.
- Bucknall, C.B., Correa, C.A. and Soares V.L.P., (1993), *Pol. Mater. Sci. Eng.*, **70**, p.241.
- Bucknall, C.B., (1977), *Toughened Plastics*, Applied Science Publishers Ltd., Essex.
- Calladine, C.R., (1969), *Engineering Plasticity*, Pergamon Press Ltd., Oxford.
- Chan W.Y.F. and Williams J.G., (1994), *Polymer*, **35**, p.1666.
- Chen, A.T., Henton, D.E., Plaver, F.M., McLaughlin, A. and Naeger, D.M., (1990), *Elastomerics*, **122**, p.19.
- Chen, C.C. and Sauer, J.A., (1990), *J. Appl. Pol. Sci.*, **40**, p.503.
- Ching, E.C.Y., Poon, W.K.Y., Li, R.K.Y. and Mai, Y.W., (2000), *Pol. Eng. Sci.*, **40**, p.2558.
- Cook, W.D. and Guise, G.B., eds., (1989), *Polymer Update: Science and Engineering*, Polymer Division, Royal Australian Chemical Institute, Melbourne.
- Cook, W.D., Zhang, T., Moad, G., Van Diepen, G., Cser, F., Fox, B. and O'Shea, M., (1996a), *J. Appl. Pol. Sci.*, **62**, p.1699.
- Cook, W.D., Zhang, T., Moad, G., Van Diepen, G., Cser, F., Fox, B. and McCarthy, L., (1996b), *J. Appl. Pol. Sci.*, **62**, p.1709.
- Cotterell, B. and Redel, J.K., (1977), *Inter. J. Fract.*, **13**, p.267.
- Cottrell A.H., (1964), *The Mechanical Properties of Matter*, John Wiley and Sons, New York.
- Crist, B., Swei, H. and Carr, S.H., (1991), *Polymer*, **32**, p.1440.
- Curtin, W.A. and Xiao, F., (1995), *Macromolecules*, **28**, p.1654.
- Deutchman, A.D., Michels, W.J. and Wilson, C.E., (1975), *Machine Design: Theory and Practice*, Macmillan Publishing Co., New York.
- Dijkstra, K. and Gaymans, R.J., (1994), *J. Mater. Sci.*, **29**, p.3231.
- Donald, A.M. and Kramer, E.J., (1982), *J. Mater. Sci.*, **17**, p.1765.

- Drucker, D.C., (1964), in *Second - Order Effects in Elasticity, Plasticity and Fluid Dynamics, International Symposium, Haifa, Israel, April 23-27, 1962*, eds. M. Reiner and D. Abir, Pergamon Press, New York, p.331.
- Dubey, R.N., (1998), *Eng. Fract. Mech.*, **60**, p.501.
- Edward, G.H., (1990), *Polymer Blends and their Interfaces*, RACI Symposium, Monash University, Melbourne.
- Eshelby, J.D., (1974), in *Prospects of Fracture Mechanics*, eds. G.C. Sih, H.C. Van Elst , D. Broek, Noordhoff, p.69.
- Frontini, P.M., Bernal, C.R. and Herrera, R., (1992), *Pol. Testing*, **11**, p.271.
- Frontini, P.M., Bernal, C.R., Sforza, M. and Bibbo, M.A., (1995), *J. Appl. Pol. Sci.*, **58**, p.1.
- Griffith, A.A., (1920), *Phil. Trans. Royal Soc. Lond.*, **A221**, p.163.
- Guagliano, M. and Vergani, L., (1994), *Fatigue Fract. Eng. Mater. Struct.*, **17**, p.1295.
- Hashemi, S. and O'Brien, D., (1993), *J. Mater. Sci.*, **28**, p.3977.
- Hashemi S., (1993), *J. Mater. Sci.*, **28**, p.6178.
- Hashemi, S., (1997), *J. Mater. Sci.*, **32**, p.1563.
- Haward, R.N. and Bucknall, C.B., (1976), *Pure and Appl. Chem.*, **46**, p.227.
- Hearn, E.J., (1995), *Mechanics of Materials, 2nd Edition, Volumes 1 and 2*, Pergamon Press Ltd., Oxford.
- Herpels, J.J. and Mascia, L., (1990), *Eur. Pol. J.*, **26**, p.997.
- Herrera, J.M., Spencer P.R., Tarin, P.M. and Stafford S.W., (1995a), *Mater. Characterisation*, **34**, p.51.
- Herrera, J.M., Spencer P.R., Tarin, P.M. and Stafford S.W., (1995b), *Mater. Characterisation*, **34**, p.57.
- Hertzberg, R.W., (1983), *Deformation and Fracture Mechanics of Engineering Materials, 2nd Edition*, John Wiley and Sons, New York.
- Horiuchi, S., Street, A. C., Ougizawa, T. and Kitano, T., (1994), *Polymer*, **35**, p.5283.

- Hosford, W.F. and Caddell R.M., (1993), *Metal Forming, Mechanics and Metallurgy, 2nd Edition*, Prentice-Hall Inc., Sydney.
- Howland, R.C.J., (1930), *Phil. Trans. Royal Soc. Lond.*, **229**, p.49.
- Huang, D.D., (1991), *49th Annual Technical Conference. ANTEC-Conference Proceedings, 37*, Society of Plastic Engineers, Brookfield, USA, p.2193.
- Huang, Y., (1991), *Microstructure-Property Relationship in Toughened Epoxy Polymers*, Ph.D. Thesis, Imperial College of Science, Technology and Medicine, London.
- Hutchinson, J.W., (1968), *J. Mech. Phys. Solids*, **16**, 1968, p.1.
- Inglis, C.E., (1913), *Fifty fourth session of the Institution of Naval Architects*, **55**, p.219.
- Irwin, G.R., (1948), *Fracturing of Metals, ASM*, p.152.
- Irwin, G.R., (1957), *J. Appl. Mech.*, **24**, p.361.
- Irwin, G.R., (1958), *Handbuch der Physik Vol. VI*, Springer, Berlin, p.551.
- Jennings, G.A., (1994), *Modern Geometry with Applications*, Springer-Verlag Inc., New York.
- Kim, B.H., Joe, C.R., Otterson, D.M. and Lavengood, R.E., (1990a), *Pol. Testing*, **9**, p.219.
- Kim, H., Keskkula, H. and Paul, D.R., (1990b), *Polymeric Science and Engineering, Proceedings of the ACS Division of Polymeric Materials Science and Engineering*, **63**, p.210.
- Kinloch, A.J. and Young, R.J., (1990), *Fracture Behaviour of Polymers*, Applied Science Publishers Ltd., Essex.
- Knott, J.F., (1973), *Fundamentals of Fracture Mechanics*, Butterworth, London.
- Knowles J.K. and Sternberg E., (1972), *Arch. Rational Mech. Analy.*, **44**, p.187.
- Knuk, M.P. and Read D.T., (1986), *Inter. J. Fract.*, **31**, p.161.
- Kreyszig, E., (1988), *Advanced Engineering Mathematics, 6th Edition*, John Wiley and Sons. New York.
- Kulshreshtha, A.K., (1993), *Pol. Plastics Technology. Eng.*, **32**, p.551.
- Kunz-Douglass, S., Beaumont, P.W.R. and Ashby, M.F., (1980), *J. Mater. Sci.*, **15**, p.1109.

- Kunz, S.C. and Beaumont P.W.R., (1981), *J. Mater. Sci.*, **16**, p.3141.
- Lin, L. and Argon A.S., (1994), *J. Mater. Sci.*, **29**, p.294.
- Lipatov, Y.S., (1992), *Inter. J. Pol. Mater.*, **17**, p.91.
- MacDonald, W.J., (1993), *Kunststoffe*, **83**, p.29.
- Mai, Y.W. and Cotterell B., (1985), *Eng. Fract. Mech.*, **21**, p.123.
- Mai, Y.W. and Cotterell B., (1986), *Inter. J. Fract.*, **32**, p.105.
- Majumdar, B., Keskkula, H. and Paul, D.R., (1994), *J. Pol. Sci. Pol. Phys. Ed.*, **32**, p.2127.
- Moad, G., Appleby, T., Cser, F., Rizzardo, E. and Stavropoulos, C., (1994), *Pol. Bulletin*, **32**, p.479.
- Montezinos, D., Wells B.G. and Burns J.L., (1985), *J. Pol. Sci., Polymer Letters Edition*, **23**, p. 421.
- Nadai, A., (1963), *Theory of Flow and Fracture of Solids Volume 2*, McGraw-Hill Book Company, Inc., New York.
- Newman Jr. J.C. and Loss F.J., (1985), eds., *Elastic-Plastic Fracture Mechanics (ASTM Special Technical Publication; 896)*, American Society for Testing and Materials, Philadelphia.
- Orowan, E., (1950), *Fatigue Fract. Metals, MIT Symposium June*, Wiley, New York.
- Parton, V.Z., (1992), *Fracture Mechanics, From Theory to Practice*, Gordon and Breach Science Publishers, Melbourne.
- Paul D.R. and Newman S., eds., (1978), *Polymer Blends - Volume 1 and 2*, Academic Press, New York.
- Paul, D.R. and Barlow, J.W., (1980), *J. Macromol. Sci. Rev. Macromol. Chem.*, **C18**, p.109.
- Paul, D.R., Keskkula, H. and Kim, H., (1991), *Pol.*, **32**, p.1447.
- Paul, D.R., Keskkula, H. and Lombardo, B.S., (1994), *J. Appl. Pol. Sci.*, **54**, p.1697.
- Peterson, R.E., (1953), *Stress Concentration Design Factors*, John Wiley and Sons Inc., New York.

- Peterson, R.E., (1974), *Stress Concentration Factors*, John Wiley and Sons Inc., New York.
- Plast. News Inter., *Plastics News International*, (1997), October, p.4.
- Raab, M., (1993), *Pol. Eng. Sci.*, **33**, p.1438.
- Rice, J.R. and Drucker, D.C., (1967), *Inter. J. Fract. Mech.*, **16**, p.19.
- Rice J.R., (1968), *J. Appl. Mech.*, **35**, p.379.
- Roe, J., (1993), *Elementary Geometry*, Oxford University Press Inc., New York.
- Rooke, D.P. and Cartwright, D.J., (1976), *Compendium of Stress Intensity Factors*, Her Majesty's Stationary Office, London.
- Santana, O.O., Maspoche, M.L. and Martinez, A.B., (1997), *Pol. Bulletin*, **39**, p.511.
- Savanije, H.B. and Berger, O.Z., (1993), *Kunststoffe*, **83**, p.27.
- Sawyer, L.C. and Grubb, D.T., (1987), *Polymer Microscopy*, Chapman and Hall Ltd., London.
- Seidler, S. and Grellman, W., (1993), *J. Mater. Sci.*, **28**, p.4078.
- Shi, Y.W., (1993), *Eng. Fract. Mech.*, **46**, p.285.
- Steenbrink, A.C., Janik, H. and Gaymans R.J., (1997), *J. Mater. Sci.*, **32**, p.5505.
- Takemori, M.T., (1990), *Polymeric Science and Engineering, Proceedings of the ACS Division of Polymeric Materials Science and Engineering*, **63**, p.568.
- Tetelman, A.S., McEvily Jr., A.J., (1967), *Fracture of Structural Materials*, John Wiley and Sons, Inc., New York.
- Timoshenko, S.P. and Goodier, J.N., (1970), *Theory of Elasticity, 3rd Edition*, McGraw-Hill Book Company, Singapore.
- Utracki, L.A., (1990), *Polymer Alloys and Blends: Thermodynamics and Rheology*, Hanser, New York.
- Ward I.M., (1986), *Mechanical Properties of Solid Polymers*, John Wiley and Sons Ltd. Sydney.
- Westergaard (1939), *J. Appl. Mech.*, **6**, p.A49.

Williams, J.G., (1984), *Fracture Mechanics of Polymers*, John Wiley and Sons Inc., Brisbane.

Wood, B.A., (1992), in *Advance in Polymer Blends and Technology, Volume 3*, ed. K. Finlayson, Technomic Publishing Company Inc., p.24.

Wu, J., Mai, Y.M. and Cotterell, B., (1993), *J. Mater. Sci.*, **28**, p.3373.

Wu, J. and Mai, Y.M., (1993), *J. Mater. Sci.*, **28**, p.6167.

Zipper, M.D., (1995), *A Free Volume and Molecular Mobility Study of Miscible Polycarbonate/Polyester Blends*, Ph.D. Thesis, Monash University, Melbourne.